UNIVERSITY OF MINNESOTA
ST. ANTHONY FALLS HYDRAULIC LABORATORY

Project Report No. 365

Hydraulic Transient Study of Fall River Tunnel System

by

Jianming He, Charles C.S. Song

and Ying Liu

Prepared for

CH2M HILL/PBG&S Team
50 Staniford St., 10th Floor
Boston, MA 02114-2517

December, 1994
Minneapolis, Minnesota

UNIVERSITY OF MINNESOTA
ST. ANTHONY FALLS HYDRAULIC LABORATORY

Project Report No. 365

Hydraulic Transient Study of Fall River Tunnel System

by

Jianming He, Charles C.S. Song,

and Ying Liu

Prepared for

CH2M HILL/PBG&S Team
50 Staniford St., 10th Floor
Boston, MA 02114-2517

December, 1994

TABLE OF CONTENTS

LIST OF FIGURES

Figure No.

I. INTRODUCTION

1.1 Problem Description

The purpose of this study is to evaluate the hydraulic transient status in the proposed Fall River Tunnel System in Southeastern Massachusetts. The tunnel system is designed to convey approximately 80% of the dry and wet weather flows generated in the Fall River combined sewer service area. The tunnel system consists of 4.5 miles of a 20–foot diameter tunnel and 2.6 miles of 8–foot (updated from 5–foot) diameter tunnel, as well as 23 dropshafts. The connection between the two different diameter tunnels is crown–to–crown (updated from invert–to–invert in the original design). The downstream end of the tunnel system is connected to a Waste Water Treatment Plant (WWTP). The WWTP is also connected to the existing interceptor system, and the water from the existing interceptor has a higher priority to enter the WWTP. Therefore, for a small storm, most inflow water to the new tunnel system will be stored in the tunnel during the storm period, and be treated later. For a large storm, however, the inflow water beyond the tunnel storage will be spilled through an extreme event overflow structure (at Arnold St.) close to the WWTP. From the hydraulic transient point of view, there are the following possible safety concerns in this tunnel system which need to be evaluated using a hydraulic transient computer simulation program.

(1) Surge phenomena induced during the initial filling stage and their effects on dropshaft structures and the downstream control facility;

(2) The reasonable weir elevation at the extreme event overflow structure based on the given diameter (30 ft. O.D.) and weir length (94.25 ft. updated from 64 ft.) to assure that overflow does not occur anywhere else.

(3) The hydraulic transient behaviors induced by the downstream flow control at the WWTP due to the limited capacity of the WWTP.

The fully dynamic transient mixed flow mathematical model (MXTRANS) developed at the University of Minnesota was used for this study. The modeling configuration is based on the current design data. Any modification of the tunnel system, including the parameters related to the tunnel diameters, dropshaft geometry, and outlet control conditions, may affect the results.

Two typical storm events, 3–month and design, provided by the project team were used in the numerical simulations. The "design" event is based on estimates of the maximum flow rates that the collection system can deliver to each dropshaft. The recurrence interval for design flows varies for each dropshaft but is generally larger than a 2–year storm.

1.2 Study Progress

This study was initiated after Prof. Charles C. S. Song visited the CH2M Hill/PBG&S Project Office (fact–find trip), on Oct. 6, 1994. Based on the information provided by CH2M Hill/PBG&S's Project Office and discussion with the project engineers, Prof. Song submitted a preliminary analysis report on Oct. 24, 1994 [1] and proposed the strategy and detailed steps to fulfill the final numerical modeling tasks.

After the computer modeling had been established, and primary results had been obtained based on the original design information, the new design information was received on Nov. 11, 1994 [2]. Prof. Song presented the modeling results at the CH2M Hill/PBG&S Project Office on Dec. 13, 1994, based on the design information to date. The results are also documented in a draft report, which includes five simulation runs. Their modeling conditions are:

Case 1: Design storm event;
Invert–to–invert connection;
No outflow to the WWTP (closed end);
The weir elevation based on the tunnel invert (13 MHW) is 53 ft. (66 MHW), and the other dropshaft surcharge elevations are the same as the design data[2].

Case 2: Design storm event;
Invert–to–invert connection;
No outflow to the WWTP (closed end);
The weir elevation based on the tunnel invert (13 MHW) is 53 ft. (66 MHW), and the other dropshaft surcharge elevations are large enough to contain any upsurge.

Case 3: 3–mouth storm event;
Invert–to–invert connection;
No outflow to the WWTP (closed end);
The weir elevation based on the tunnel invert (13 MHW) is 53 ft. (66 MHW), and the other dropshaft surcharge elevations are the same as the design data[2].

Case 4: 3–month storm event;
Invert–to–invert connection;
Outflow to the WWTP is controlled by the difference between the WWTP capacity and the existing interceptor hydrograph (3–month) at the same time.
The weir elevation based on the tunnel invert (13 MHW) is 53 ft. (66 MHW), and the other dropshaft surcharge elevations are the same as the design data[2].

Case 5: Design storm event;
Invert–to–invert connection;
Outflow to the WWTP is controlled by the difference between the WWTP capacity and the existing interceptor

hydrograph (design storm) at the same time.
The weir elevation based on the tunnel invert (13 MHW) is 53 ft. (66 MHW), and the other dropshaft surcharge elevations are the same as the design data[2].

The above modeling results will be described in Chapter III of the report.

After the completion of the above-mentioned five cases and the draft report, some design data were further updated by the CH2M Hill/PBG&S Team [3]. The changes included:

1. The weir length increased to 94 feet from 64 feet.
2. The tunnel diameters in the upstream reaches that were 5-foot increased to 8-foot diameter.
3. Tunnel connection changed from invert-to-invert to crown -to-crown.
4. The Arnold Street weir elevation was set 30-feet above the tunnel invert 14.78 MHW (updated from 13 MHW).
5. The Manning coefficient for the transient analyses changed from 0.013 to 0.015.
6. The diameters of the following dropshafts were updated to

Dropshaft Name	Updated(ft)	Original(ft)
Wilson	10	15
Quequechan	10	15
Arnold	30	30
North Park	20	30
Lowell	20	30

Based on the newly-updated data, two more simulation runs were conducted:

Case 6: Updated design data;
Design storm event;
No outflow to the WWTP (closed end);
All the dropshaft surcharge elevations were large enough to contain any upsurge.

Case 7: Updated design data;
3-month storm event;
Outflow to the WWTP was controlled by the difference between the WWTP capacity and the existing interceptor hydrograph (3-month) at the same time.
The dropshaft surcharge elevations were the same as the design data[2].

The results of the above two modeling cases will be discussed in Chapter IV of the report.

II. THE MIXED TRANSIENT FLOW MODEL

2.1 Modeling Equations

The flow to be simulated is very unsteady and contains highly dynamic phenomena such as pressurization surge. The model used, then, must be able to simultaneously calculate unsteady open–channel flows and unsteady pressurized flows, including the abrupt change that occurs at the shock or the surge front.

The well–known St. Venant equations:

$$\frac{\partial y}{\partial t} + v \frac{\partial y}{\partial x} + \frac{c^2}{g} \frac{\partial v}{\partial x} = 0 \qquad (1)$$

$$g \frac{\partial y}{\partial x} + \frac{\partial v}{\partial t} + v \frac{\partial v}{\partial x} + g(S_f - S_o) = 0 \qquad (2)$$

are used to represent the unsteady open–channel flow. In the above equations, y is the flow depth, v is the flow velocity, c is the gravity wave speed, S_o is the channel slope, S_f is the energy slope, and g is the acceleration due to gravity, x is the distance along a tunnel, and t is time.

The corresponding equations for unsteady pressurized flow are:

$$\frac{\partial y}{\partial t} + V \frac{\partial y}{\partial x} + \frac{a^2}{g} \frac{\partial v}{\partial x} = 0 \qquad (3)$$

$$g \frac{\partial y}{\partial x} + \frac{\partial v}{\partial t} + v \frac{\partial v}{\partial x} + g(S_f - S_o) = 0 \qquad (4)$$

in which a is the pressure wave speed, while y takes the meaning of piezometric head measured from the tunnel invert. The systems of equations (1) ~ (4) are solved by the methods of characteristics [4].

Because the transition from the open–channel flow condition to pressurized flow condition must be abrupt, as in the case of a hydraulic jump, the special shock boundary conditions must be applied. It was shown by Cardle and Song [4], for a pressurization surge or a positive surge, that three characteristic equations plus two shock boundary conditions can be used to calculate five unknowns at the interface. These five unknowns are v and y on both sides of the interface and the speed of the interface movement. The model can also simulate the negative surge which occurs during the depressurization process. The detailed physical nature of the surging process has been discussed by Guo and Song [5].

A number of other boundary conditions representing junctions, dropshafts, upstream end, downstream end, reservoirs, and other accessories are also provided in the model. Inflow hydrographs, outflow conditions, and other active or passive flow control methods can also be included in the input data file. Velocity, depth, discharge, and other variables at any location and any time may be specified as outputs.

For more than twenty years, the above dynamic transient mixed flow mathematical model has been widely applied to a number of large sewer tunnel systems, such as Chicago TARP Phase I [6, 7, 8] and TARP Phase II [9, 10]; Milwaukee Inline Storage System [11, 12]; Rochester, New York, Genesee River Storage–Conveyance System [13]; and New York Passaic River Flood Protection Tunnel System [14].

2.2 Modeling Configuration

The general geometric information of the tunnel system is shown in Fig. 2.1. The schematic and stationing for transient modeling purposes are displayed in Fig. 2.2. There are a total of 199 computation stations with the modeling configuration. The distance between two stations is 200 ft, except the junction stations (Stations 89, 126, and 127) which represent the same location. The stationing of the main tunnel, excluding the Quequechan St. Branch, is displayed in Fig. 2.3, which will be used to show the water elevation along the main tunnel. The Manning's coefficient of 0.013 is used for the entire tunnel system in Case 1 to Case 5, and 0.015 in Case 6 and Case 7.

2.3 Downstream Condition

As mentioned before, the proposed tunnel system is connected to the WWTP at the downstream end. Because of the limited capacity (106 MGD = 164 cfs) of the WWTP, the outflow of the new tunnel system to the WWTP has to be limited to the difference between the WWTP capacity and the existing interceptor hydrograph. Therefore, a flow control at the downstream end is imposed. In the modeling condition, the outflow control means that the flow rate is given. For the closed–end condition, the downstream flow rate is zero.

Based on the given flow rate, water head at the downstream end can be easily calculated using the C^+ characteristic equation from the governing equations (3) and (4).

2.4 Inflow Hydrographs

The 3–month hydrographs at each dropshaft were provided by the CH2M Hill/PBG&S Team. Fig. 2.4 shows the total inflow to the new tunnel system at all the flow collection dropshafts, the existing interceptor hydrograph (3–month), and the capacity of the WWTP. The total inflow to the new tunnel system has a peak value of 633 cfs. The peak value of the existing interceptor hydrograph is 82.3 cfs. The capacity of WWTP is 164 cfs (106 MGD). The accumulative water volumes of the 3–month event for the total inflow to the new tunnel and the existing interceptor hydrograph is shown in Fig. 2.5.

Similar hydrographs for the design storm event are shown in Figs. 2.6 and 2.7. Since the design storm event hydrograph is not available, Fig. 2.6 is obtained by scaling–up the 3–month hydrograph patterns at each dropshaft using the given peak values of the design event, as shown in Table 1. At each dropshaft, the scale–up factor is the difference between the peak values of the design event and 3–month event. The design storm hydrograph at a dropshaft can be obtained by multiplying the 3–month hydrograph by the scale–up factor for the entire hydrograph period. The design event hydrograph of the existing interceptor is also scaled up using the total peak difference between the 3–month and design storm events for the new tunnel system. As indicated in Fig. 2.6, during 6.5 to 12 hours, the outflow of the existing tunnel to the WWTP is larger than the capacity of the WWTP.

Table 1

FALL RIVER TUNNEL SYSTEM - FLOW COLLECTION HYDRAULIC DATA

FLOW COLLECTION LOCATION	SWMM CONDUIT # UPSTREAM OF FLOW COLLECTION LOCATION	DESIGN RATE (CFS)	SURCHARGE ELEVATION BASED ON INVERT OF INFLOW PIPE AT DROP SHAFT
Plymouth North (Ply-n OF and QVI)	552C & 662C	185.00	114.58
Pleasant (PSI)	525	50.00	121.08
Quequechan (Que. OF)	805	95.00	125.00
Lowell (OF)	37	150.00	123.25
Rodman (RHI)	540	65.00	124.43
Third (Area H)	535	50.00	115.28
Pocassett (small BSF component)	not used	50.00	66.72
N. Main	810C	140.00	78.10
Central	32	160.00	99.00
Elm	793C	50.00	94.46
President	774C	90.00	77.69
Jones	783C	85.00	84.84
Langley	781C	55.00	78.20
Stewart	779C	55.00	57.46
Herman	785C	40.00	60.34
North Park	787C	30.00	137.00
Columbia	800C	140.00	81.00
Middle	772C	120.00	130.40
Globe	770C	220.00	96.00
Birch	768C	210.00	92.78
Woodman	766C	50.00	89.70
Mt. Hope	764C	120.00	79.75
Wilson Road Pump Station	not applicable	10.00	160*
TOTAL		**2220.00**	
* Estimated at 30 feet below ground elevation.			

III. GENERAL HYDRAULIC TRANSIENT CHARACTERISTICS (ORIGINAL DESIGN DATA — CASE 1 TO CASE 5)

The first step is to determine the weir elevation at the Arnold extreme event overflow structure to assure that no overflow occurs at the other dropshafts. Apparently, the worst case for the tunnel system is that no outflow to WWTP is allowed under the design storm event. Under these conditions, if the weir elevation is set at the ground elevation (94.58 MHW), a large amount of overflow was found at a number of dropshafts. After a number of testing runs, the weir elevation at 66 MHW (53 ft above the invert 13 MHW) is found to be reasonable. Therefore all the results presented in this report is based on this weir elevation at the Arnold extreme event overflow structure.

3.1 Design Storm with Closed End (Case 1)

Figs. 3.1(a) and 3.1(b) show the time variation of water elevations at the eight dropshaft locations during the design storm event with closed end at the WWTP. In this case, due to the steep increase of the hydrograph as indicated in Fig. 2.6, the tunnel system is pressurized after about 6.5 hours, and the flow becomes a closed conduit flow. The pressurization starts from the downstream end about 6.5 hours after the beginning of the storm. As the tunnel continues to be filled and the pressurized portion expands, surge develops at the interface between the pressurized zone and the free surface zone. The magnitude of the surge increases as the inflow rate increases. When the surge migrates to the upstream ends, it produces a sudden water level rise. A more detailed short period near the sharp peak is displayed in Figs. 3.1(c) and 3.1(d). When the surge arrives at the Wilson Road Pump Station, the water surface elevation rises from 30 ft. to 98 ft. MHW in about 8 minutes. This is a severe surge, but it doesn't result in backflow (spilling over the intake) at the inlet since the peak is still lower than the ground surface elevation (189.08 MHW).

Fig. 3.1(e) gives the instantaneous hydraulic gradelines along the main tunnel (excluding the Quequechan branch) during this storm. The station number in this figure is referred to in Fig. 2.3. The dashed lines represent the dropshaft locations and outlet elevations. As shown in this figure, the water level increases rapidly during 6 to 7 hours of this storm due to the rapidly increased inflow. Fig. 3.1(f) shows the maximum water surface elevation in the main tunnel stations. Note that the maximum elevation at different locations may occur at different times. As shown in the figure, the maximum value at the Herman and Stewart dropshafts is higher than the top of the shaft elevation. It will be found that the duration of the higher water surface elevation at the two dropshafts is very short.

The inflow and overflow of the tunnel system is shown in Fig. 3.1(g). The difference between the total inflow and overflow is water volume stored in the tunnel at that moment. The detailed variation of the overflow at the beginning of the overflow is shown in Fig. 3.1(h). The modeling results indicate that overflow at the Arnold extreme event overflow structure starts at t=6.67 hours, and rapidly increases to the total inflow rate. This means that after the overflow starts, no available storage is left in the tunnel system; consequently, all the inflow becomes overflow.

The results also show that there is a small amount of overflow at the Herman St. dropshaft during a very short period due to the transient surge. The maximum overflow at the Herman St. dropshaft is 216 cfs occurring at t=6.75 hours. A very small amount of overflow also takes place at the Stewart dropshaft since it has the lowest dropshaft height. Several runs have been tested to avoid the overflow at the dropshafts by lowering the weir elevation at the Arnold extreme event overflow structure. But the results indicate that lowering weir elevation does not help the overflow problem since the Arnold extreme event overflow structure is too far away from the two dropshafts. There are a number of possible solutions to this problem, such as increasing the outlet elevation at the two dropshafts, enlarging the dropshaft diameters to reduce the surge strength, modifying the tunnel diameter and the tunnel connection, or implementing inflow control, etc..

3.2 Design Storm with Closed End and Modified Dropshaft Height (Case 2)

As stated in the above case, the overflow at Herman and Stewart can not be avoided by lowering the weir elevation at the Arnold extreme event dropshaft. This case uses the same conditions as Case 1 except that the outlet elevations at the Herman and Stewart dropshafts are set high enough to contain an upsurge, so that the potential surge height can be determined.

Figs. 3.2(a) to 3.2(h) show the modeling results with the dropshaft modification stated above. By comparing the results of Case 1 and Case 2, it can be found that the maximum water surface elevation above the tunnel invert at Herman (invert 26.15 MHW) and Stewart (invert 23.57 MHW) increases from 62.3 (88.45 MHW) to 80.3 ft. (106.45 MHW) and 65.3 (88.87 MHW) to 68.0 ft. (91.57 MHW), respectively. These are 20.0 and 10.5 ft. higher than the design elevation, respectively. Therefore, if the elevation at Herman and Stewart can be increased to 80.3 and 68.0 ft. based on the tunnel invert at the dropshafts, overflow occurs only at the Arnold extreme event overflow structure. As mentioned before, there are other alternatives to achieve the same goal. Besides the the higher maximum surface elevation at the upstream area, the other hydraulic transient characteristics of the two cases are very similar.

3.3 3–month Storm with Closed End (Case 3)

Figs. 3.3(a) to 3.3(h) show the modeling results during the 3–month storm event with closed end at the WWTP. In this case, due to the smaller amount of the inflow hydrograph, the tunnel system is fully pressurized at about t=9.02 hours when the total inflow reaches the second peak, as shown in Fig. 3.3(g).

Figs. 3.3(a) to 3.3(d) show that the water surface elevations in the entire tunnel system experience strong oscillations which are caused by both transient surge and fluctuating inflow hydrographs (two peak pattern). The amplitude of the surge is the greatest at the Wilson Road Pump Station. The two peaks occur during the transient period, which worsens the unsteadiness. However, Fig. 3.3(f) shows that the maximum water surface elevations are lower than the design dropshaft outlet elevation except at the Arnold extreme event overflow structure. This means that there is no overflow at the dropshafts during the 3–month storm event.

As shown in Fig. 3.3(g), the first peak of the overflow at Arnold St. is as large as 1,100 cfs at t=8.0 hours, but lasts a very short time. After that, the water elevation at Arnold St. fluctuates strongly below the weir elevation, and at t=9.02 hours the water surface elevation rises to higher than the weir elevation, and generates the second overflow peak.

3.4 3–month Storm under Controlled Outflow to the WWTP (Case 4)

Figs. 3.4(a) to 3.4(g) shows the modeling results during the 3–month storm event under controlled outflow to the WWTP. In this case, since the remaining capacity of the WWTP after treating the water volume from the existing interceptor plus the new tunnel storage is larger than the total water volume of the 3–month storm, the tunnel system is not fully pressurized during this storm period. As shown in Fig. 3.4(f), the maximum water surface elevation at the section between Wilson Rd. Pump Station to Herman is lower than the pipe diameter of 5 feet.

For the same reason as above, plus the outflow control, the water surface elevations at the downstream area fluctuate strongly, as shown in Figs. 3.4(a) to 3.4(d). The oscillations must be considered in the final gate design at the downstream end.

Fig. 3.4(g) shows the total inflow hydrograph and the flow to the WWTP. The existing interceptor hydrograph to the WWTP is given by CH2M Hill engineers. The dashed line represents the capacity of the WWTP. So the difference between the dashed line and cross–symbol solid line is the flow rate allowed to enter the WWTP from the new tunnel. As the figure shows, the outflow from the new tunnel starts to decrease at t=6.4 hours, and and increase after t=9.5 hours, in response to the changing inflow from the existing interceptor. After t=13.3 hours, the remaining capacity of the WWTP is larger than the total inflow to the new tunnel system. Hence the WWTP begins to treat the water stored in the new tunnel system.

3.5 Design Storm under Controlled Outflow to the WWTP (Case 5)

Figs. 3.5(a) to 3.5(h) shows the modeling results during the design storm event under controlled outflow to the WWTP. In this case, since the remaining capacity of the WWTP, after treating the water volume from the existing interceptor, is relatively small as compared with the inflow to the new tunnel, the outflow allowed to the WWTP has little effect on hydraulic transient characteristics. Therefore, the results in this case are very similar to those in Case 1. Since the outflow to the WWTP is not controlled until t=5.5 hours, overflow at Arnold St. starts at 9.5 hours, which is 22 minutes later than that in Case 1. After t=12.2 hours the WWTP again has some capacity to treat the water from the new tunnel.

IV. GENERAL HYDRAULIC TRANSIENT CHARACTERISTICS (UPDATED DESIGN DATA — CASE 6 AND CASE 7)

As mentioned before, the above modeling results in Case 1 to Case 5 are based on the original design data received before the draft report was finished. Later, some of the design data are modified by the CH2M HIll/PBG&S team. The changes include:

1. The weir length increased to 94 feet from 64 feet.
2. The tunnel diameters in the upstream reaches that were 5–foot increased to 8–foot diameter.
3. Tunnel connection changed from invert–to–invert to crown –to–crown.
4. The Arnold Street weir elevation was set 30–feet above the tunnel invert 14.78 MHW (updated from 13 MHW).
5. The Manning coefficient for the transient analyses changed from 0.013 to 0.015.
6. The diameters of the following dropshafts were updated as

Dropshaft Name	Updated(ft)	Original(ft)
Wilson	10	15
Quequechan	10	15
Arnold	30	30
North Park	20	30
Lowell	20	30

The modeling results described in this chapter referred to as Case 6 and Case 7 are based on the updated design data.

4.1 Design Storm with Closed End and Updated Design Data (Case 6)

Figs. 4.1(a) to 4.1(h) show the modeling results without flow to the WWTP during the design storm event based on the updated design data. Compared with the results in Case 1 and Case 2 with the same hydrograph, the hydraulic surge in this case is dramatically reduced. As shown in Fig. 4.1(f), the maximum water surface elevations are no longer over the dropshaft outlets. This means that there is no overflow at any dropshaft under the updated design. It is believed that the significant improvement is mainly due to the change in tunnel connection from invert–to–invert to crown–to–crown. Since the invert elevation in the upstream reaches is increased, and the weir elevation at Arnold St. is decreased, the small diameter upstream reaches are pressurized for only a very short time interval, as shown in Fig. 4.1(e).

4.2 3–Month Storm with Updated Design Data under Controlled Outflow to the WWTP (Case 7)

Figs. 4.2(a) to 4.2(e) show the modeling results during the 3–month storm event under controlled outflow to the WWTP based on the updated design data. Compared with the results in Case 4 with the same hydrograph, it is clear that the hydraulic transient behavior is also improved. As shown in Fig. 4.2(b), only small amplitude oscillations occurred at the Globe dropshaft and at the Arnold St. extreme overflow structure. The hydraulic surge does not reach the North Park dropshaft, as shown in Fig. 4.2(d). The peak maximum water surface elevations between two dropshafts are apparently due to a water hammer phenomena.

V. CONCLUSIONS AND RECOMMENDATIONS

Following is a list of important conclusions based on the modeling results and analyses.

5.1 Under the Original Design Data

1. Based on the design storm event without water allowed to the WWTP, the reasonable weir height of the Arnold extreme event overflow is 53 feet above the pipe invert (or 66 MHW based on the tunnel invert 13 MHW) with a given weir length of 64 feet. The weir height is strongly affected by the dropshaft height at Pocasset. In other words, if the dropshaft height at Pocasset could be increased, the weir elevation can also be higher.

2. Strong surge is identified in cases where design storm events occur under modeling conditions. The main reason for this is the large rate of increase of the inflow hydrographs. The two–peak pattern distribution of the inflow hydrographs is also a cause of the water surface oscillations.

3. Under the above weir condition, there are still small amounts of overflow from the Herman and Stewart dropshafts lasting less than 2 minutes due to the pressurization surge. The overflow cannot be avoided by further lowering the weir elevation of the Arnold extreme event overflow structure since it is too far away from the two dropshafts. There are five possible methods to eliminate the overflow. They are: 1) changing the tunnel connection from invert–to–invert to crown–to–crown; 2) increasing the outlet elevation of the two dropshafts; 3) enlarging the diameter of the two dropshafts; 4) increasing the pipe diameter of the section; 5) controlling the inflow.

4. If the outlet elevation of the two dropshafts is increased to avoid the overflow problem, the dropshaft height above the tunnel pipe invert must be higher than 80.3 feet (106.48 MHW) at Herman and 68.0 feet (91.47 MHW) at Stewart.

5. In the case of a 3–month storm and no flow into the WWTP, no overflow occurs at all the dropshafts except at the Arnold extreme event overflow structure. But strong oscillations are identified during the surge period due to unsteady inflow and surge movement.

6. The preferential treatment policy of the tunnel system works well for the 3–month storm. All the inflow can be treated by the WWTP except a small amount of overflow from the Arnold extreme event overflow structure, which lasts less than 2 minutes. But due to the inflow control, the water surface oscillations become even worse at the downstream area. The oscillations must be considered when the control gate is designed.

7. For the design storm, the treatment capacity of the WWTP is so insignificant that the transient characteristics in the new tunnel under the design storm condition are about the same with or without the treatment.

5.2 Under the Updated Design Data

8. The updated design of the tunnel system has satisfactorily improved hydraulic transient conditions. In the case of the design storm without flow to WWTP, the maximum water surface elevations are all lower than the dropshaft outlets. This means that the outflow occurs only at the Arnold St. extreme overflow structure.

9. The updated design also reduces the water pressure oscillation in the downstream reach in the case of the 3–month storm under controlled outflow to the WWTP.

Some comments and recommendations are listed below:

1. The outflow to the WWTP from the new tunnel system is controlled based on the remaining capacity of the WWTP. How to control the outflow is closely related to the detailed design of the connection structure of the new tunnel to the WWTP and the WWTP pump operation. Therefore, when the detailed design of the connection and the operating procedures are modified, they may have effects on the modeling results.

2. If the existing interceptor hydrograph used for the present analysis is not the actual recorded data, it is suggested that the two–tunnel systems be simultaneously modeled. The results will be more accurate.

3. As mentioned before, the design storm inflow hydrographs are patterned after the 3–month storm event. The assumption of pattern similarity may have some effects on the modeling results in the design storm cases. If the actual patterns of the design storm are less concentrated, the surge condition will be improved.

REFERENCES

1. Charles C.S. Song, "Task 2 – Preliminary Analysis" a letter to Dr. Allen L. Davis, Oct. 24, 1994.

2. Facsimile Transmittal from Rita Fordiani of CH2M Hill Boston Office to Dr. Jianming He," Nov. 11, 1994.

3. Facsimile Transmittal from Dr. Allen L. Davis of CH2M Hill to Dr. Charles C. S. Song, "Memorandum — Revised Data for MXTRANS Model Update," Dec. 15, 1994.

4. Cardle, J. A. and Song, C.C.S., "Mathematical Modeling of Unsteady Flow in Storm Sewers." *International Journal of Engineering Fluid Mechanics*, Vol. 1, No. 4, 1988.

5. Guo, Q. and Song, C.C.S., "Surging in Urban Storm Drainage Systems," ASCE, *Journal of Hydraulic Engineering*, Vol. 116, No. 12, June, 1989.

6. Song, C.C.S., Guo, Q., and Zheng, Y., "Hydraulic Transient Modeling of TARP Systems," St. Anthony Falls Hydraulic Laboratory, Project Report No. 270, March 1988.

7. Song, C.C.S., Lin, W., and Gong, C., "Hydraulic Transient Modeling of TARP Systems," St. Anthony Falls Hydraulic Laboratory, University of Minnesota, Project Report No. 332, March 1992.

8. He, J., Song, C.C.S., Liu, Y., and Gong, C., "Hydraulic Transient Study of Mainstream Tunnel System and Control Operation," St. Anthony Falls Hydraulic Laboratory, University of Minnesota, Project Report No. 361, Oct. 1994.

9. Guo, Q., and Song, C.C.S., "Hydraulic Transient Analysis of TARP Phase II O'Hare System," St. Anthony Falls Hydraulic Laboratory, University of Minnesota, Project Report No. 276, July 1988.

10. Song, C.C.S., He, J., Liu, Y., and Gong, C., "Hydraulic Transient Study of Mainstream & Des Plaines TARP Phase II Systems," St. Anthony Falls Hydraulic Laboratory, University of Minnesota, Project Report No. 353, July 1994.

11. Song, C.C.S., and Lin, W., "Study of Potential Hydraulic Transient for Milwaukee Inline Storage System," St. Anthony Falls Hydraulic Laboratory, University of Minnesota, Project Report No. 297, July 1990.

12. Lin, W., and Song, C.C.S., "Hydraulic Transient Analysis of Tunnels and Dropshaft for Milwaukee Inline Storage System," St. Anthony Falls Hydraulic Laboratory, University of Minnesota, Project Report No. 340, July 1993.

13. Song, C.C.S., Cardle, J.A., and Gavali, S., "Mathematical Modeling of the Genesee River Storage–Conveyance System, Rochester, N.Y., St. Anthony Falls Hydraulic Laboratory, University of Minnesota, Project Report No. 215, July 1982.

14. He, J., Song, C.C.S., Liu, Y., and Gong, C., "Hydraulic Transient Study of Passaic River Flood Protection Tunnel," St. Anthony Falls Hydraulic Laboratory, University of Minnesota, Project Report No. 354, Sept. 1994.

APPENDIX I

Figures 2.1 through 4.2

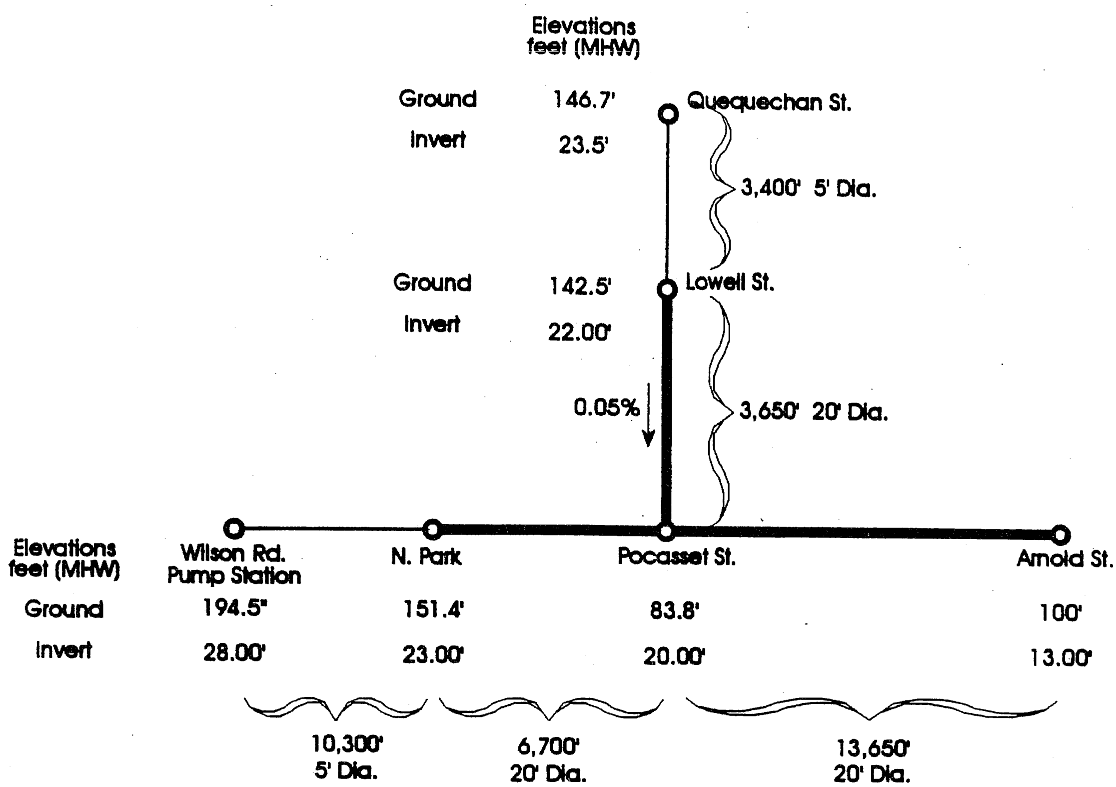

Notes:

Assume Slope = 0.05%

Total Length Swift to Wilson = 30,650'

Total Length Pocasset to Quequechan = 7,050'

2.72 feet NGVD = 0 feet Mean High Water (MHW) = Fall River Datum

Fig. 2.1 General layout of the Fall River Tunnel System

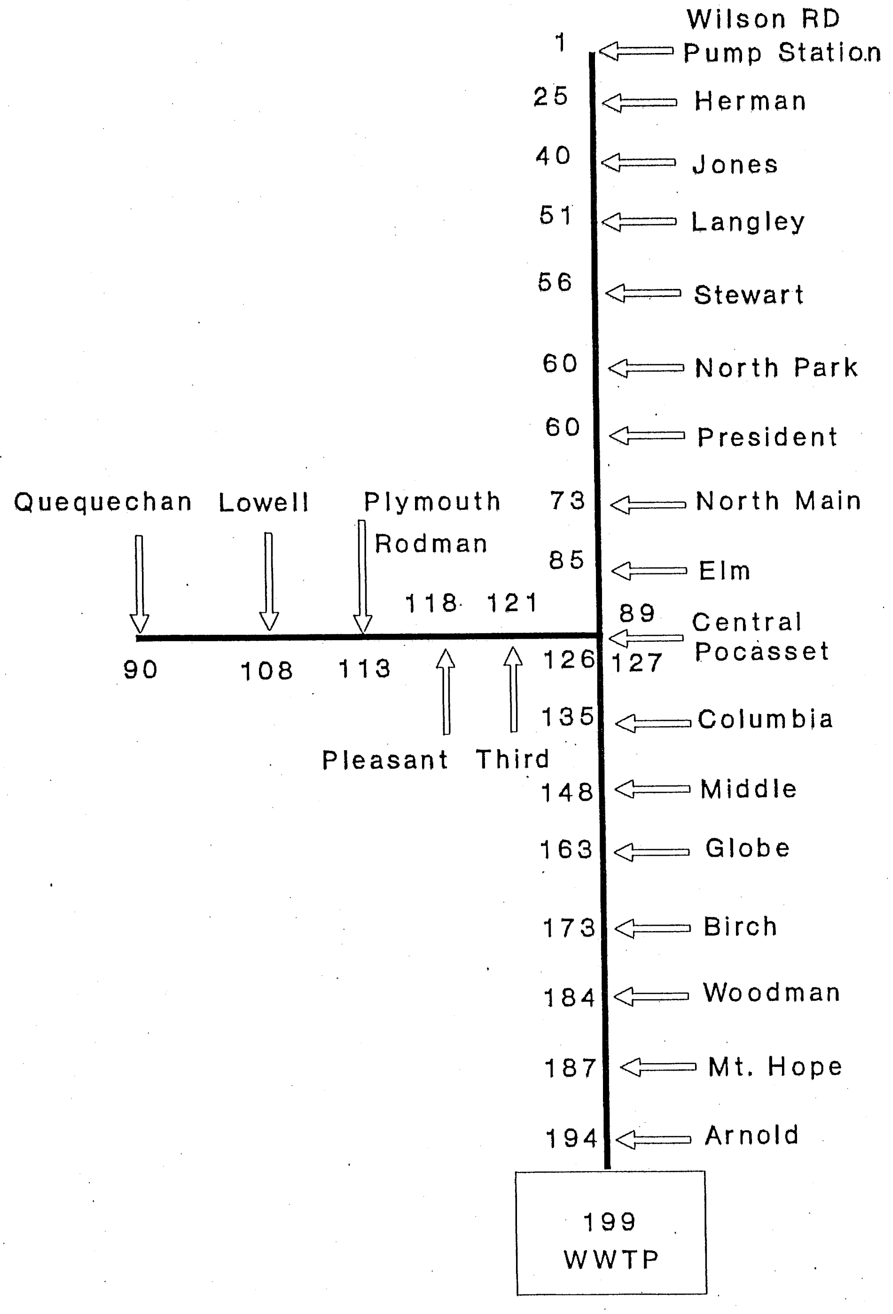

Fig. 2.2 Modeling configuration of the Fall River Tunnel System and the computation stations

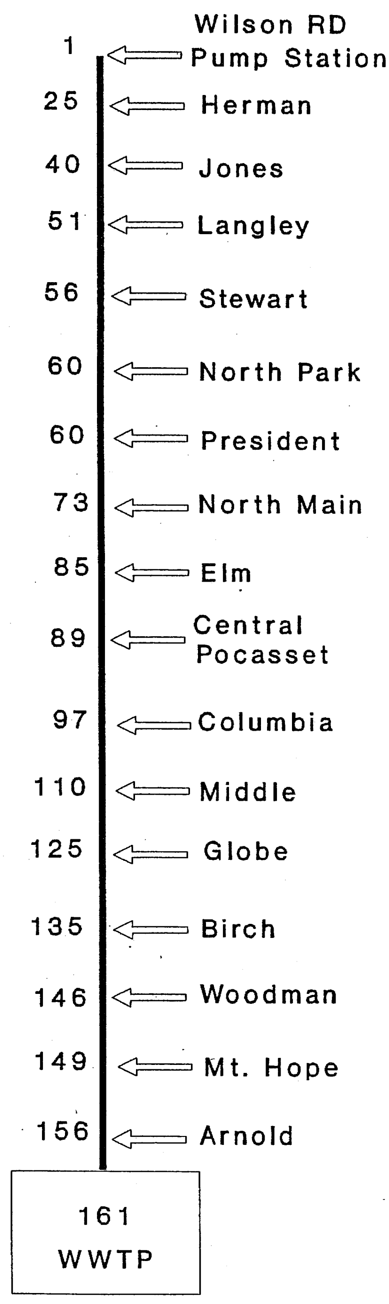

Fig. 2.3 Schematic of the main tunnel, excluding the Quequechan Branch, and the station numbers for showing the hydraulic gradeline along the main tunnel

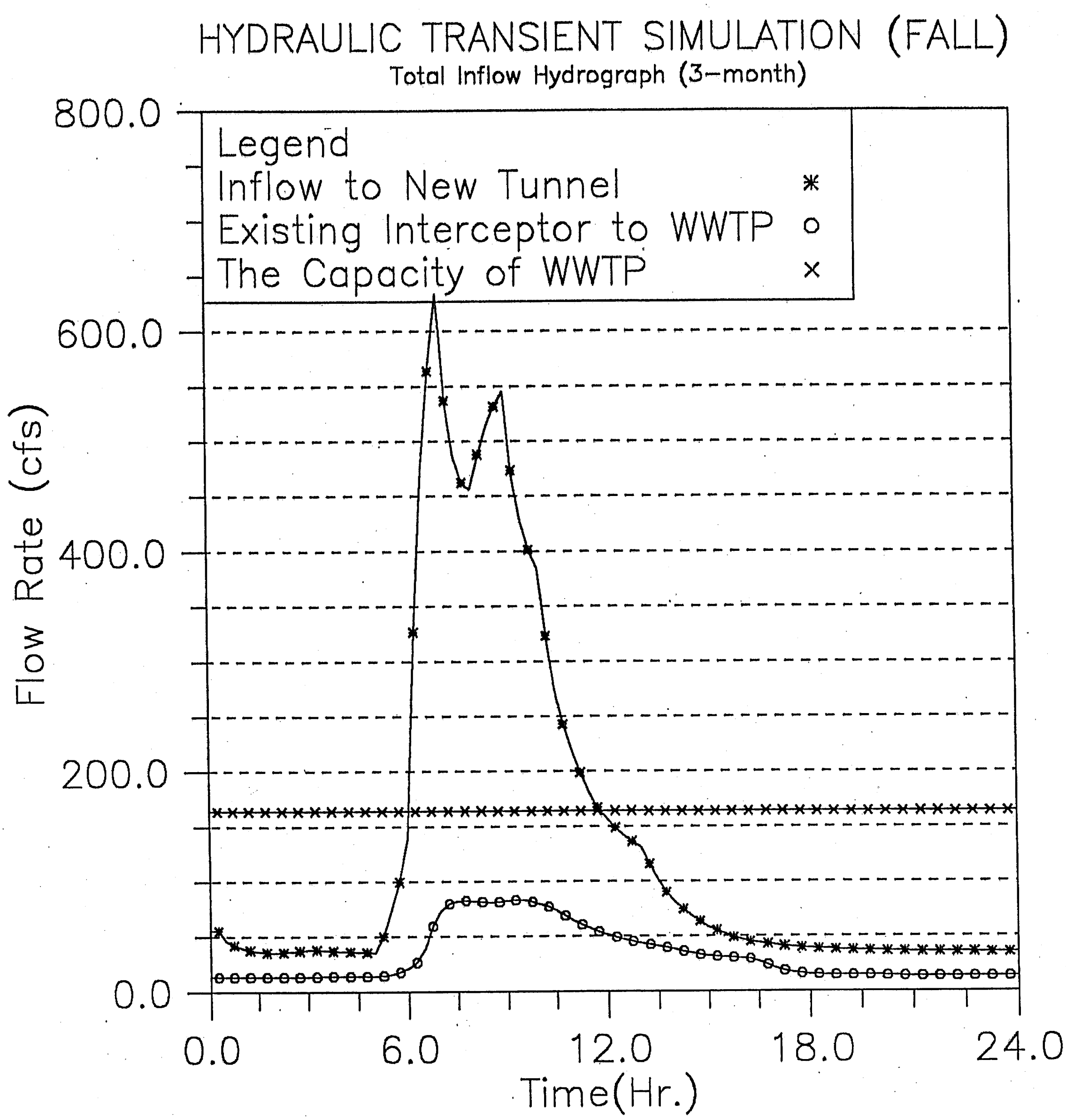

Fig. 2.4 3–month storm total inflow hydrograph, existing interceptor 3–month hydrograph, and the WWTP capacity

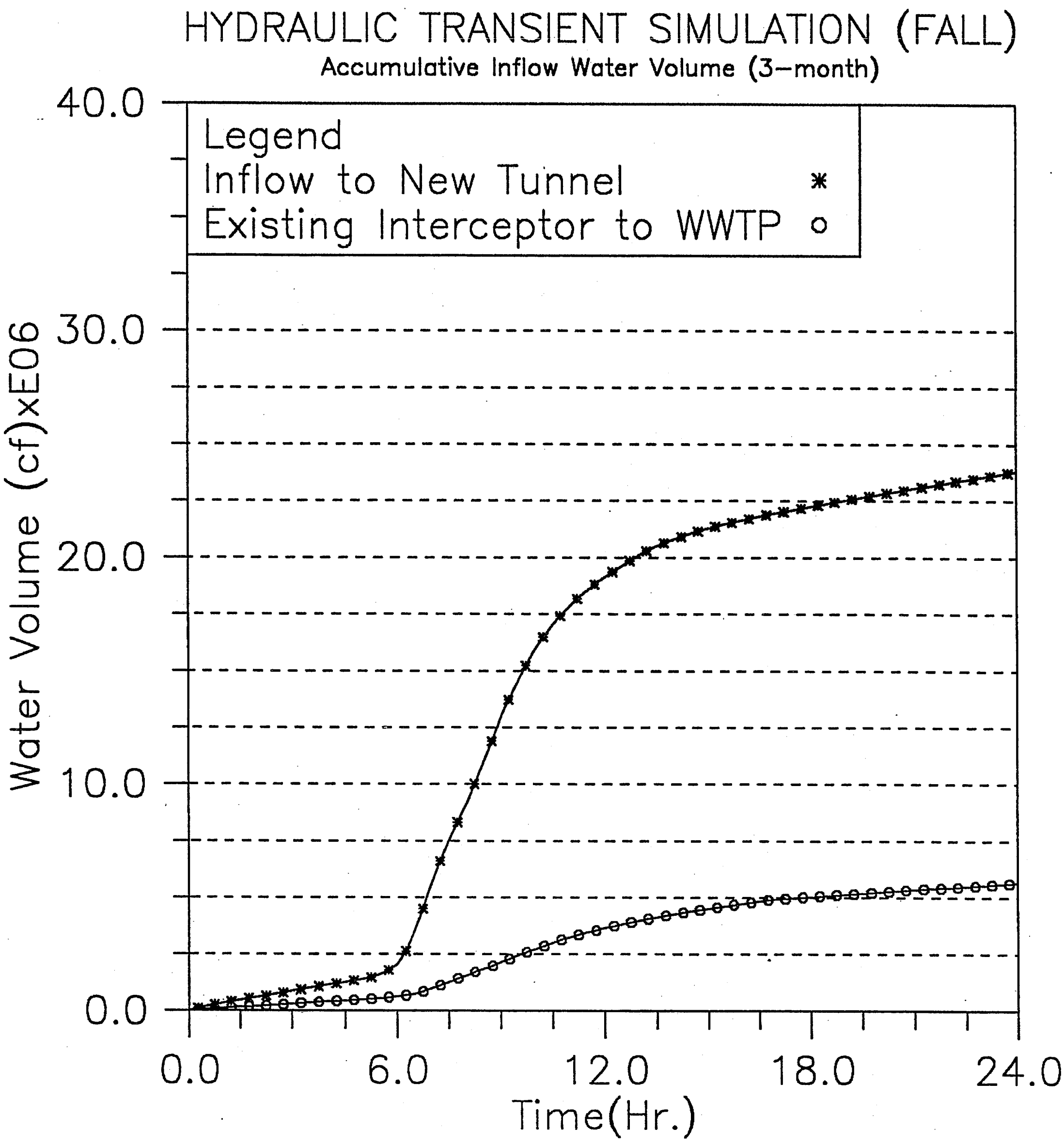

Fig. 2.5 The total accumulative water volume of the 3-month inflow hydrograph and existing interceptor hydrograph.

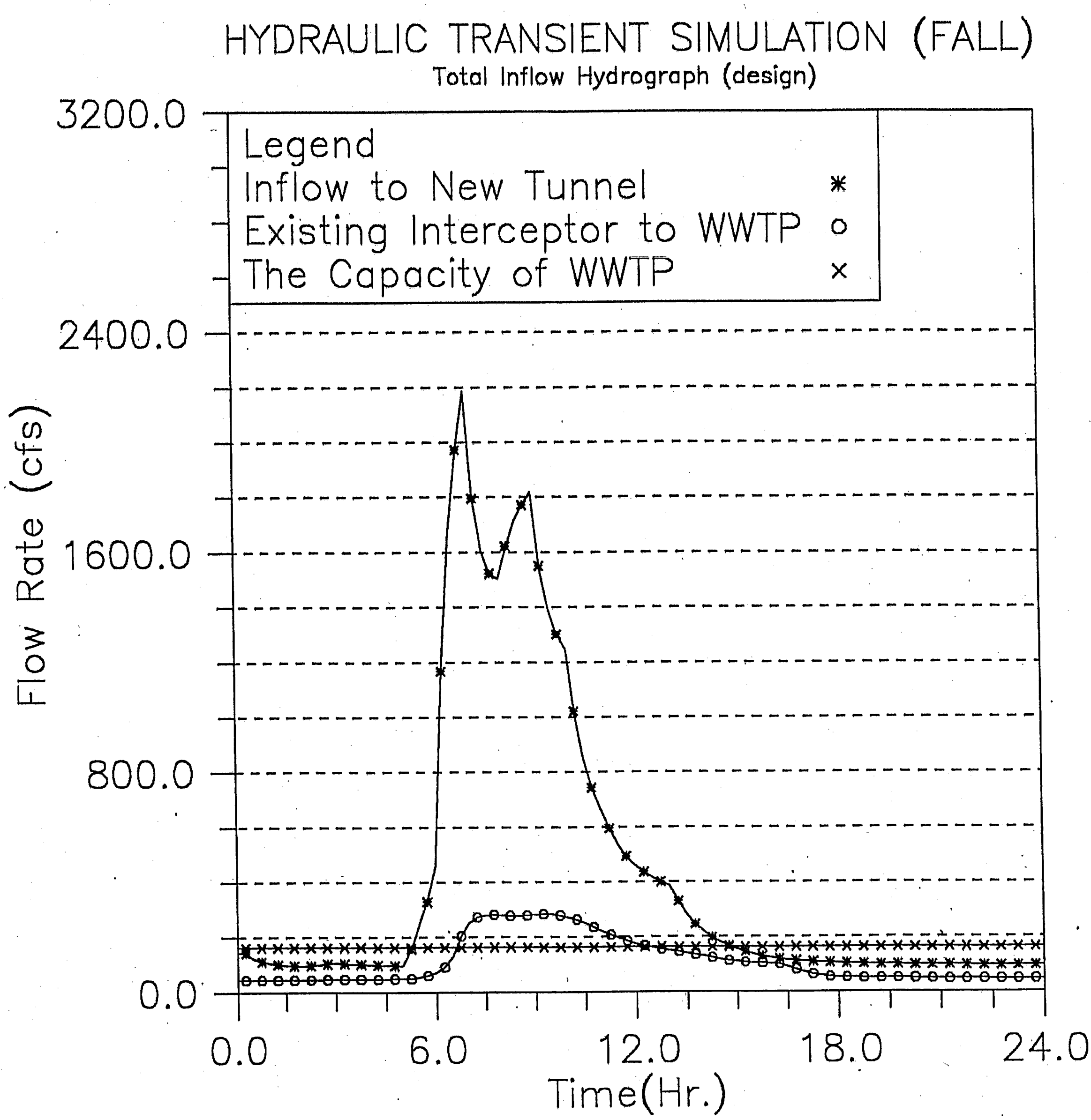

Fig. 2.6 The design storm total inflow hydrograph, existing interceptor design hydrograph, and the WWTP capacity

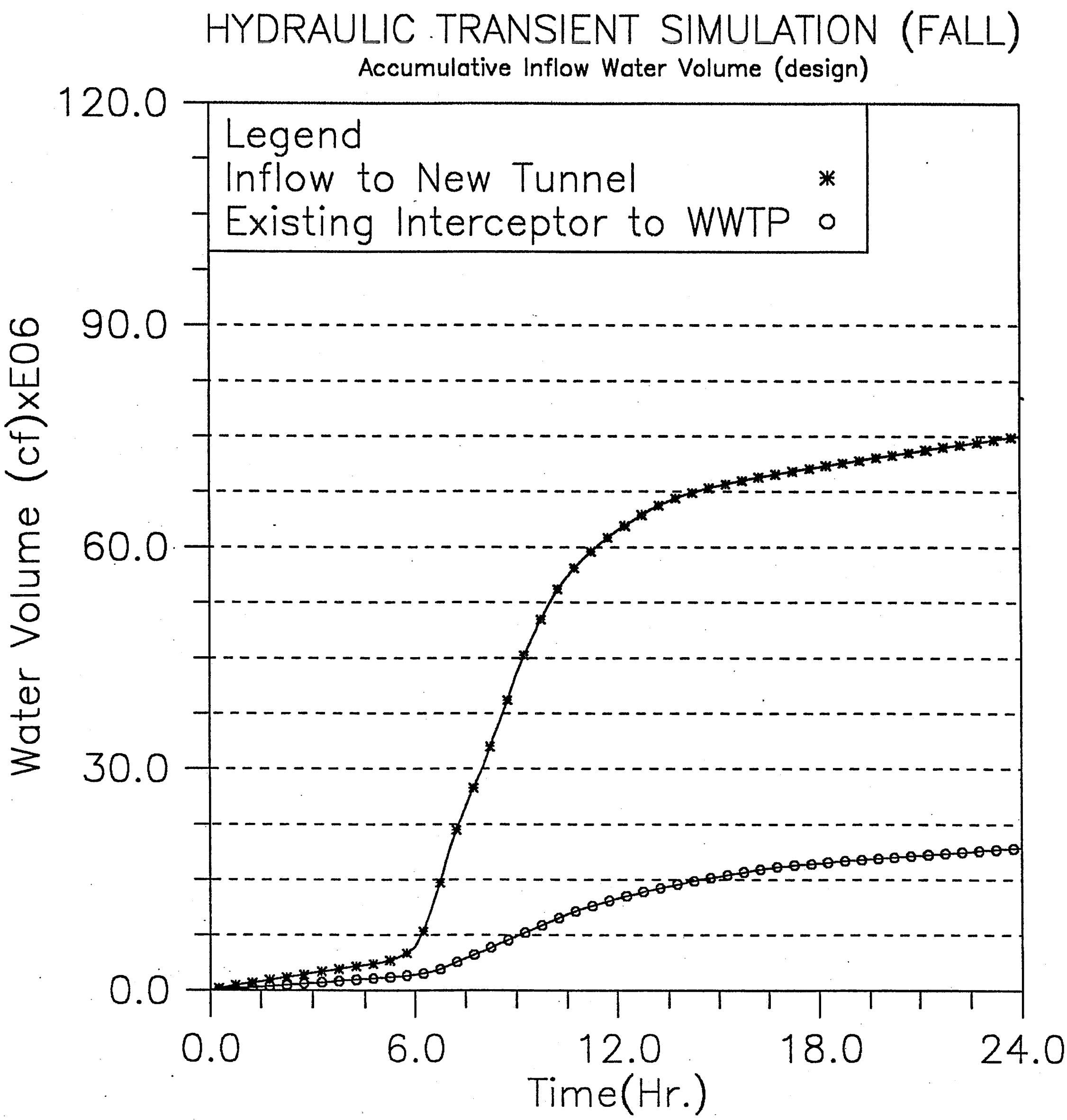

Fig. 2.7 The total accumulative water volume of the design inflow hydrograph and existing interceptor design hydrograph.

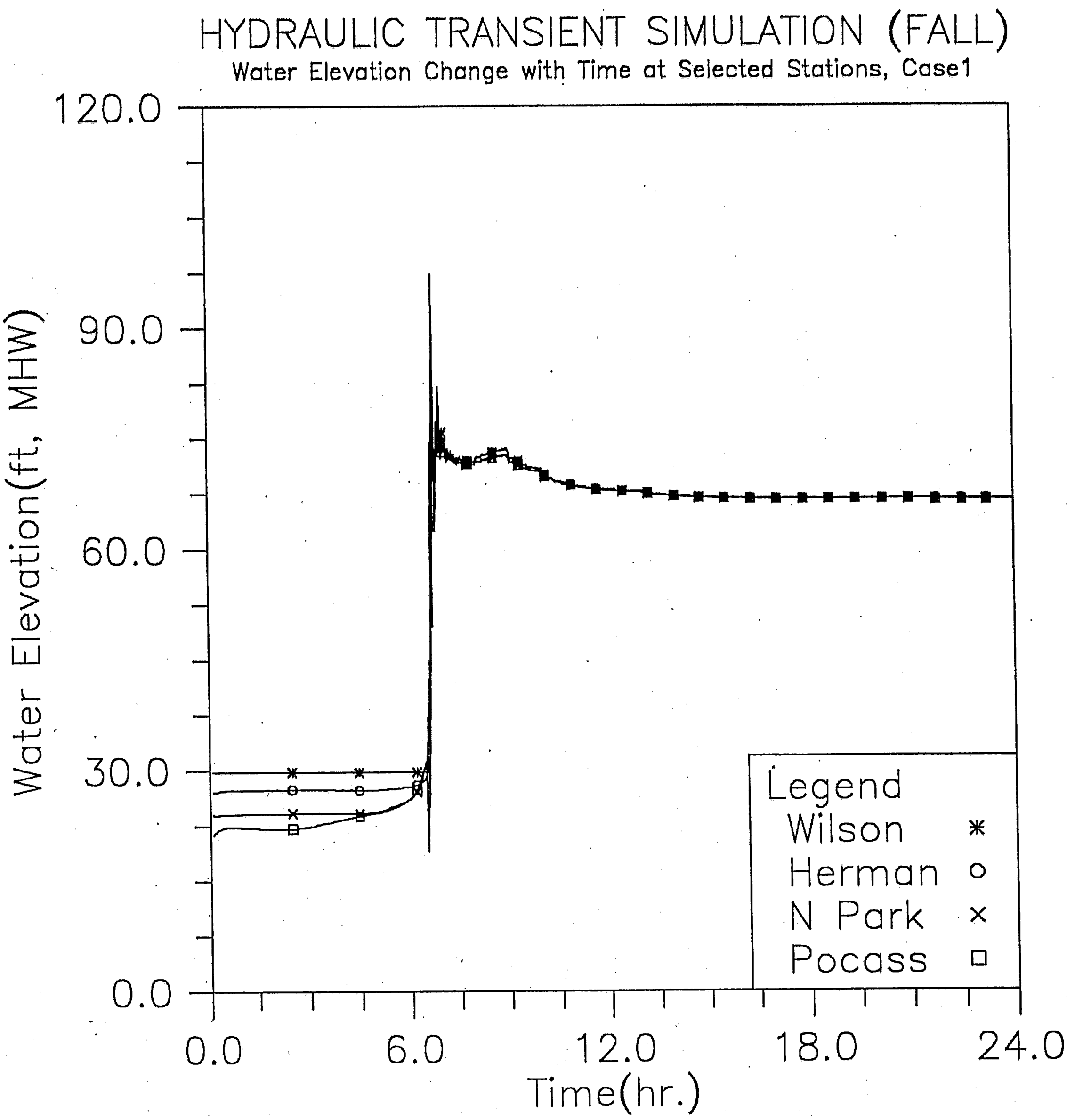

Fig. 3.1(a) Time variation of water surface elevations at four upstream dropshafts; modeling case: design storm without flow to the WWTP (Case 1).

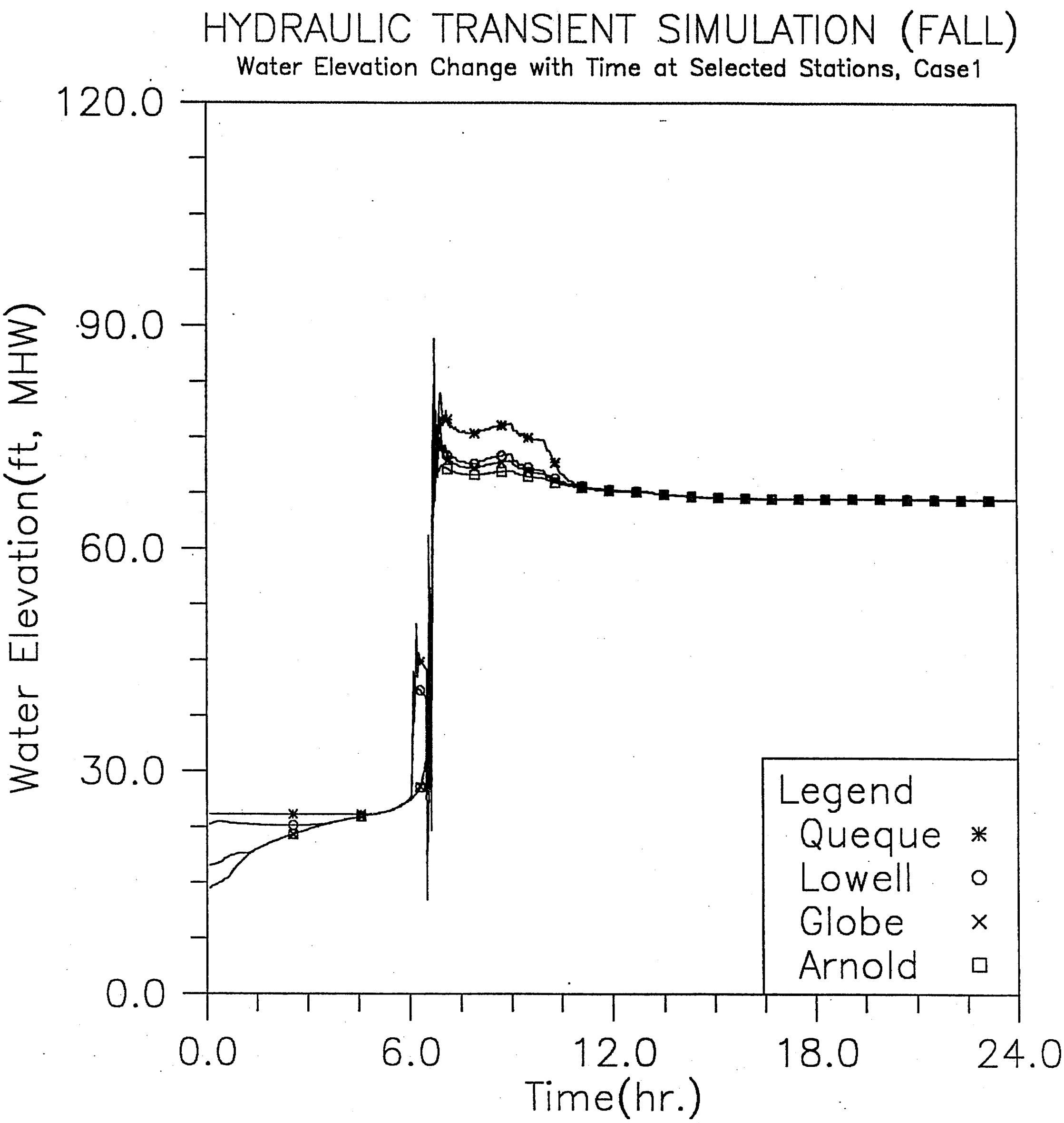

Fig. 3.1(b) Time variation of water surface elevations at Quequechan and three downstream dropshafts; modeling case: design storm without flow to the WWTP (Case 1).

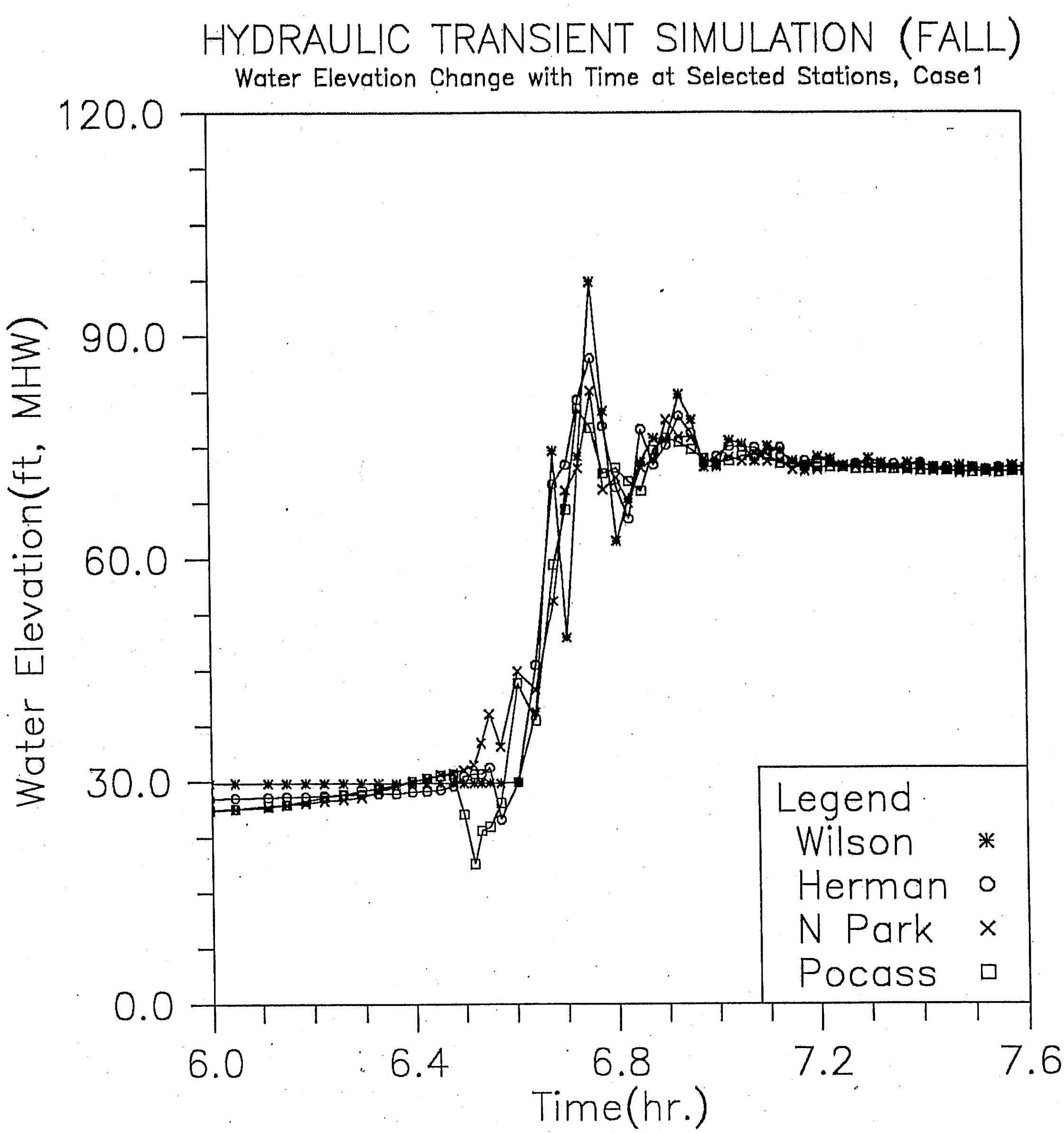

Fig. 3.1(c) Detailed time variation of water surface elevations at four upstream dropshafts during the surge period; modeling case: design storm without flow to the WWTP (Case 1).

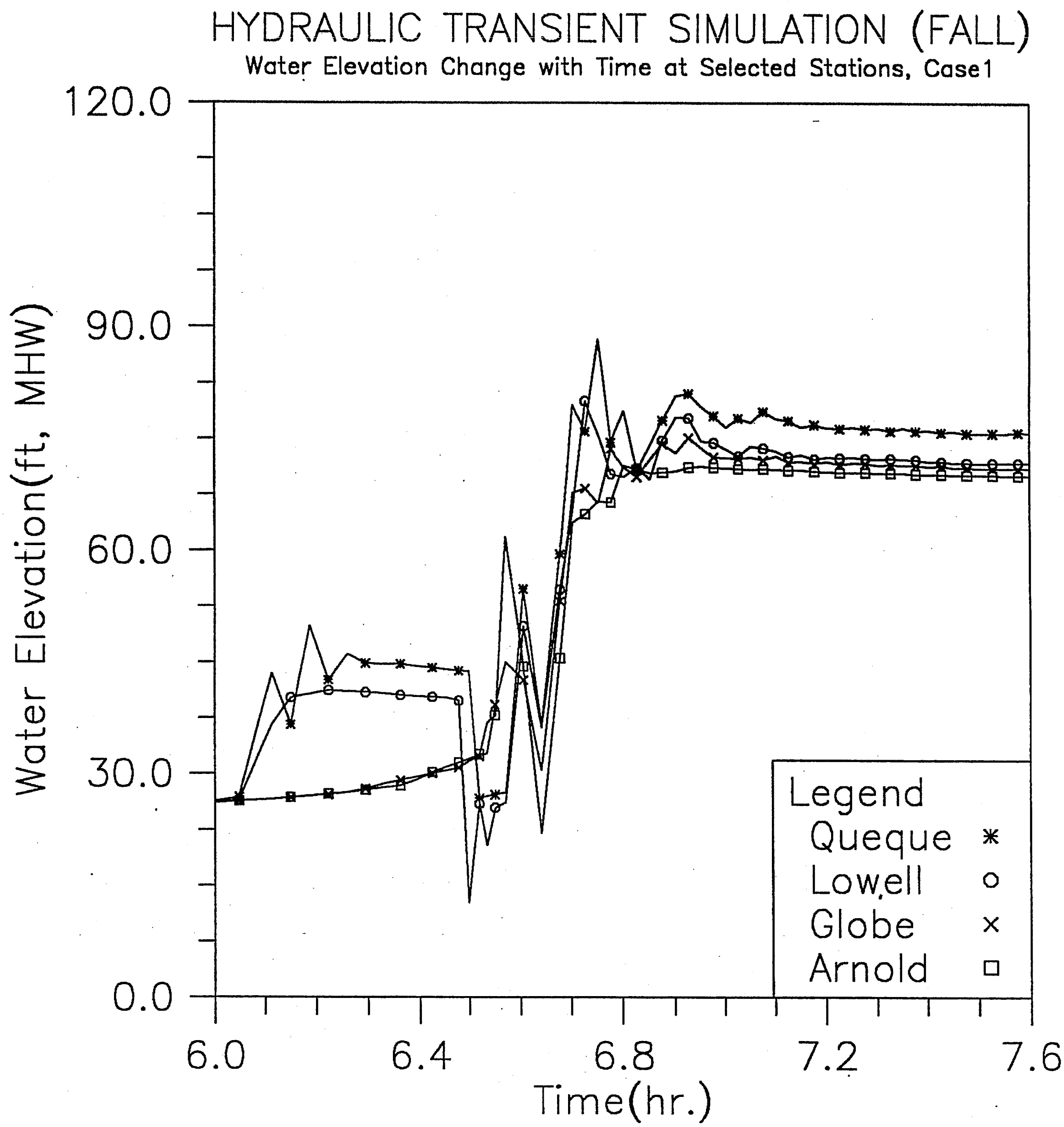

Fig. 3.1(d) Detailed time variation of water surface elevations at Quequechan and three downstream dropshafts during the surge period; modeling case: design storm without flow to the WWTP (Case 1).

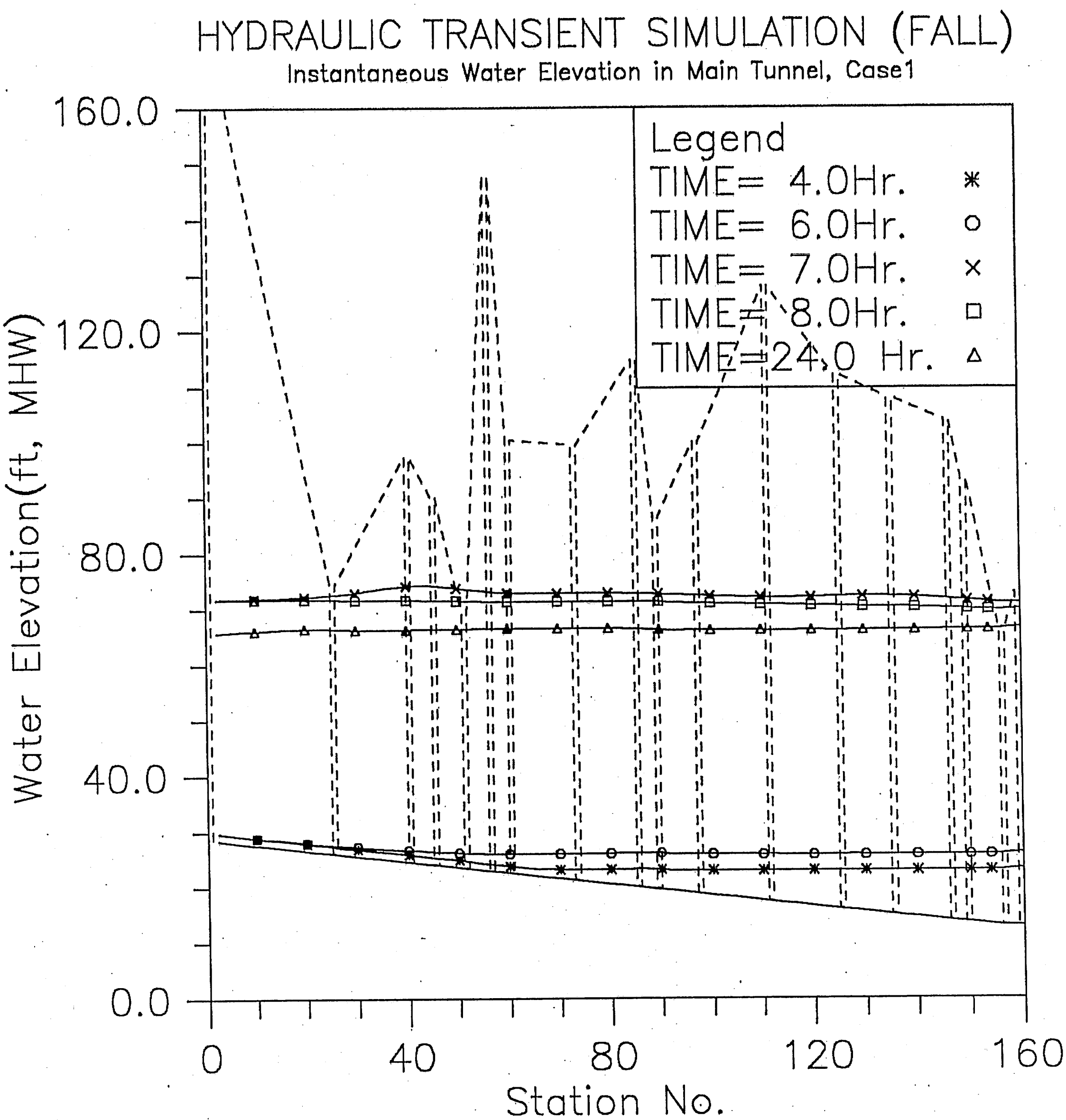

Fig. 3.1(e) Instantaneous hydraulic gradelines along the main tunnel; modeling case: design storm without flow to the WWTP (Case 1).

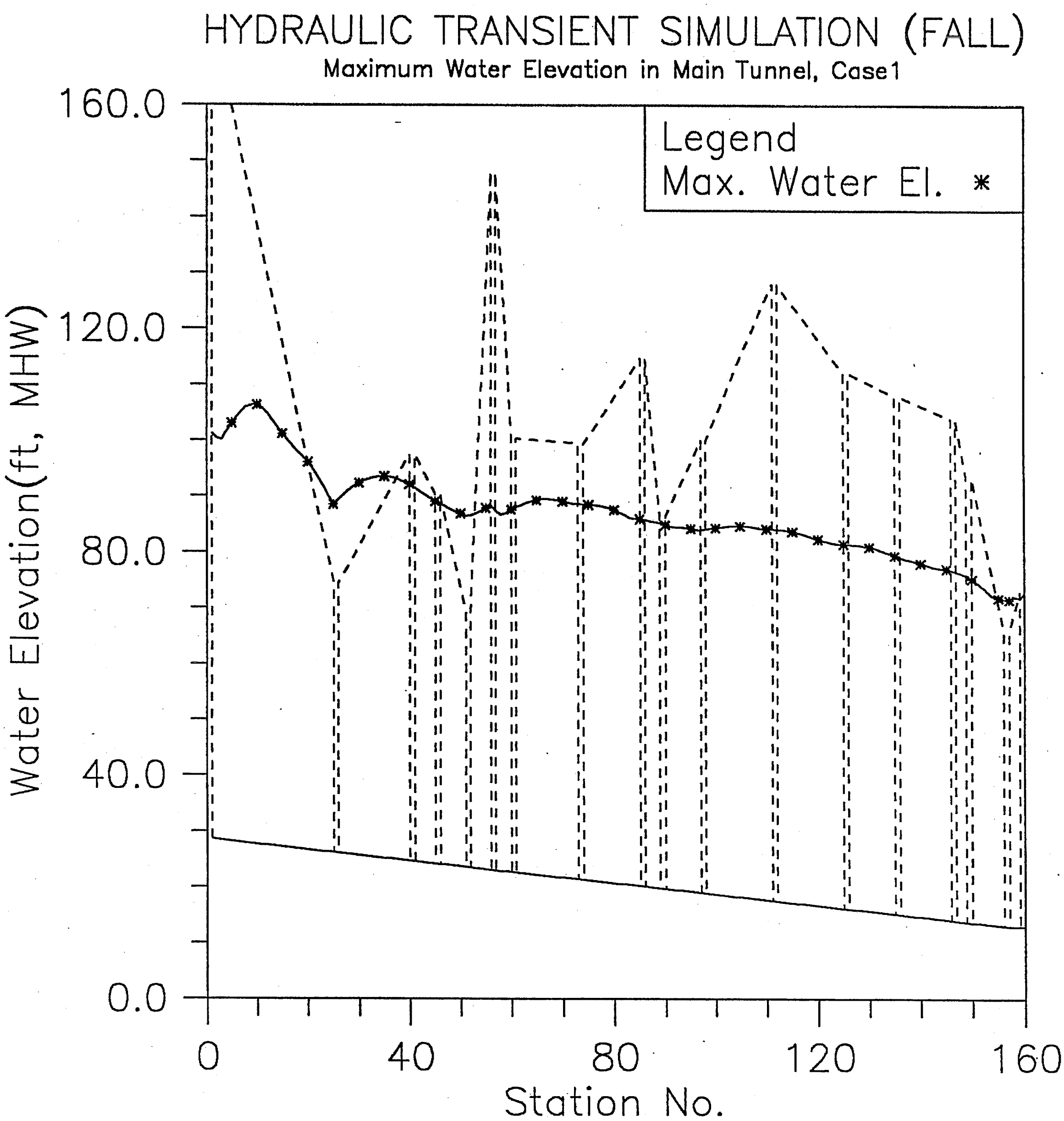

Fig. 3.1(f) The maximum water surface elevations along the main tunnel; modeling case: design storm without flow to the WWTP (Case 1).

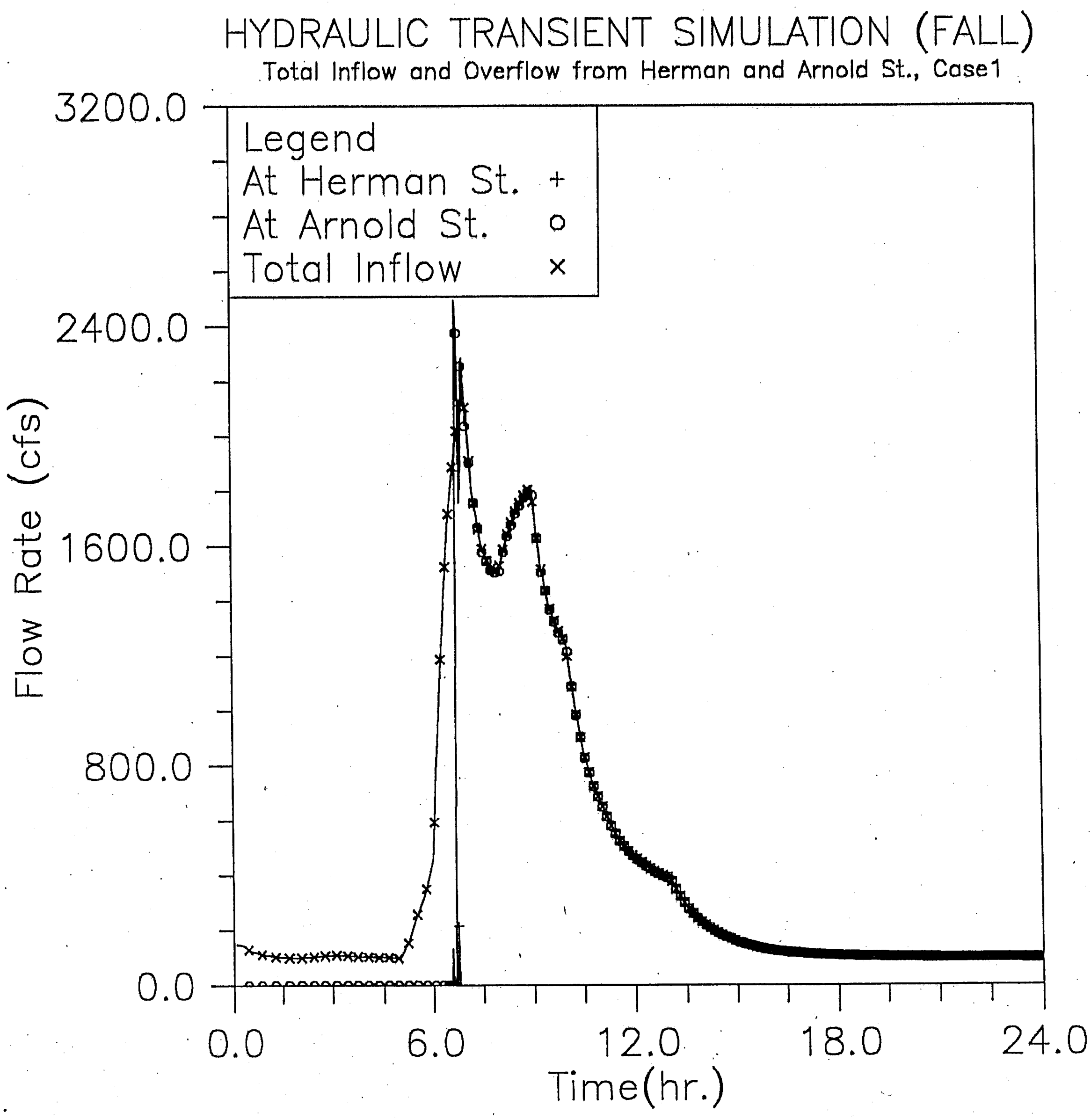

Fig. 3.1(g) Time variation of the overflow and the total inflow; modeling case: design storm without flow to the WWTP (Case 1).

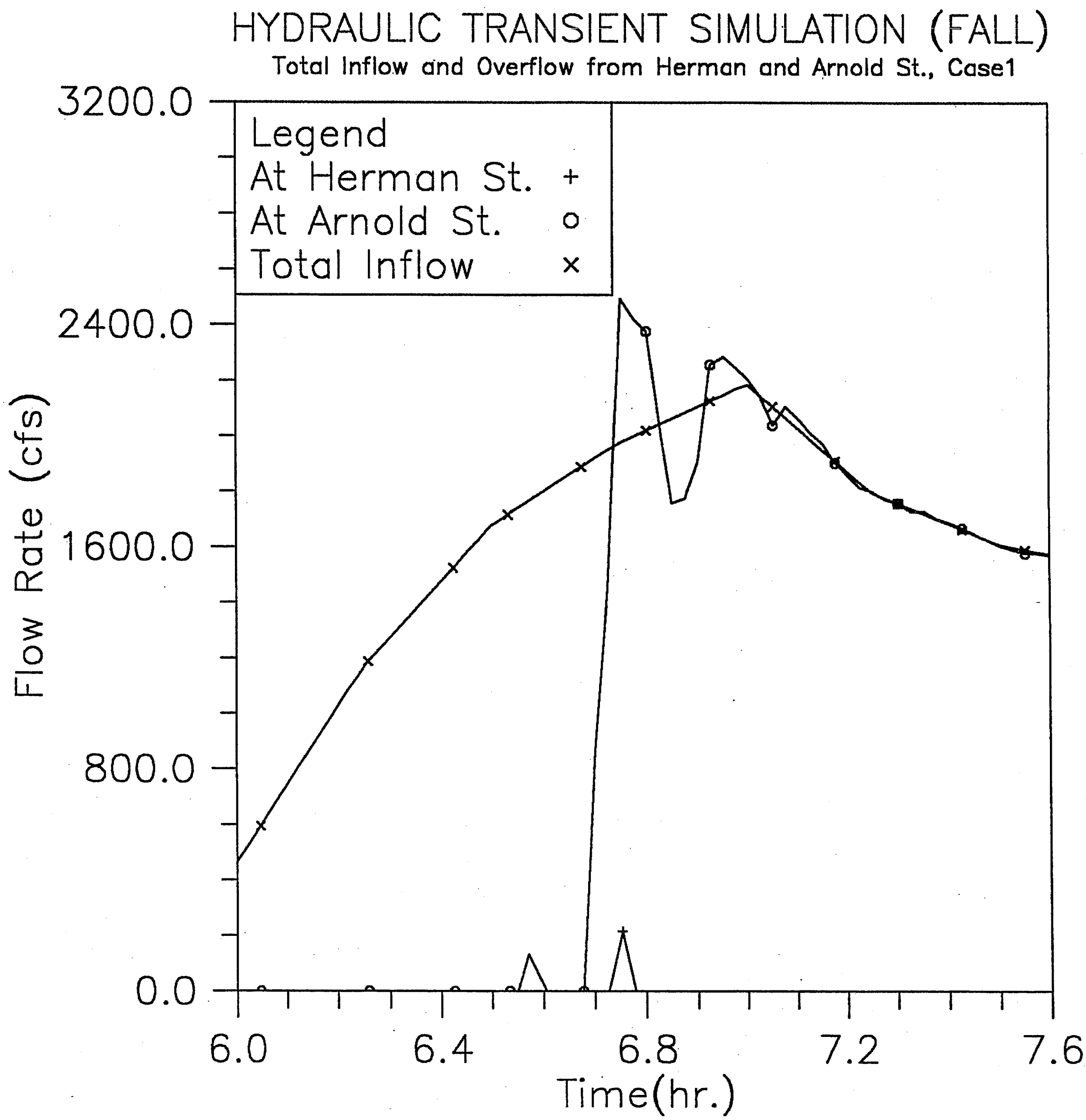

Fig. 3.1(h) Detailed time variation of the overflow and the total inflow during the initial stage of the overflow; modeling case: design storm without flow to the WWTP (Case 1).

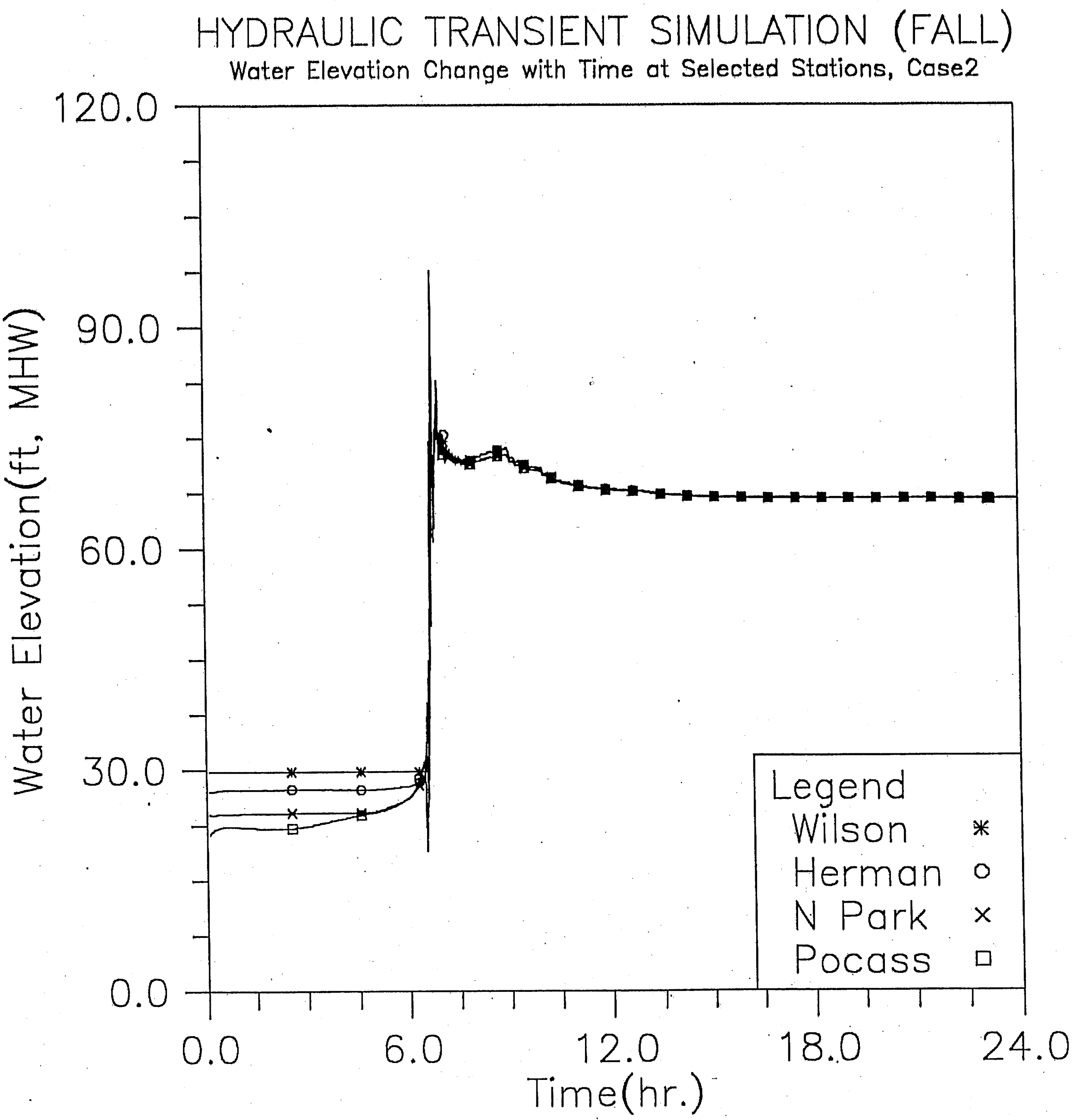

Fig. 3.2(a) Time variation of water surface elevations at four upstream dropshafts; modeling case: design storm without flow to the WWTP and increased dropshaft height (Case 2).

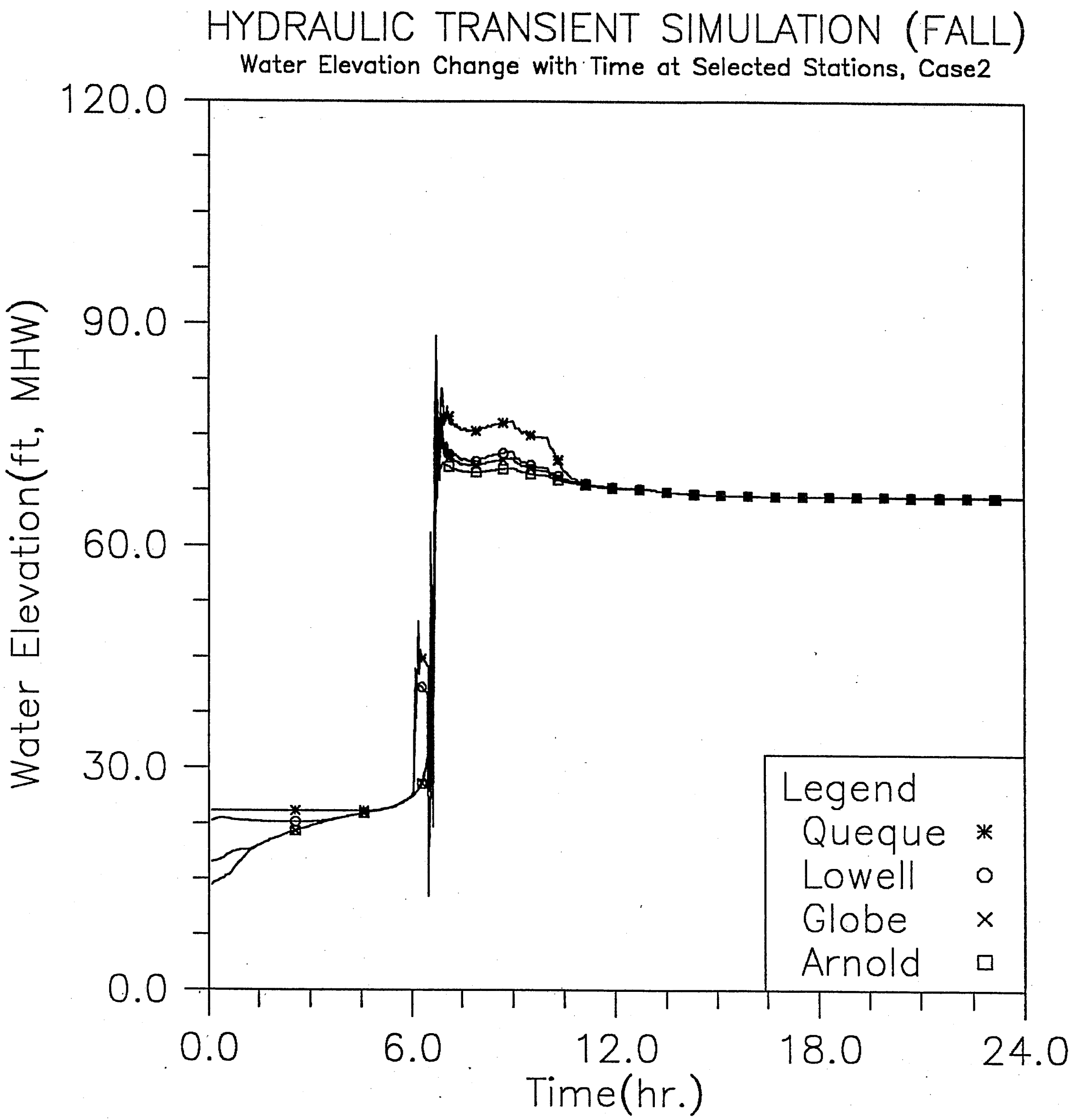

Fig. 3.2(b) Time variation of water surface elevations at Quequechan and three downstream dropshafts; modeling case: design storm without flow to the WWTP and increased dropshaft height (Case 2).

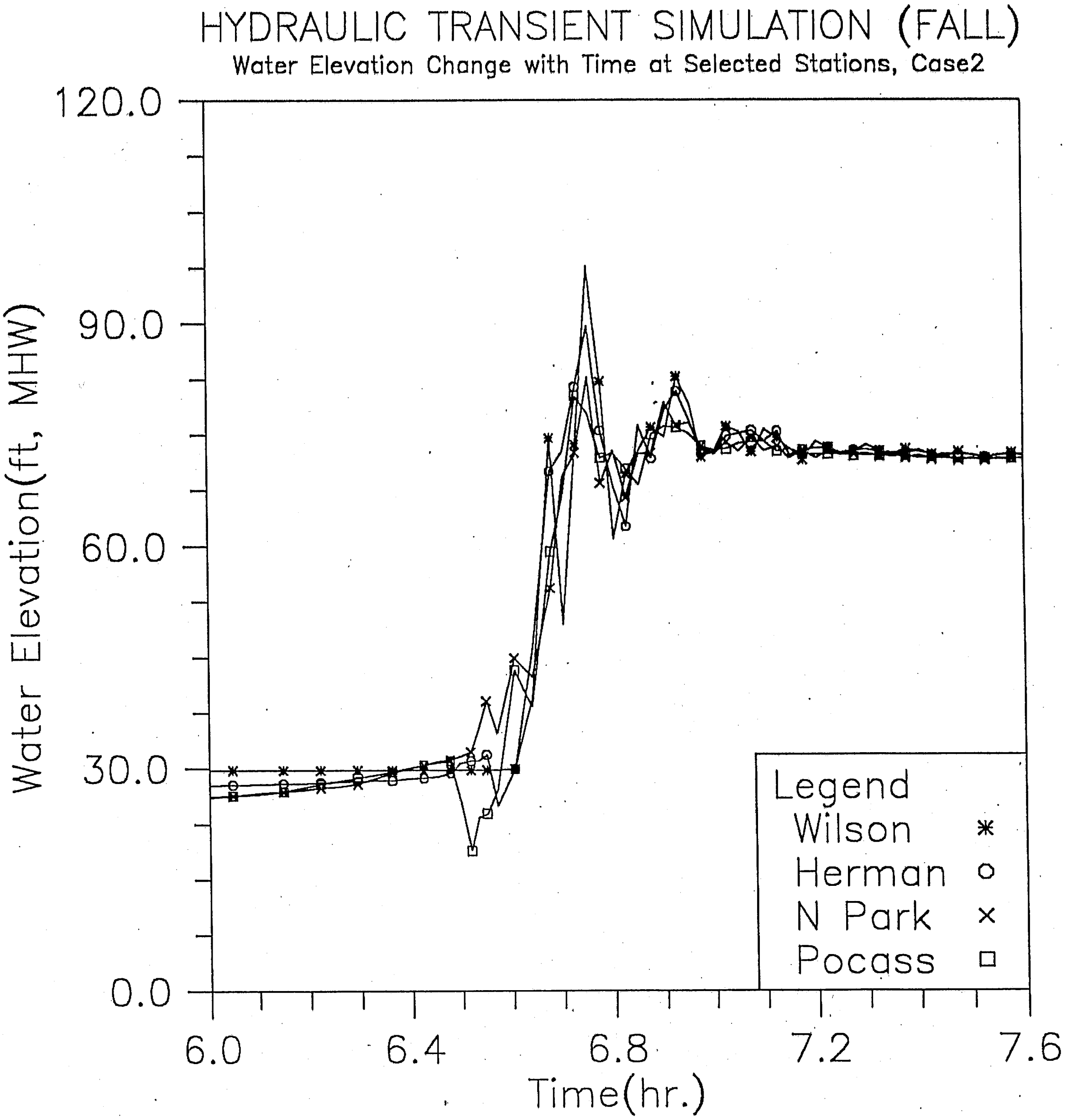

Fig. 3.2(c) Detailed time variation of water surface elevations at four upstream dropshafts during the surge period; modeling case: design storm without flow to the WWTP and increased dropshaft height (Case 2).

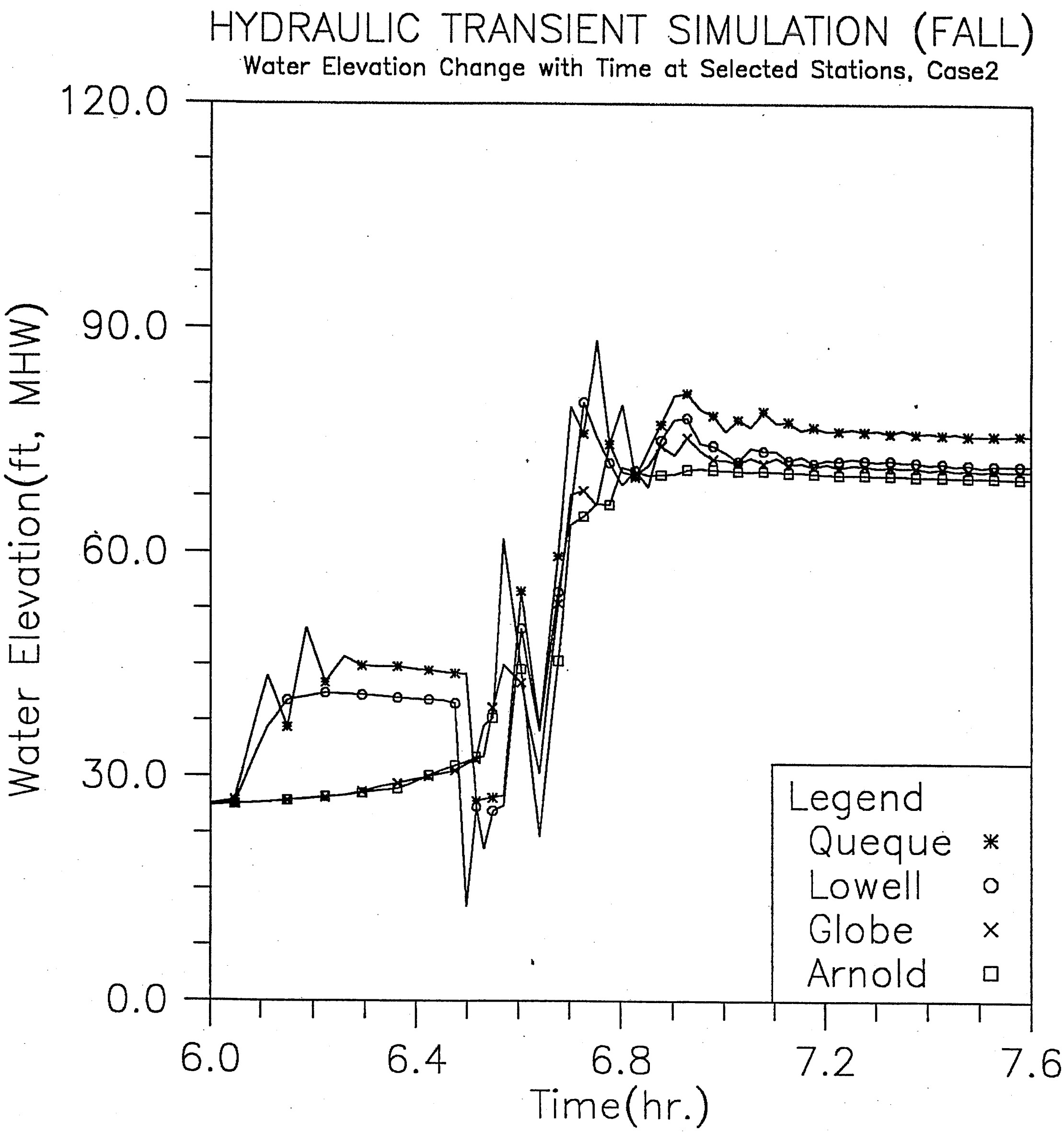

Fig. 3.2(d) Detailed time variation of water surface elevations at Quequechan and three downstream dropshafts during the surge period; modeling case: design storm without flow to the WWTP and increased dropshaft height (Case 2).

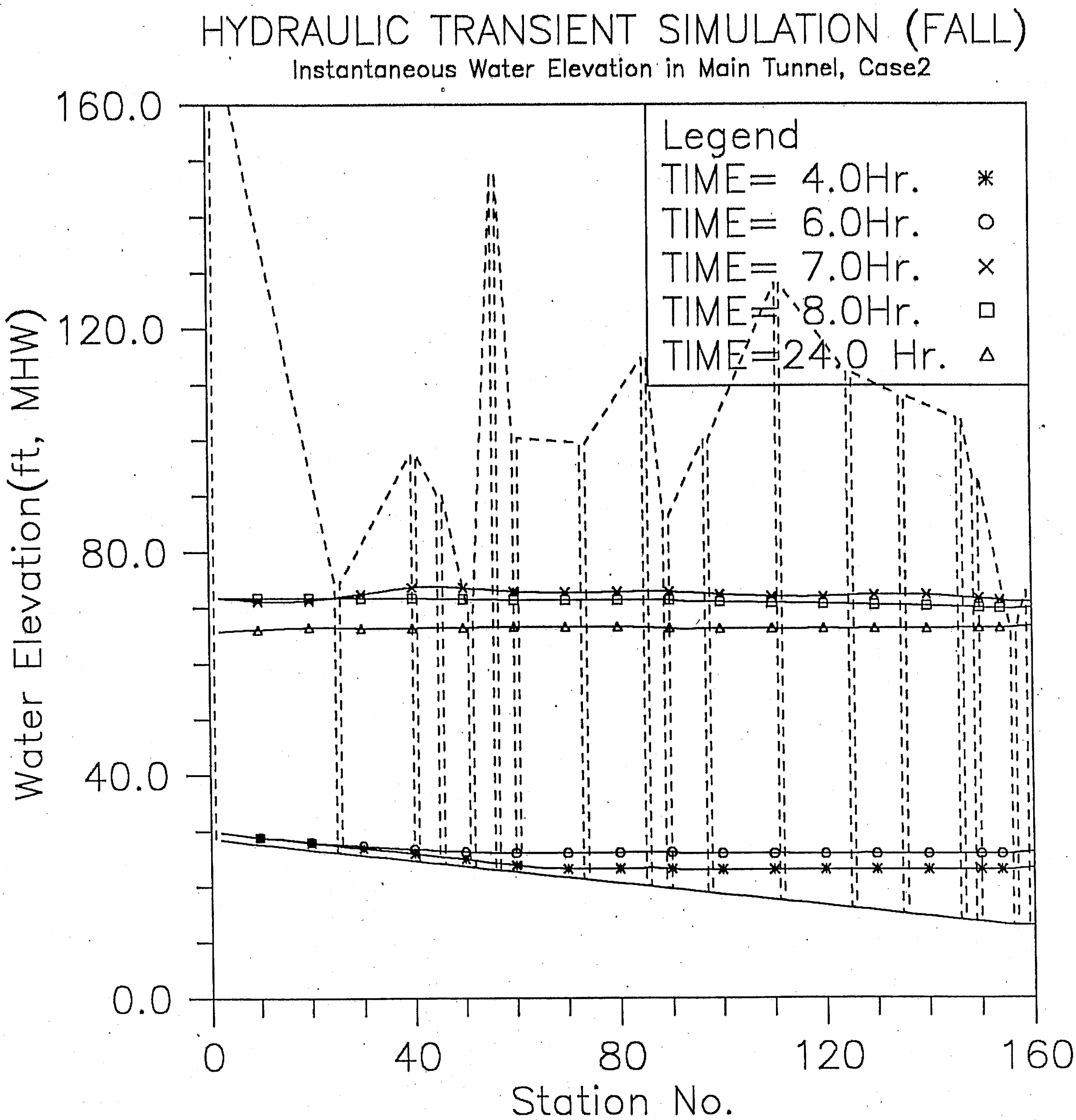

Fig. 3.2(e) Instantaneous hydraulic gradelines along the main tunnel; modeling case: design storm without flow to the WWTP and increased dropshaft height (Case 2).

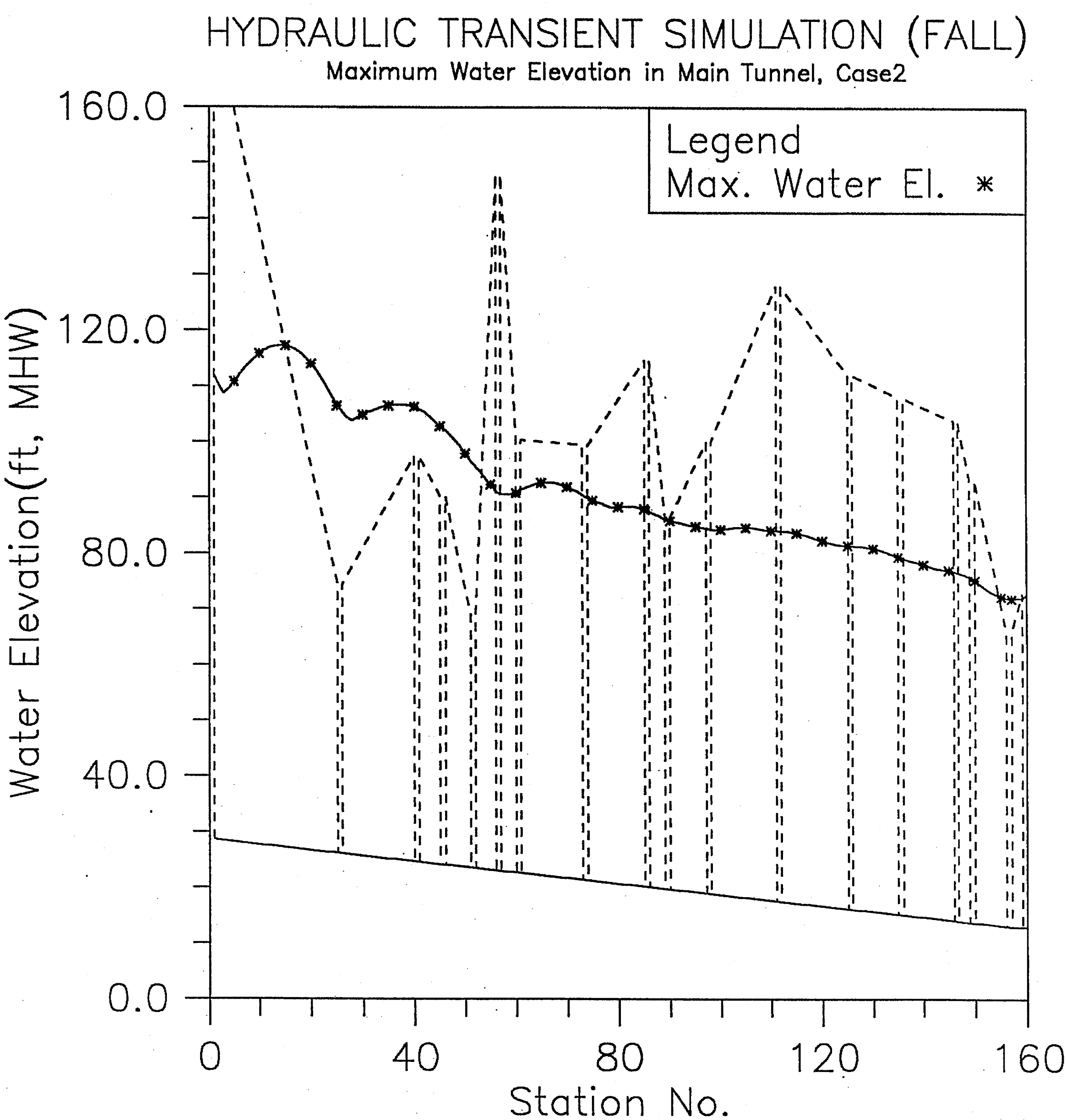

Fig. 3.2(f) The maximum water surface elevations along the main tunnel; modeling case: design storm without flow to the WWTP and increased dropshaft height (Case 2).

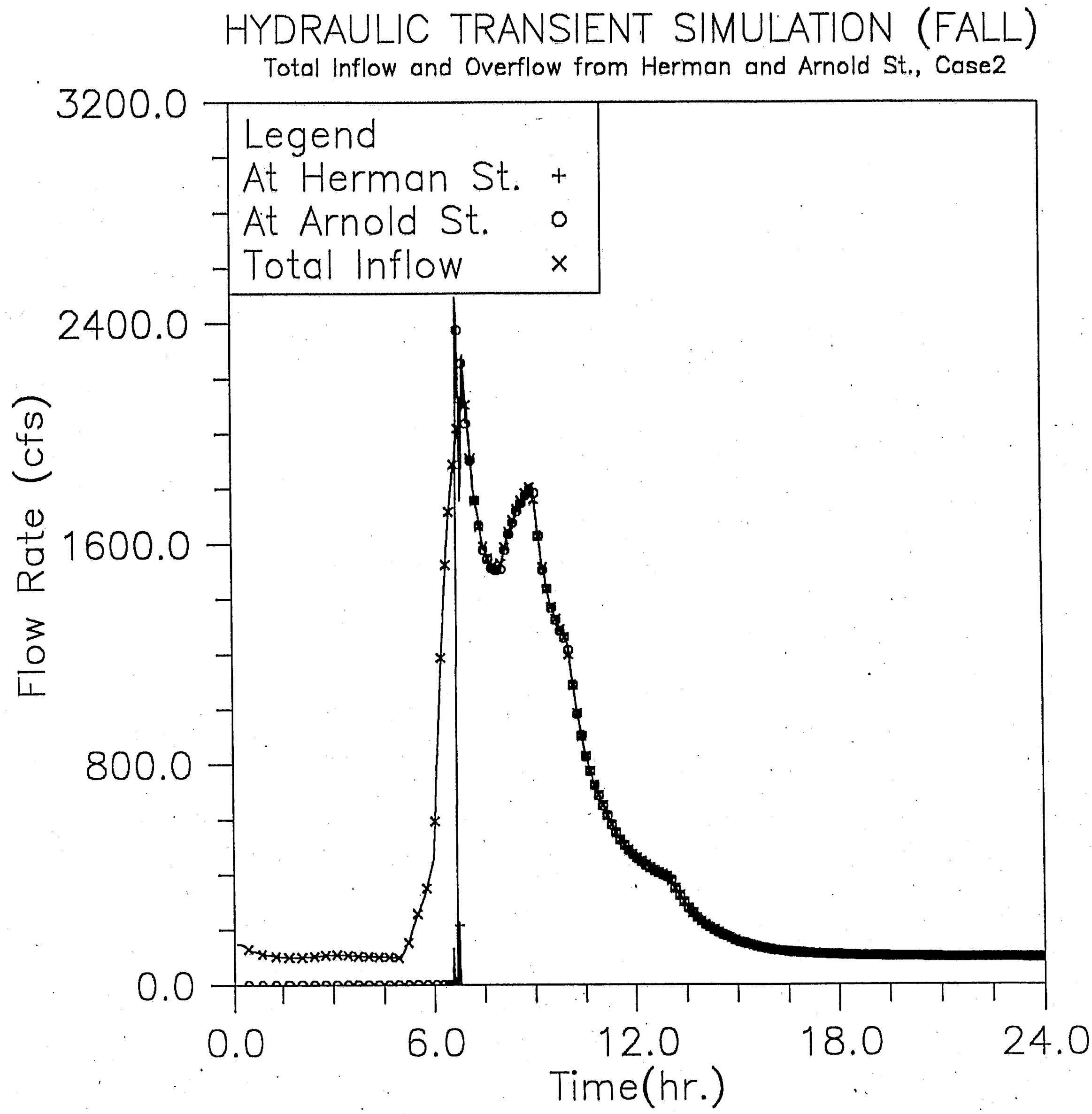

Fig. 3.2(g) Time variation of the overflow and the total inflow; modeling case: design storm without flow to the WWTP and increased dropshaft height (Case 2).

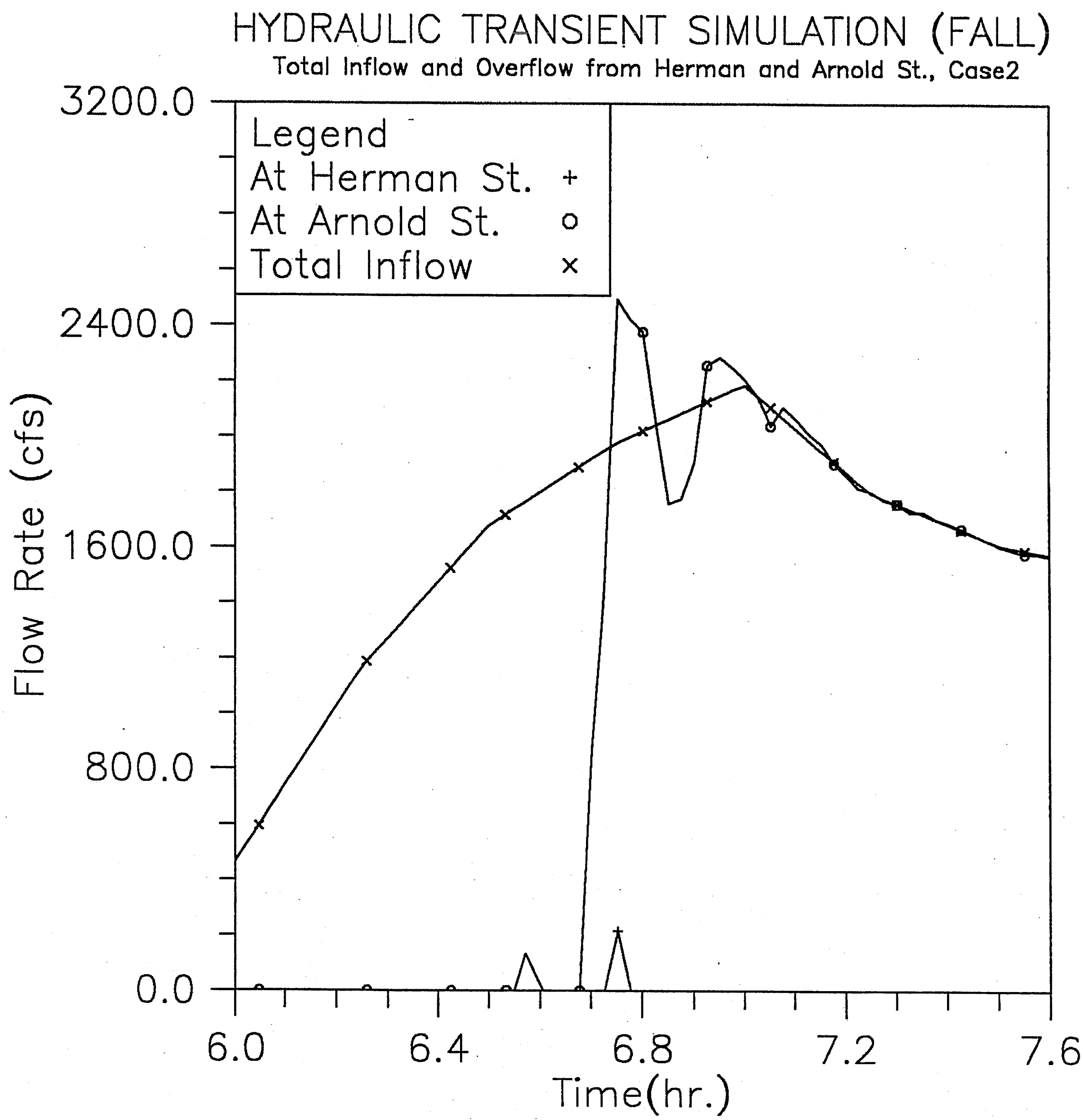

Fig. 3.2(h) Detailed time variation of the overflow and the total inflow during the initial stage of the overflow; modeling case: design storm without flow to the WWTP and increased dropshaft height (Case 2).

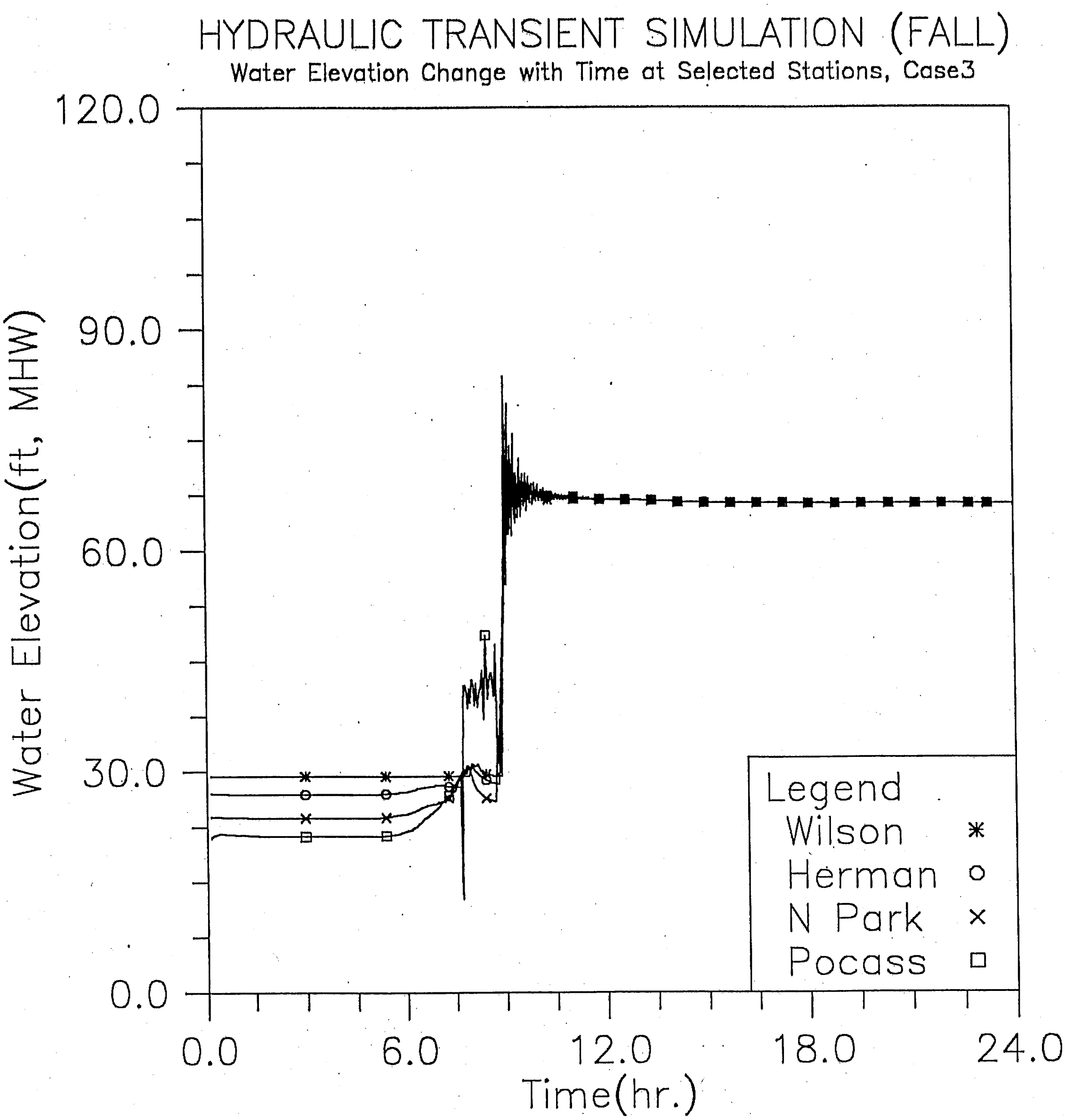

Fig. 3.3(a) Time variation of water surface elevations at four upstream dropshafts; modeling case: 3–month storm without flow to the WWTP (Case 3).

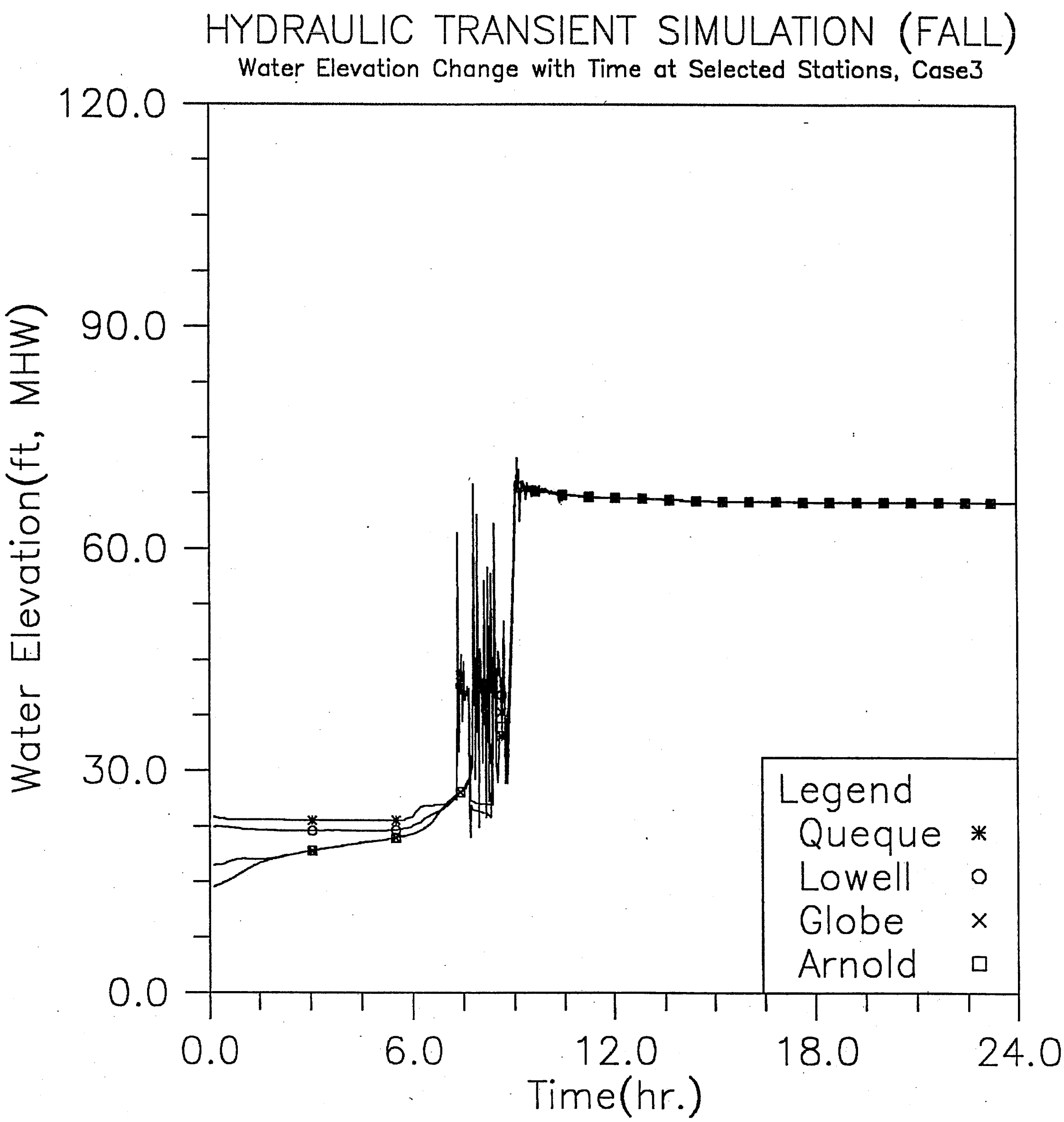

Fig. 3.3(b) Time variation of water surface elevations at Quequechan and three downstream dropshafts; modeling case: 3–month storm without flow to the WWTP (Case 3).

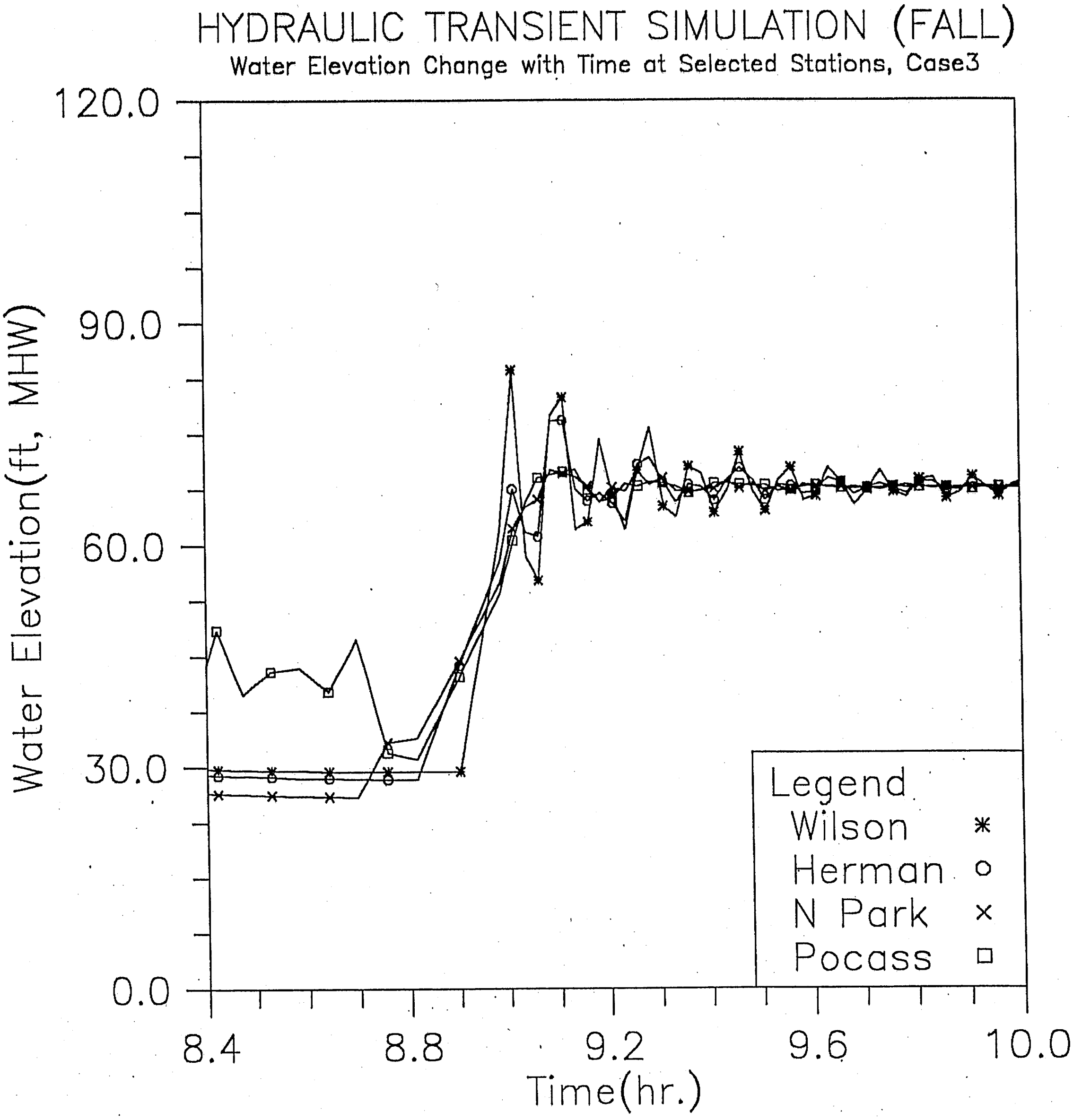

Fig. 3.3(c) Detailed time variation of water surface elevations at four upstream dropshafts during the surge period; modeling case: 3–month storm without flow to the WWTP (Case 3).

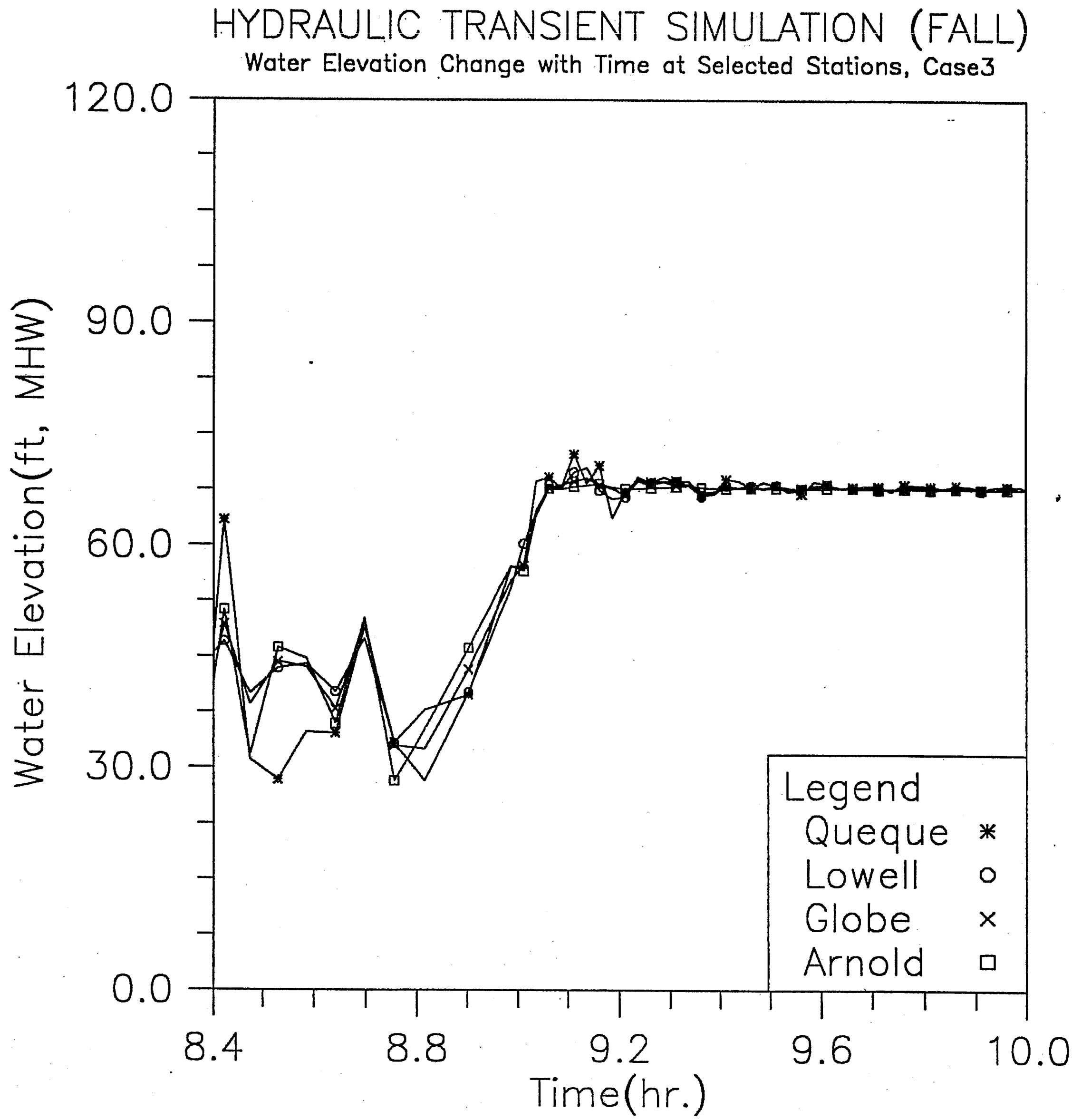

Fig. 3.3(d) Detailed time variation of water surface elevations at Quequechan and three downstream dropshafts during the surge period; modeling case: 3–month storm without flow to the WWTP (Case 3).

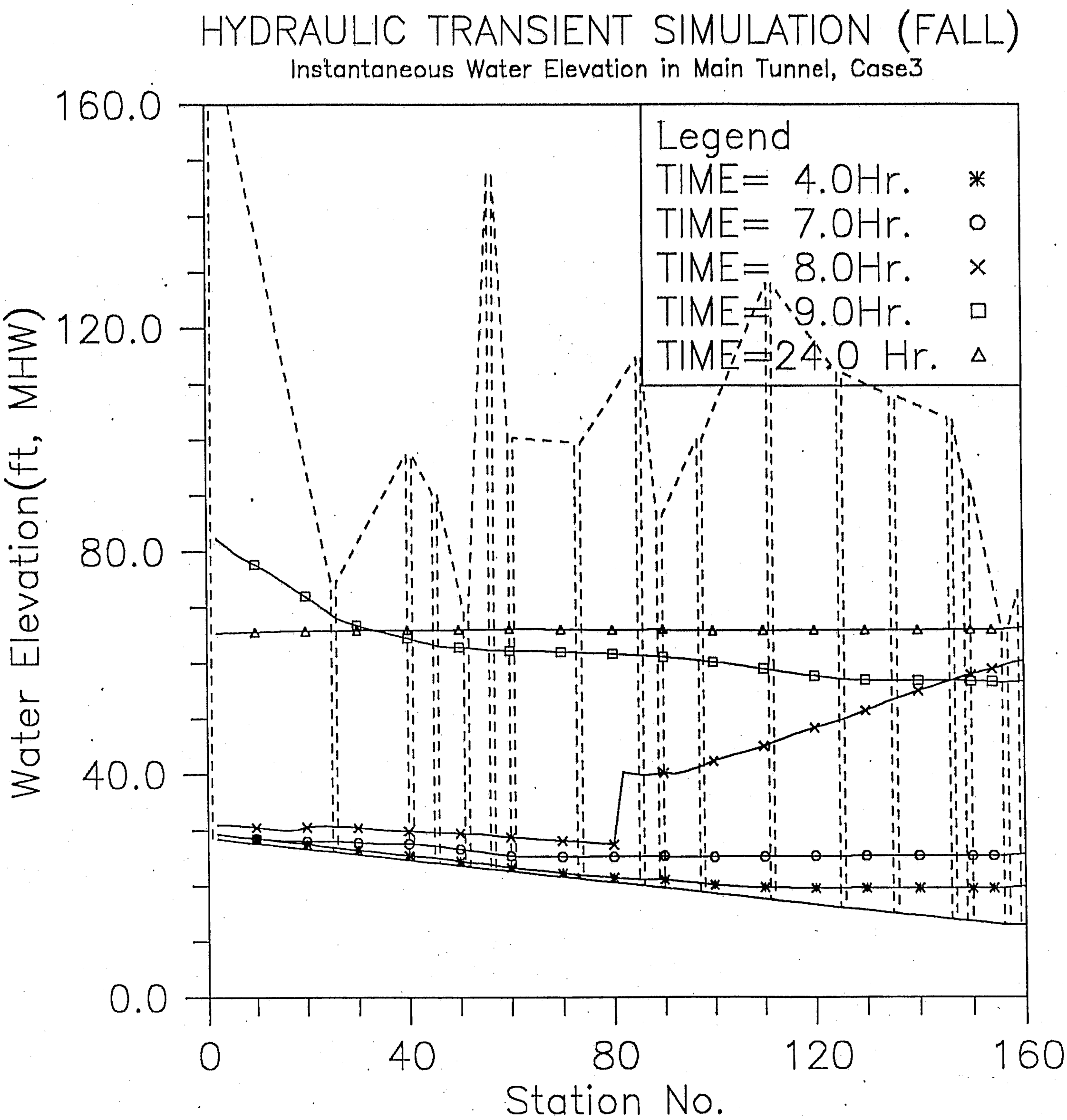

Fig. 3.3(e) Instantaneous hydraulic gradelines along the main tunnel; modeling case: 3–month storm without flow to the WWTP (Case 3).

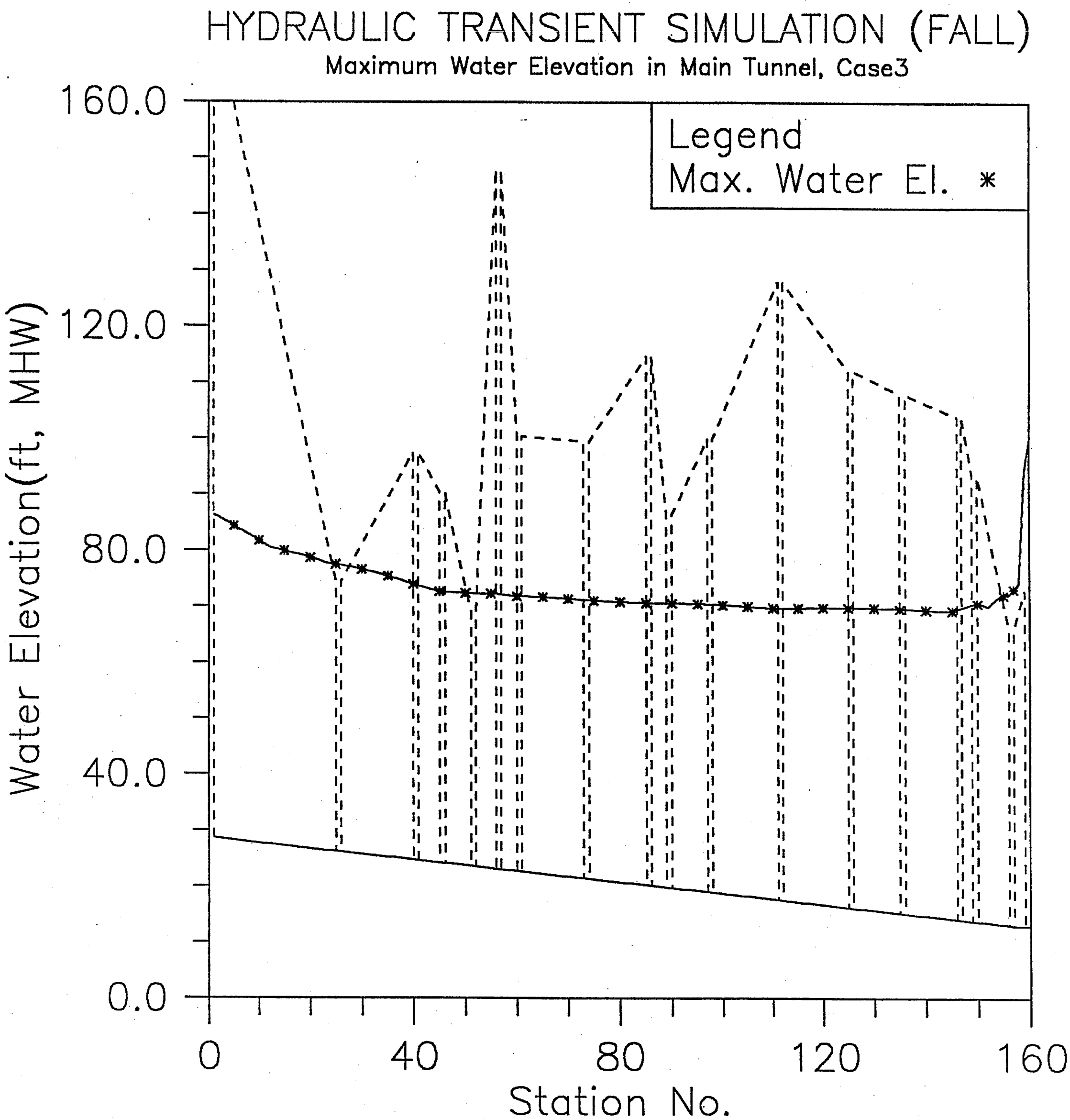

Fig. 3.3(f) The maximum water surface elevations along the main tunnel; modeling case: 3–month storm without flow to the WWTP (Case 3).

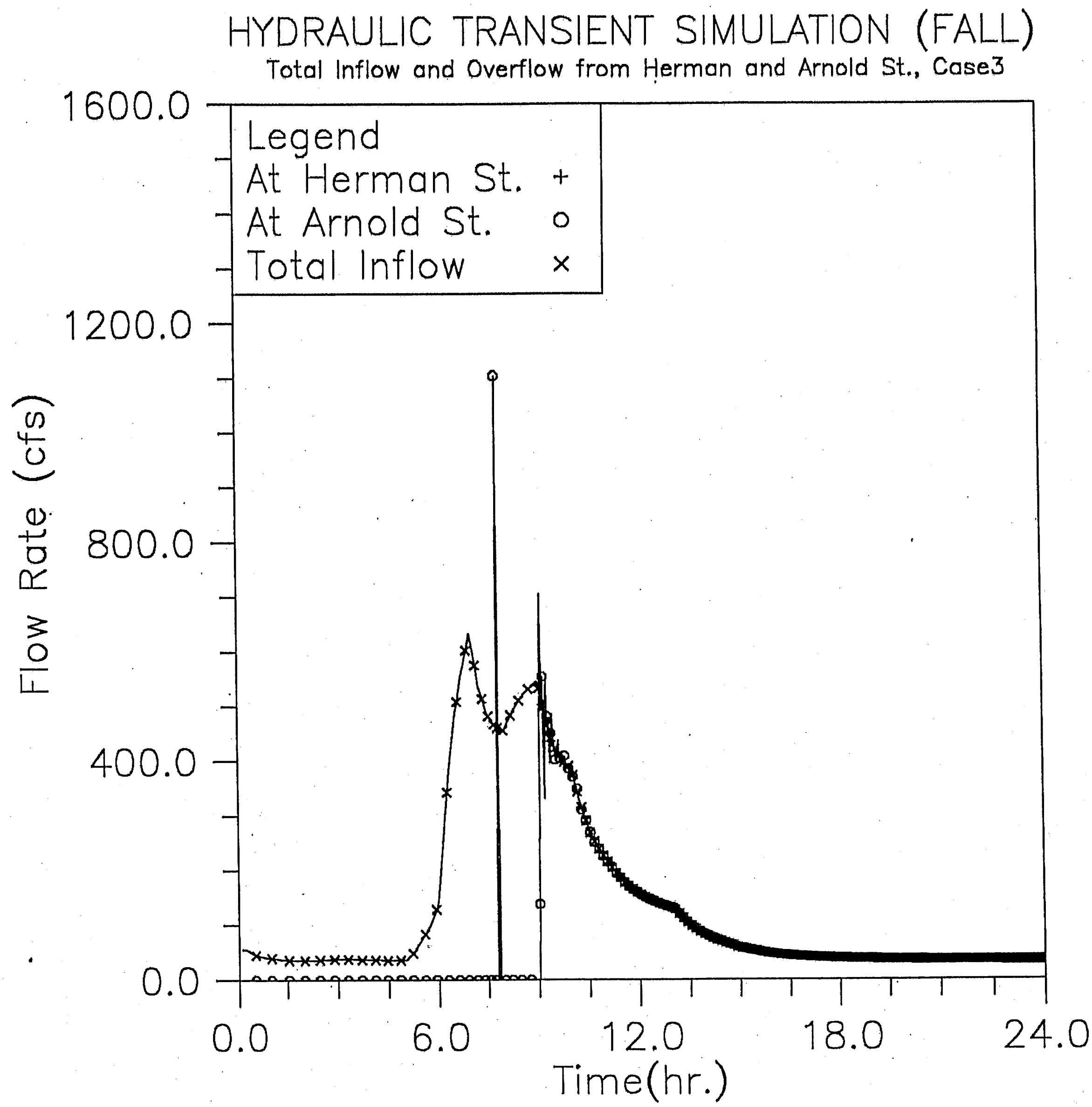

Fig. 3.3(g) Time variation of the overflow and the total inflow; modeling case: 3–month storm without flow to the WWTP (Case 3).

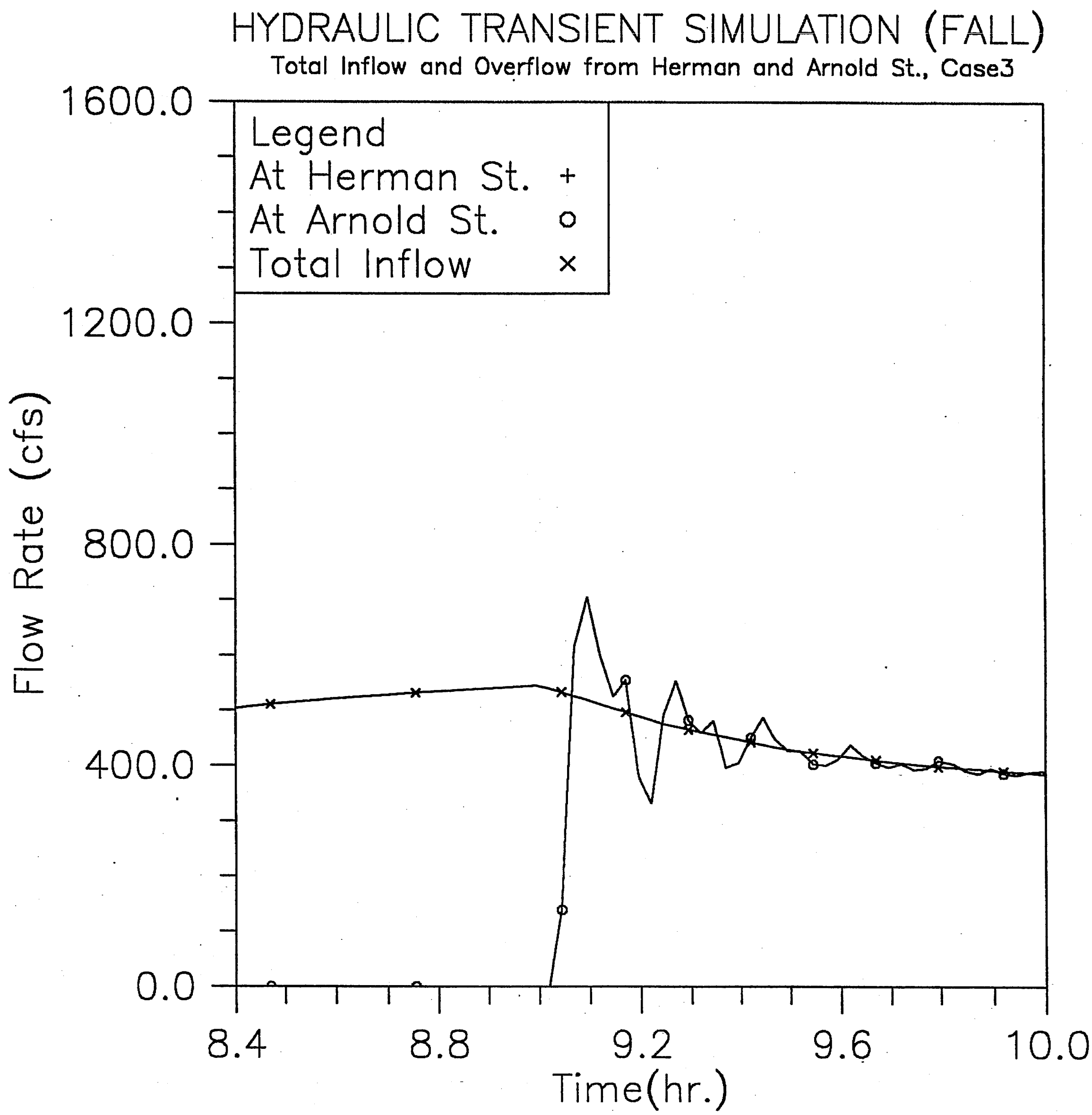

Fig. 3.3(h) Detailed time variation of the overflow and the total inflow during the initial stage of the overflow; modeling case: 3–month storm without flow to the WWTP (Case 3).

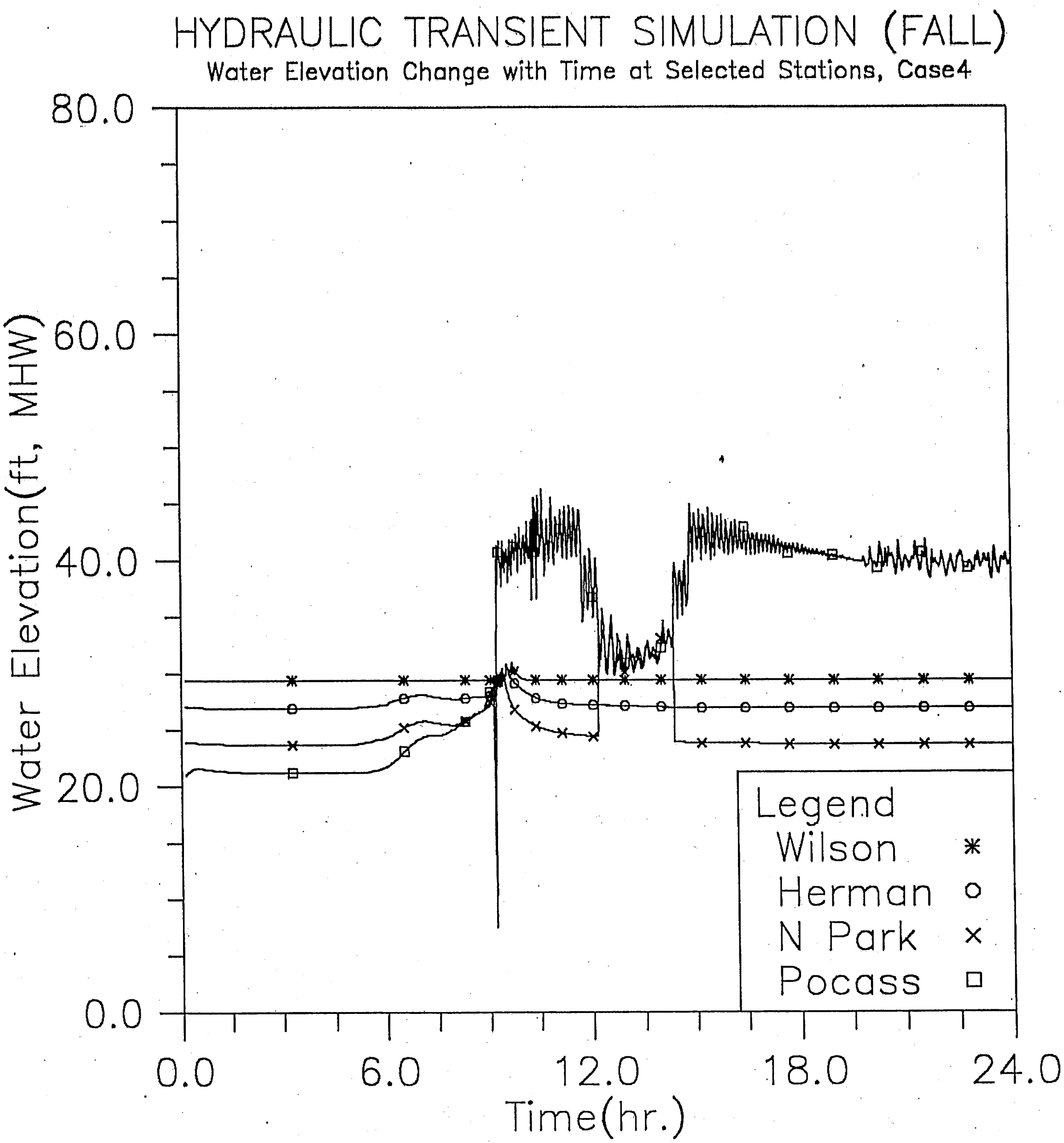

Fig. 3.4(a) Time variation of water surface elevations at four upstream dropshafts; modeling case: 3–month storm and limited outflow to the WWTP (Case 4).

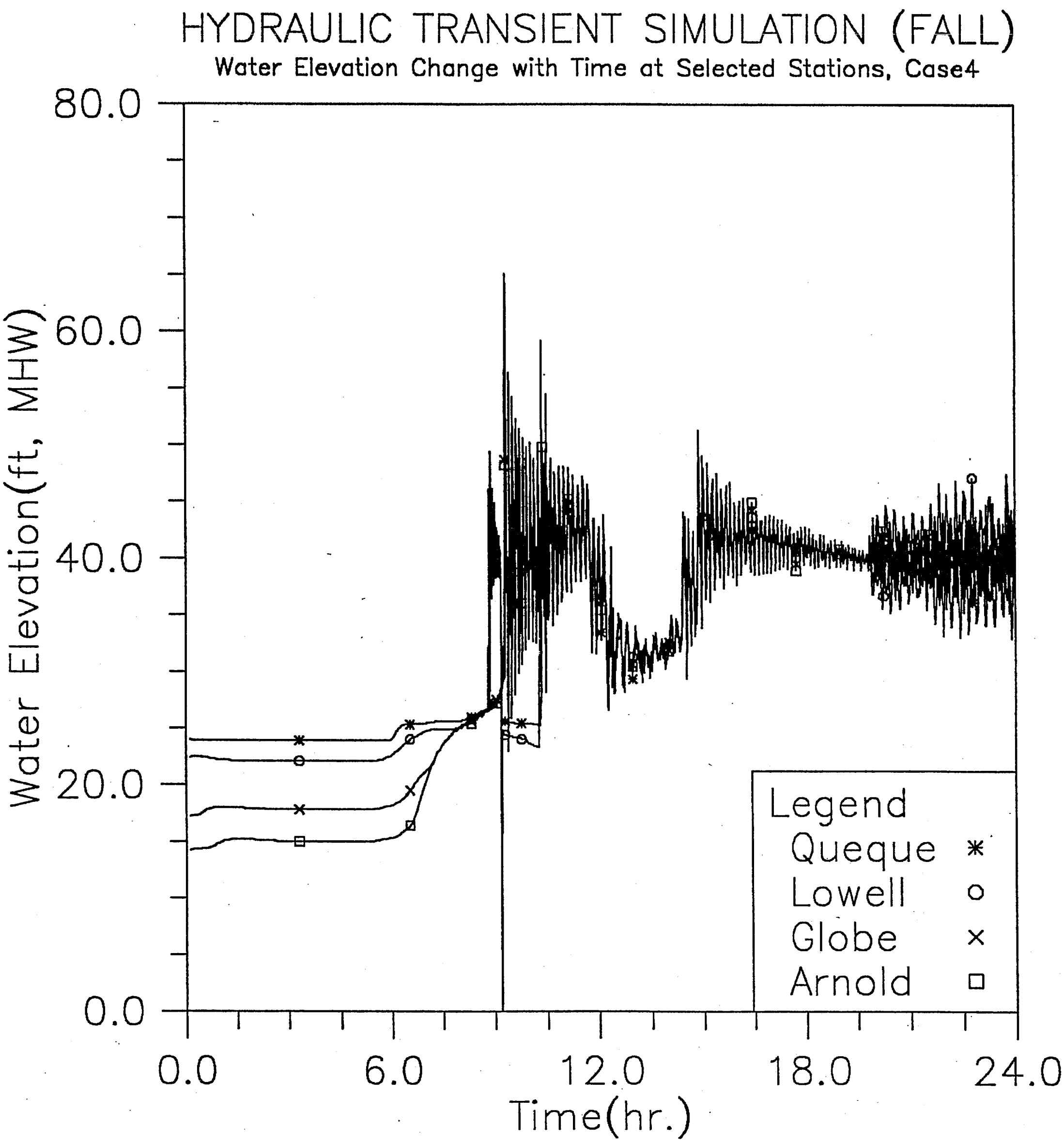

Fig. 3.4(b) Time variation of water surface elevations at Quequechan and three downstream dropshafts; modeling case: 3–month storm and limited outflow to the WWTP (Case 4).

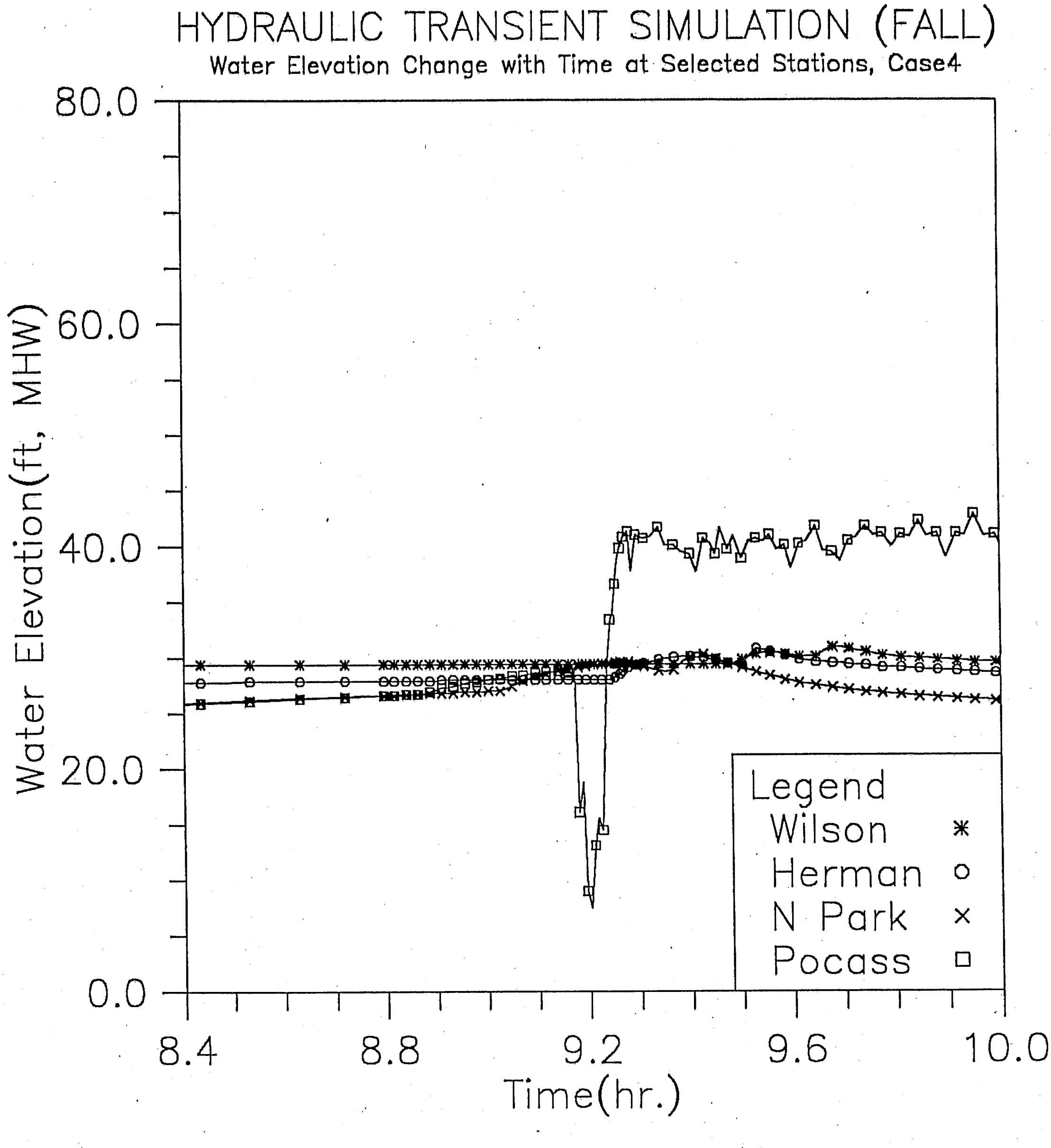

Fig. 3.4(c) Detailed time variation of water surface elevations at four upstream dropshafts during the surge period; modeling case: 3–month storm and limited outflow to the WWTP (Case 4).

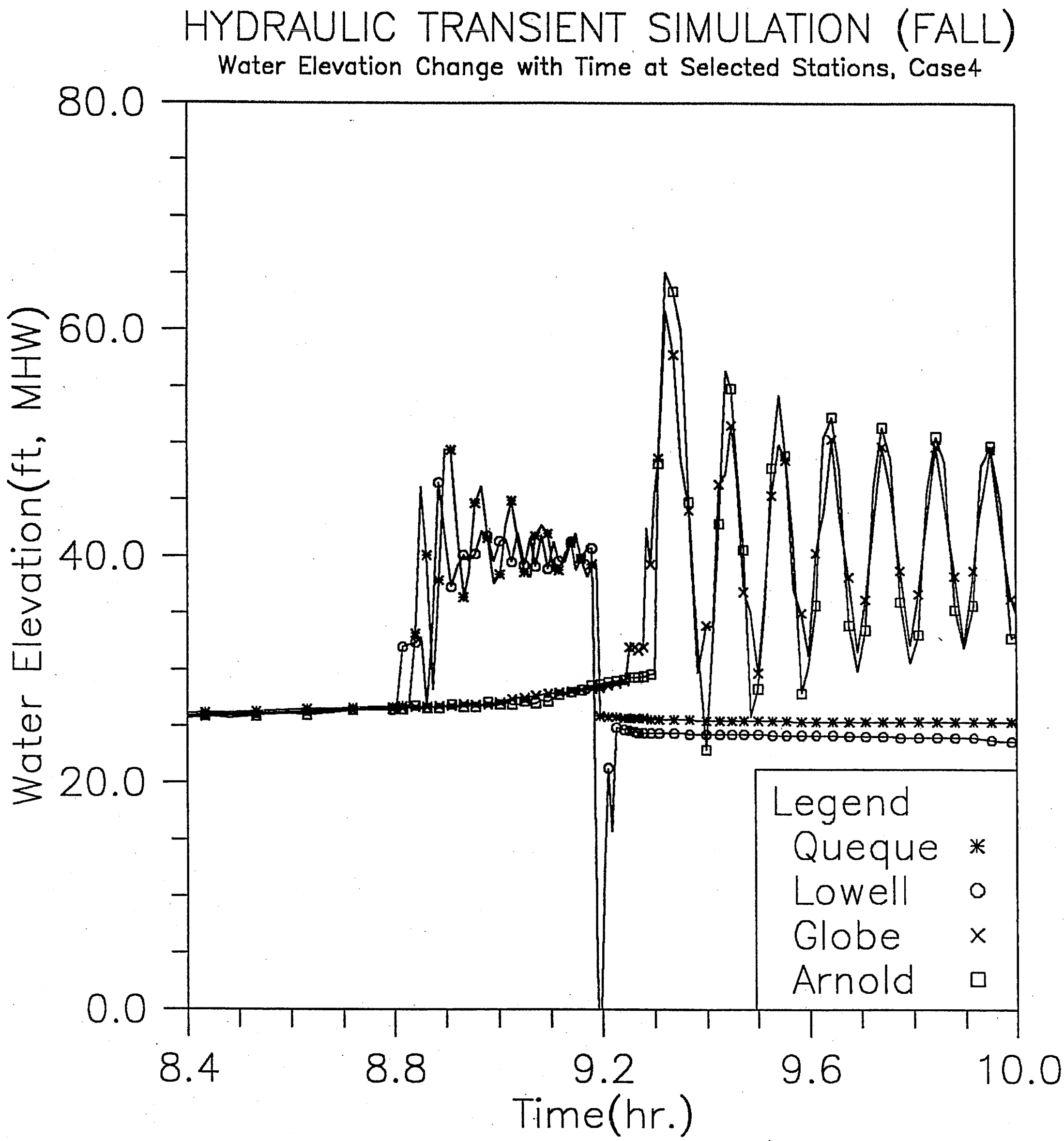

Fig. 3.4(d) Detailed time variation of water surface elevations at Quequechan and three downstream dropshafts during the surge period; modeling case: 3–month storm and limited outflow to the WWTP (Case 4).

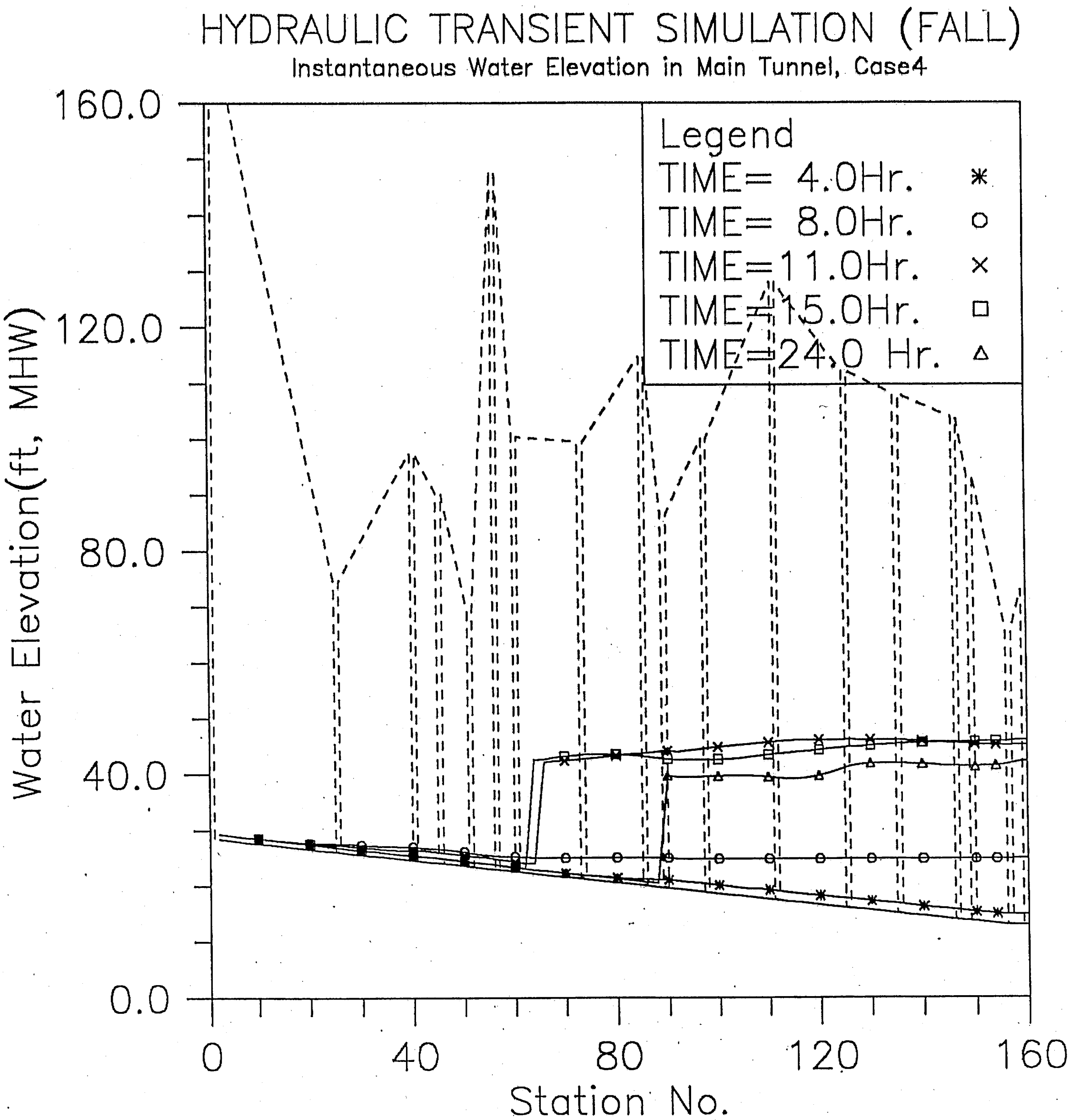

Fig. 3.4(e) Instantaneous hydraulic gradelines along the main tunnel; modeling case: 3–month storm and limited outflow to the WWTP (Case 4).

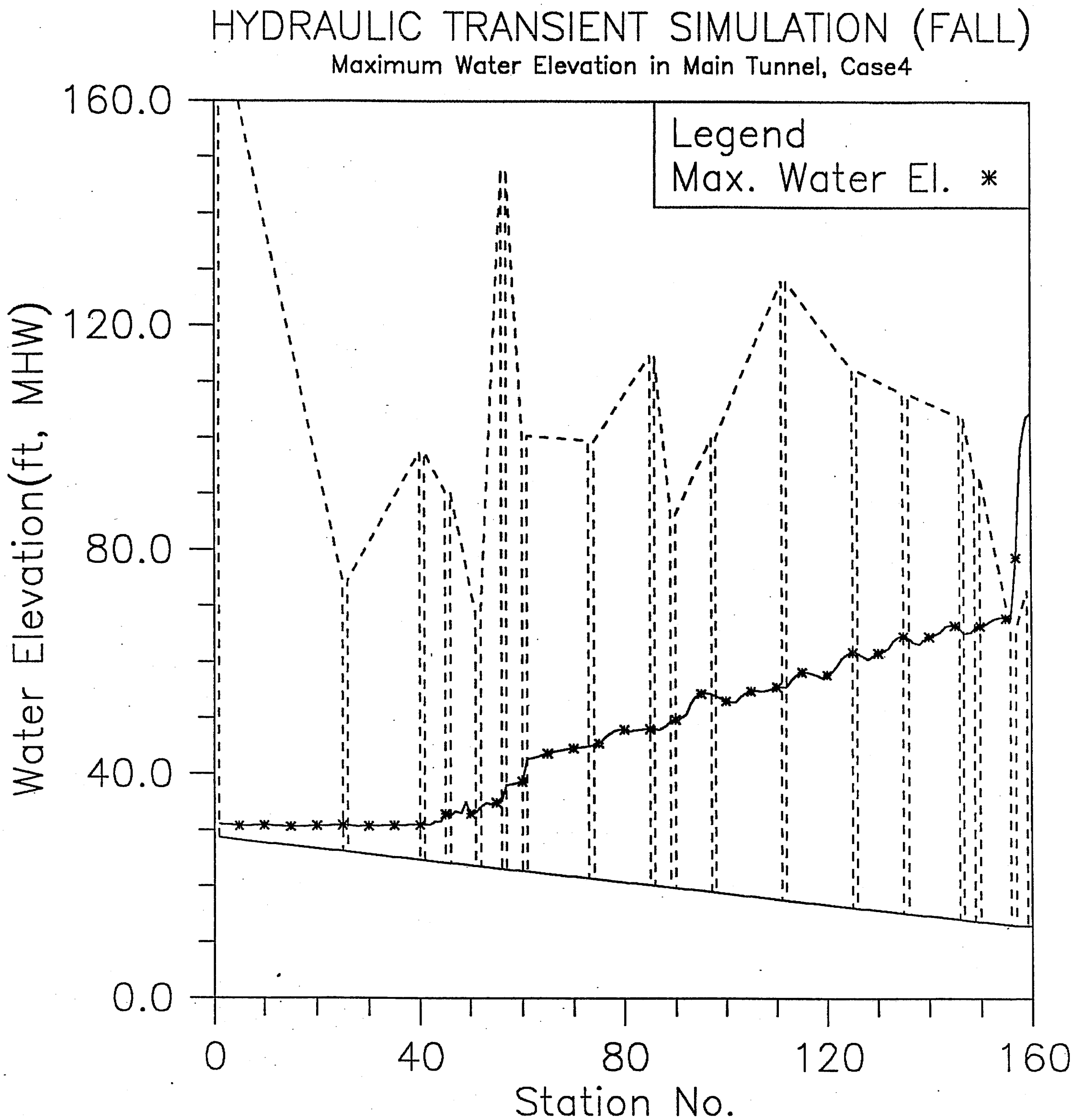

Fig. 3.4(f) The maximum water surface elevations along the main tunnel; modeling case: 3–month storm and limited outflow to the WWTP (Case 4).

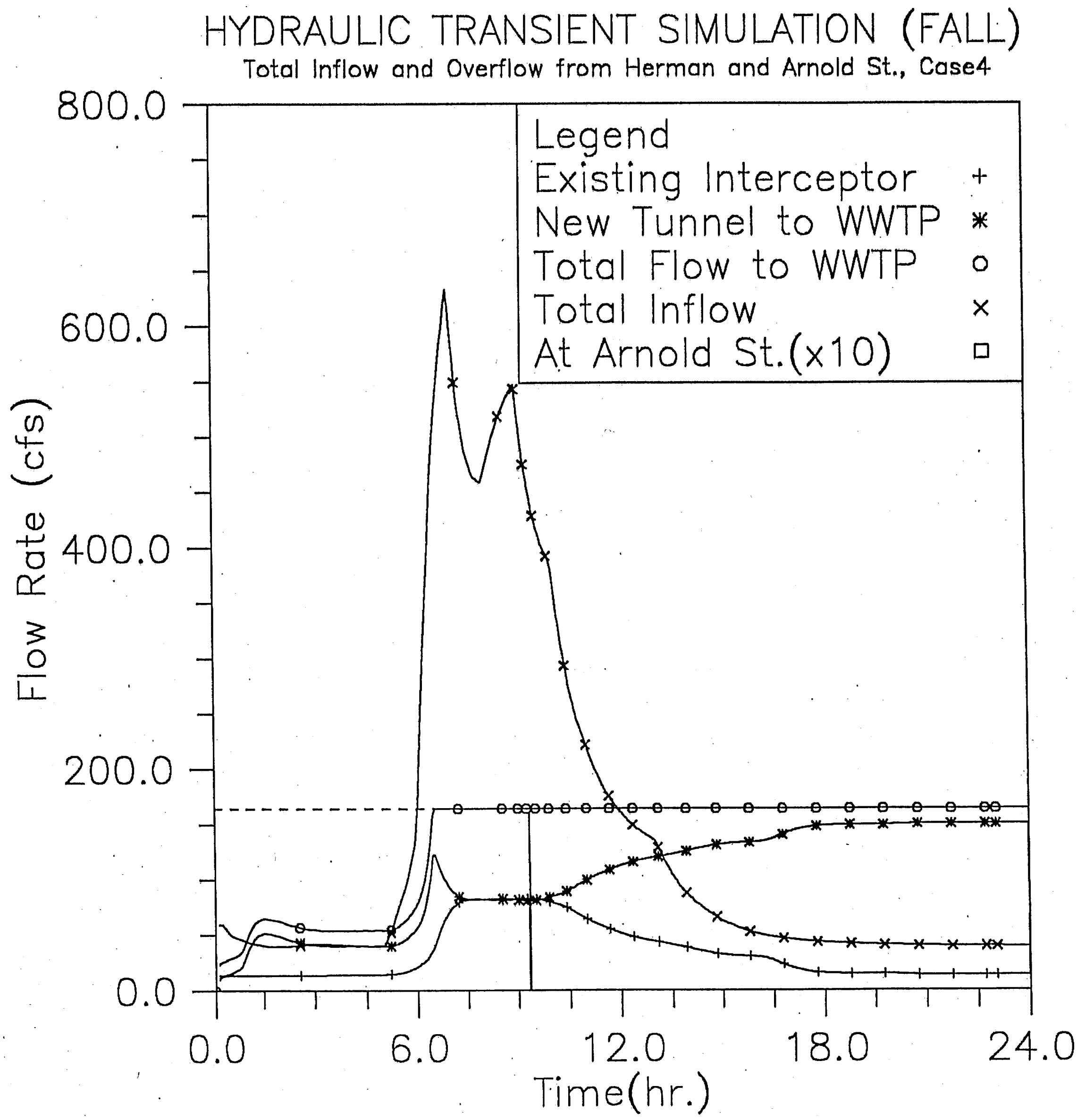

Fig. 3.4(g) Time variation of the overflow and the total inflow; modeling case: 3–month storm and limited outflow to the WWTP (Case 4).

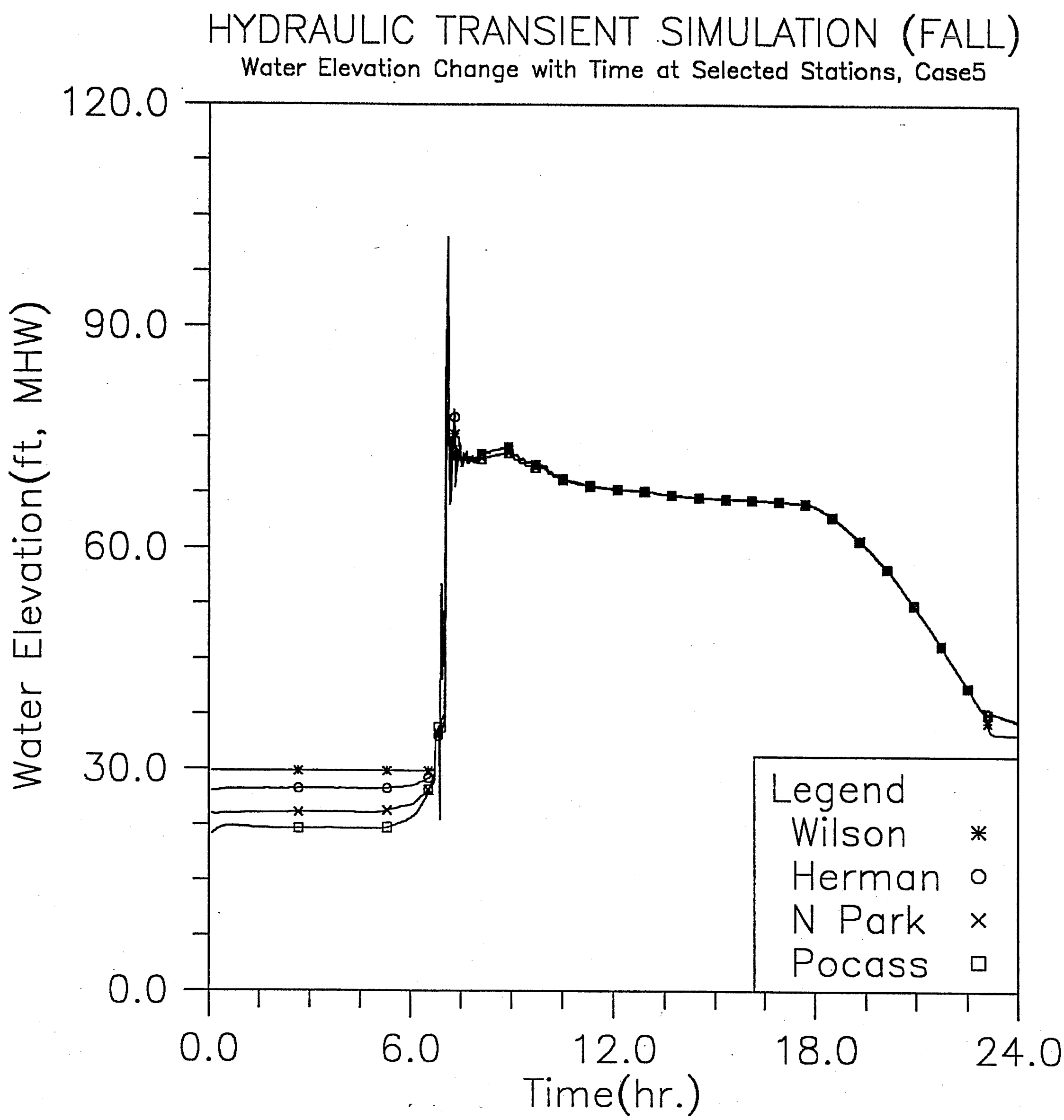

Fig. 3.5(a) Time variation of water surface elevations at four upstream dropshafts; modeling case: design storm and limited outflow to the WWTP (Case 5).

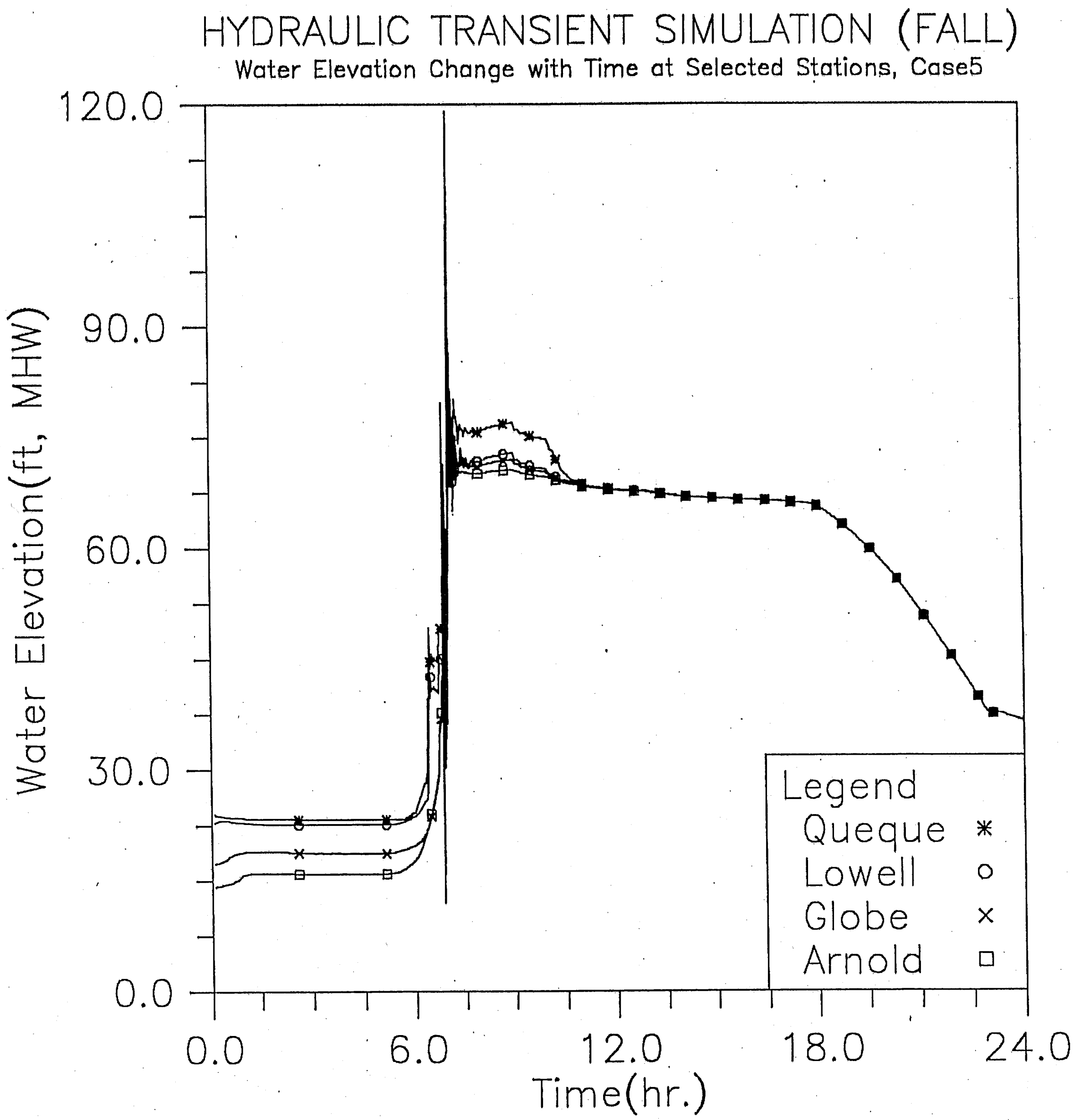

Fig. 3.5(b) Time variation of water surface elevations at Quequechan and three downstream dropshafts; modeling case: design storm and limited outflow to the WWTP (Case 5).

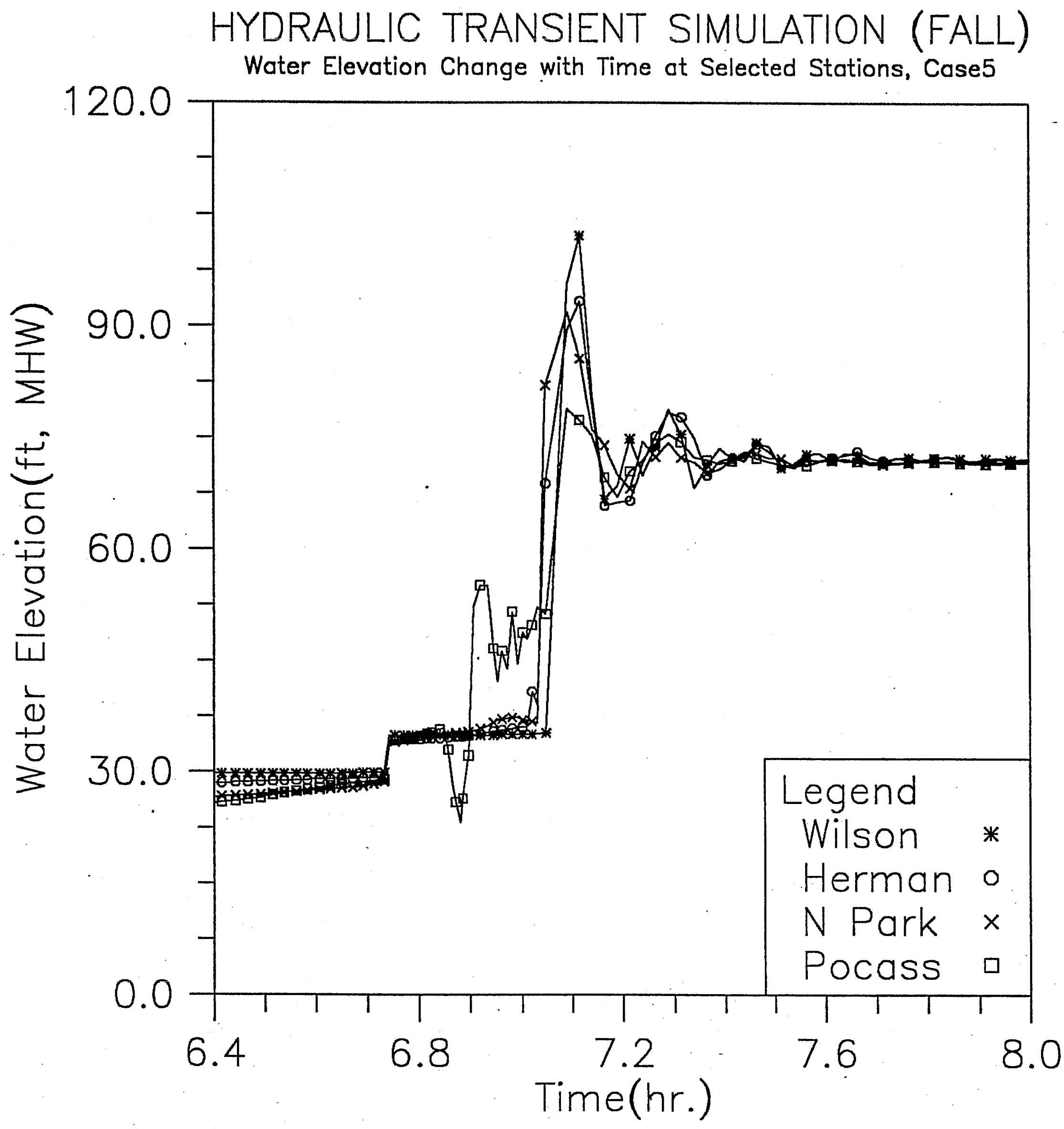

Fig. 3.5(c) Detailed time variation of water surface elevations at four upstream dropshafts during the surge period; modeling case: design storm and limited outflow to the WWTP (Case 5).

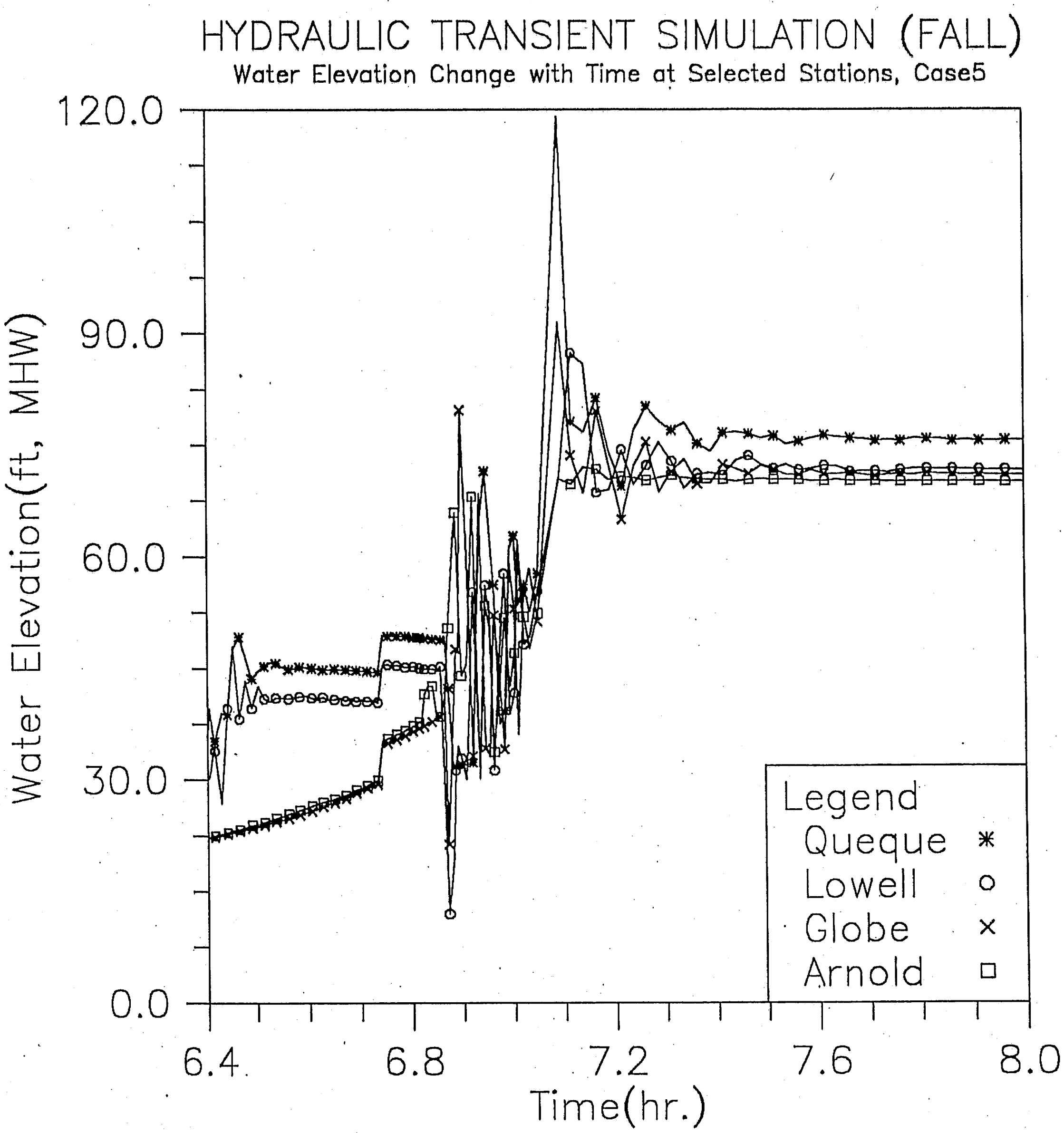

Fig. 3.5(d) Detailed time variation of water surface elevations at Quequechan and three downstream dropshafts during the surge period; modeling case: design storm and limited outflow to the WWTP (Case 5).

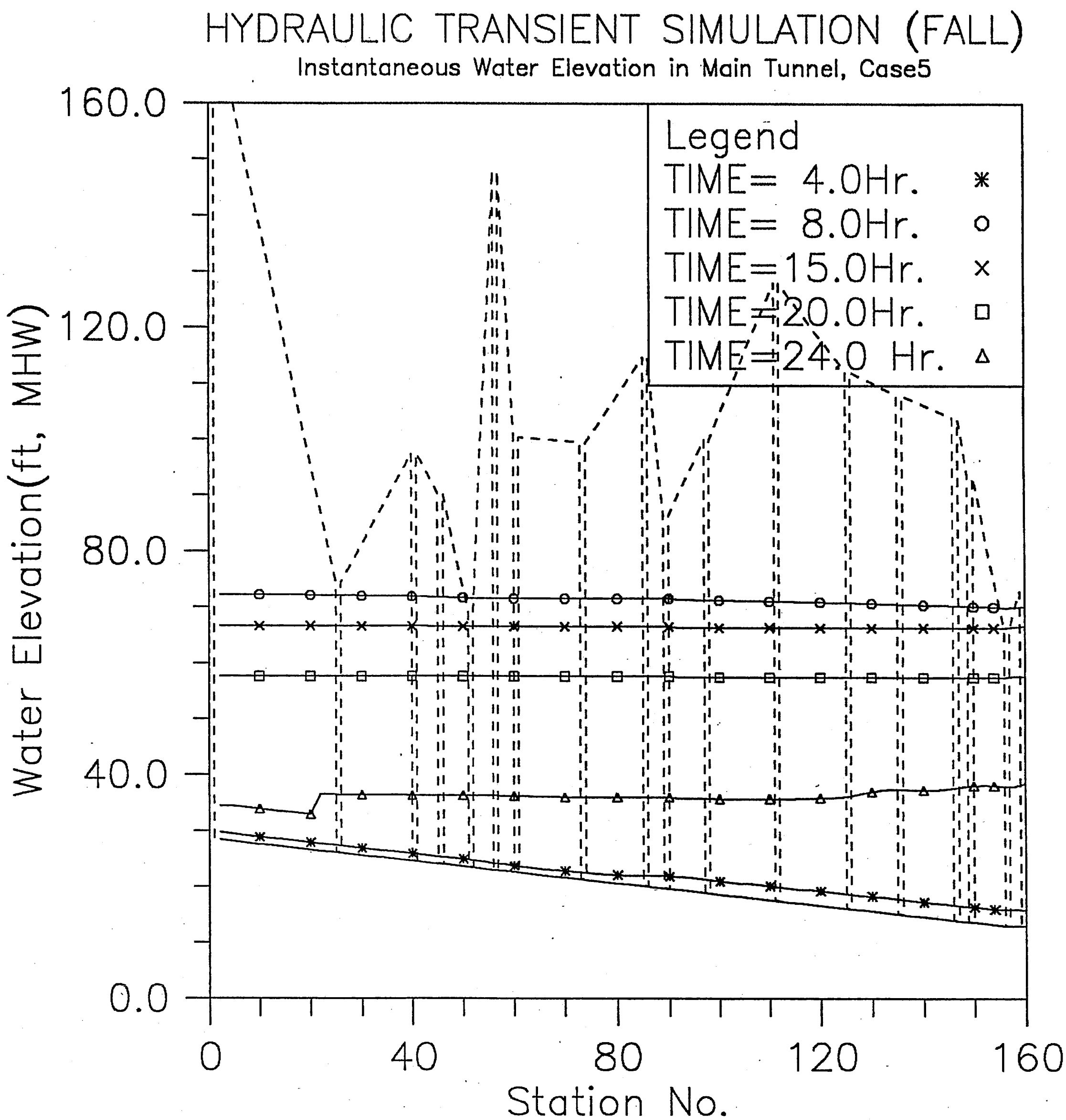

Fig. 3.5(e) Instantaneous hydraulic gradelines along the main tunnel; modeling case: design storm and limited outflow to the WWTP (Case 5).

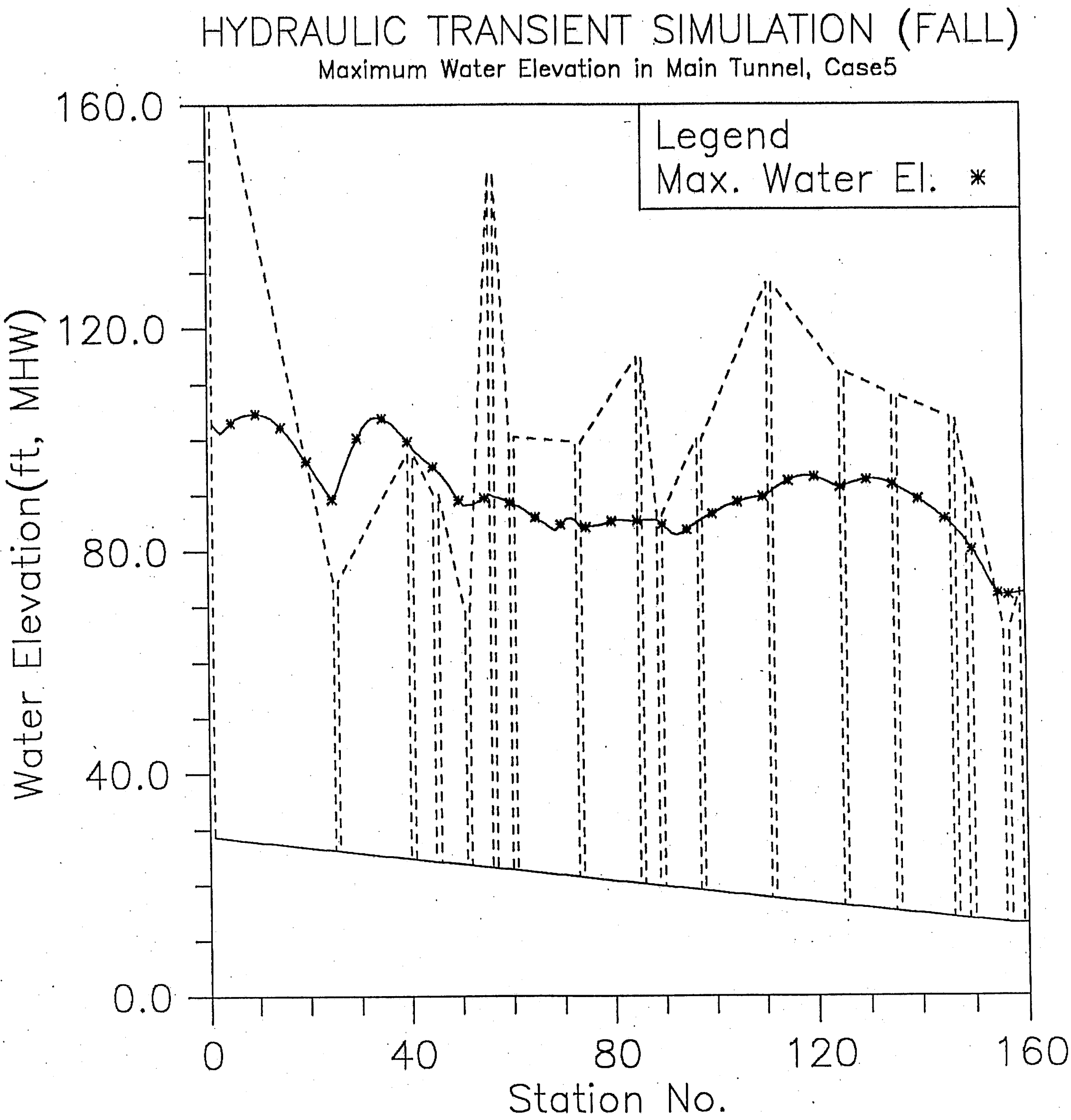

Fig. 3.5(f) The maximum water surface elevations along the main tunnel; modeling case: design storm and limited outflow to the WWTP (Case 5).

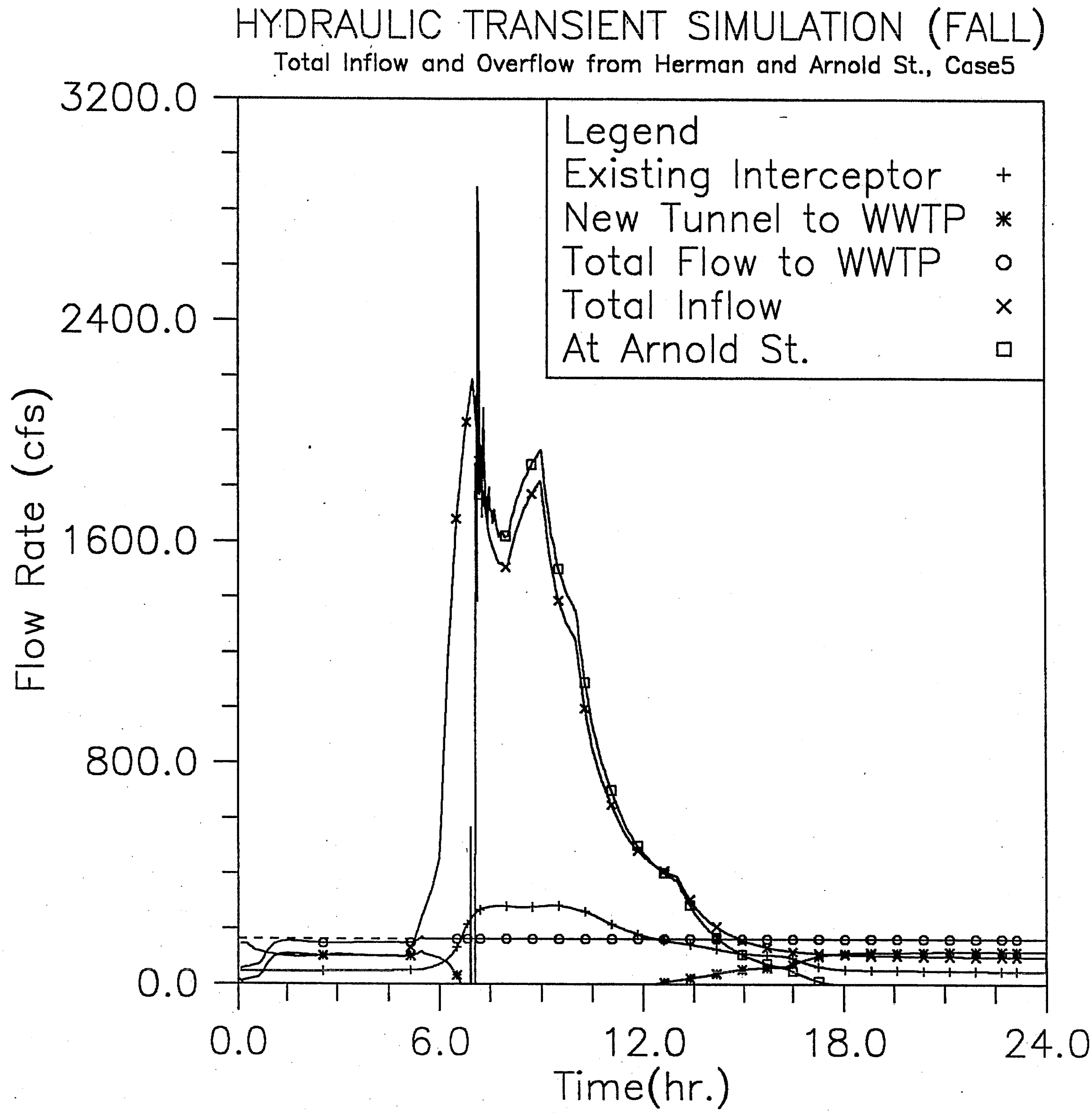

Fig. 3.5(g) Time variation of the overflow and the total inflow; modeling case: design storm and limited outflow to the WWTP (Case 5).

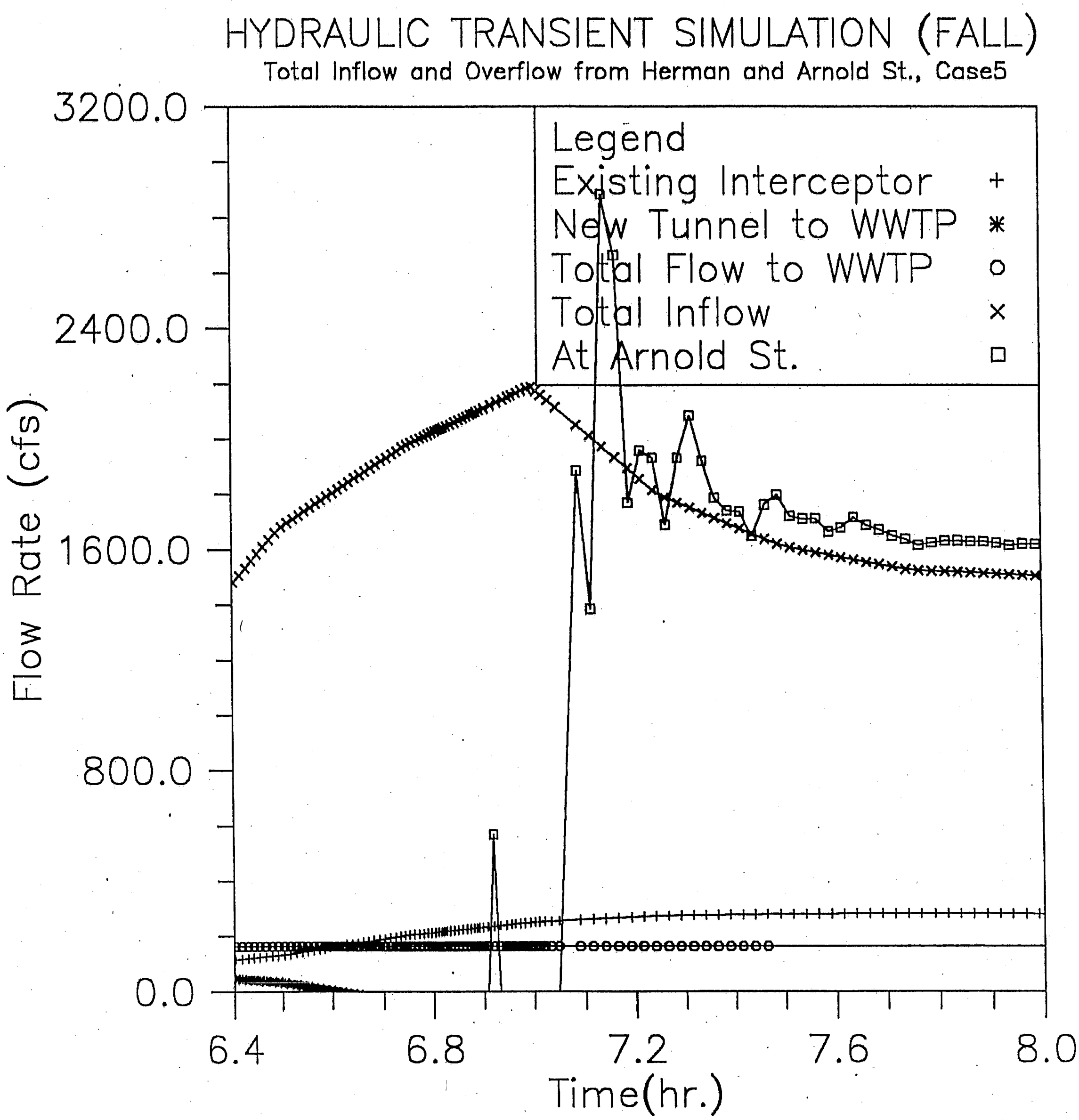

Fig. 3.5(h) Detailed time variation of the overflow and the total inflow during the initial stage of the overflow; modeling case: design storm and limited outflow to the WWTP (Case 5).

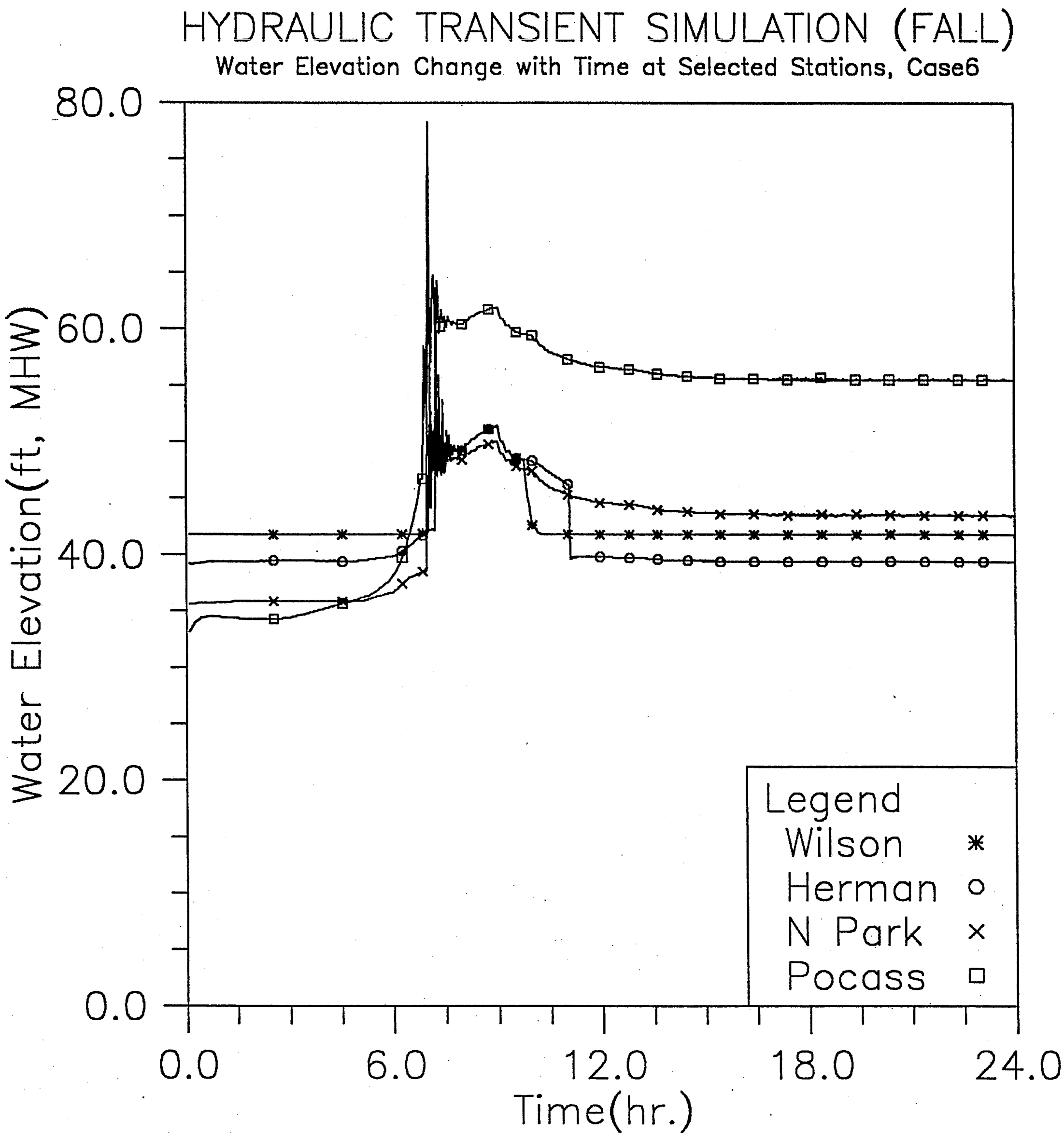

Fig. 4.1(a) Time variation of water surface elevations at four upstream dropshafts; modeling case: design storm without flow to the WWTP, and updated design data (Case 6).

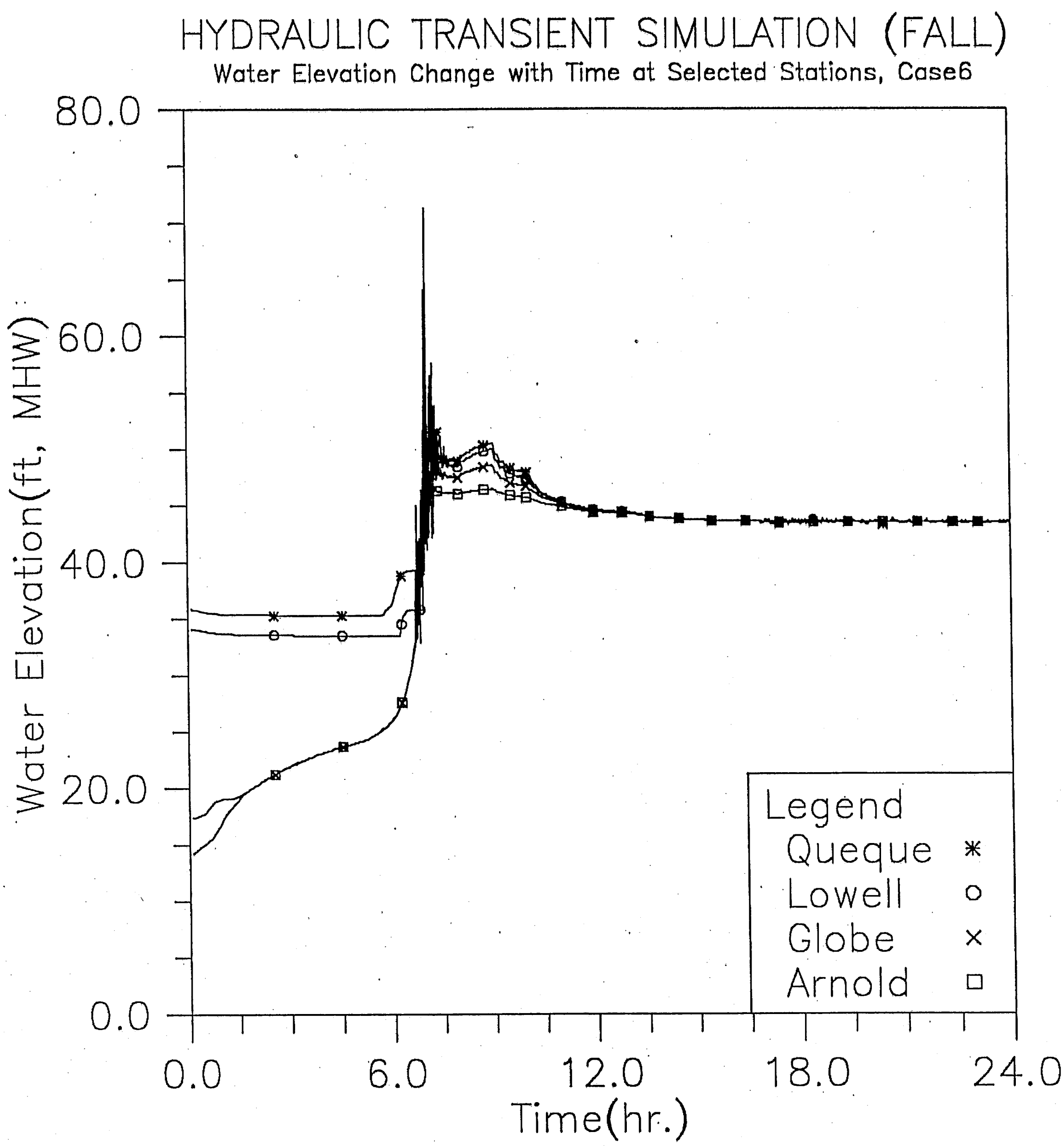

Fig. 4.1(b) Time variation of water surface elevations at Quequechan and three downstream dropshafts; modeling case: design storm without flow to the WWTP, and updated design data (Case 6).

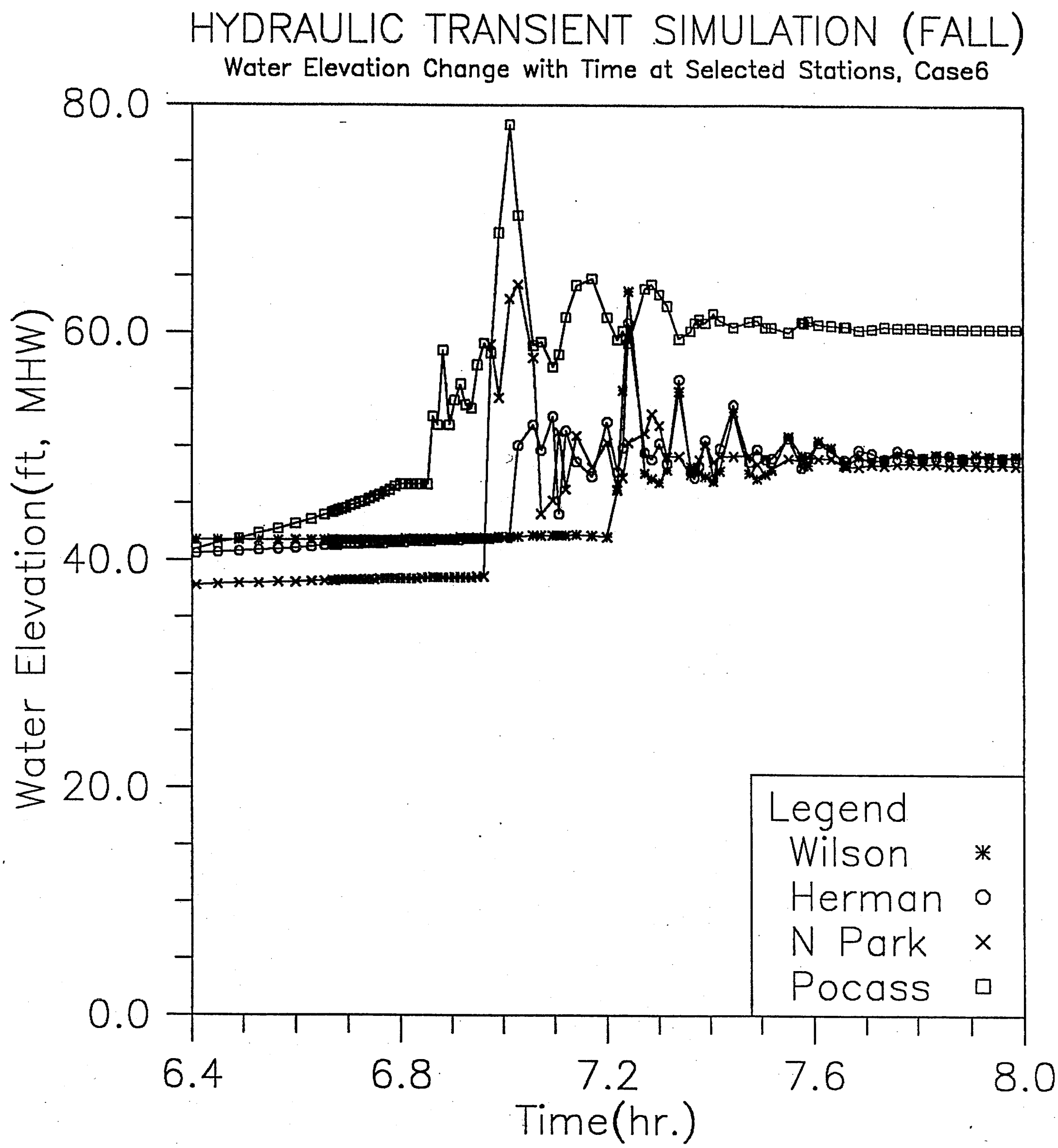

Fig. 4.1(c) Detailed time variation of water surface elevations at four upstream dropshafts during the surge period; modeling case: design storm without flow to the WWTP, and updated design data (Case 6).

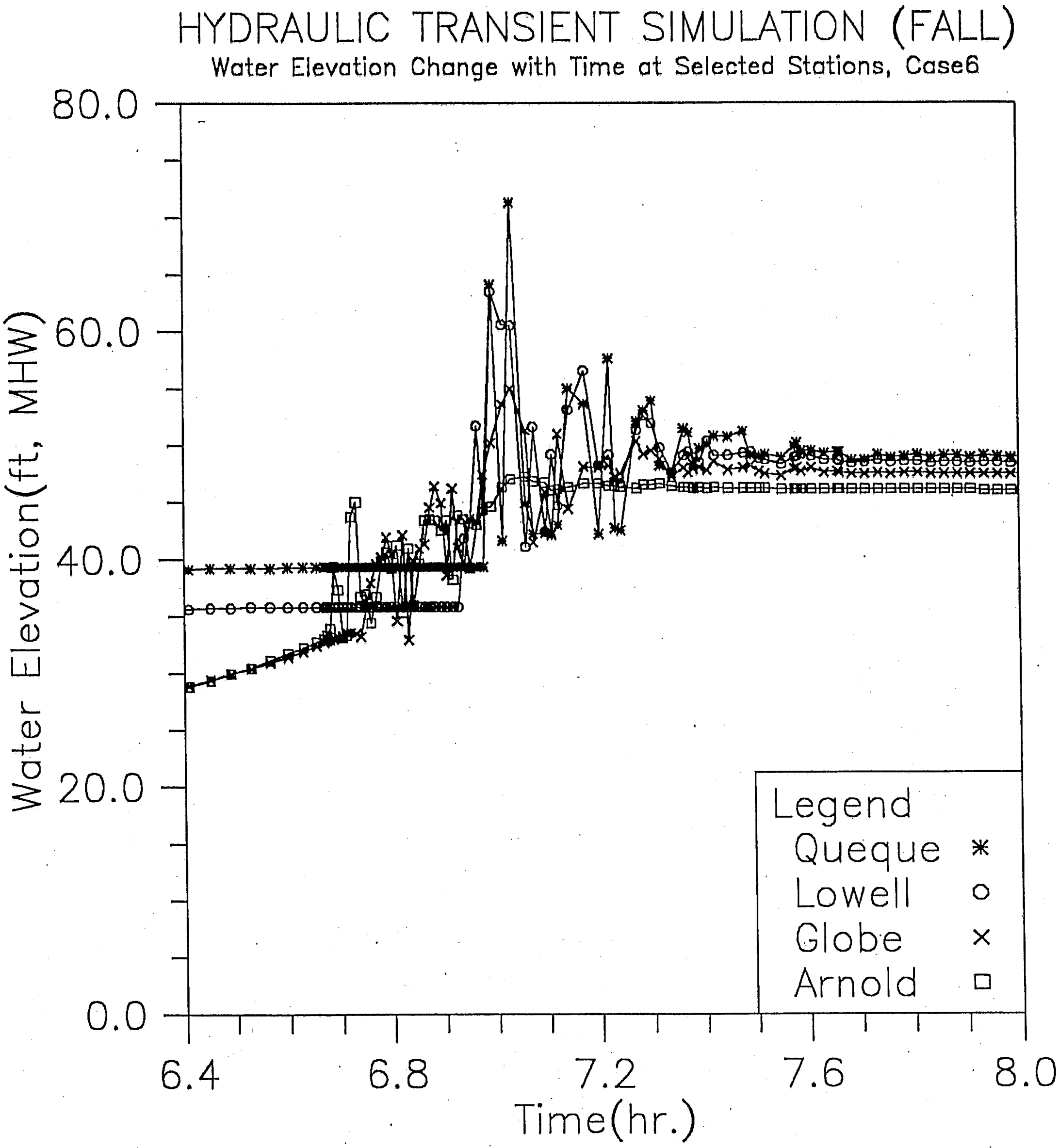

Fig. 4.1(d) Detailed time variation of water surface elevations at Quequechan and three downstream dropshafts during the surge period; modeling case: design storm without flow to the WWTP, and updated design data (Case 6).

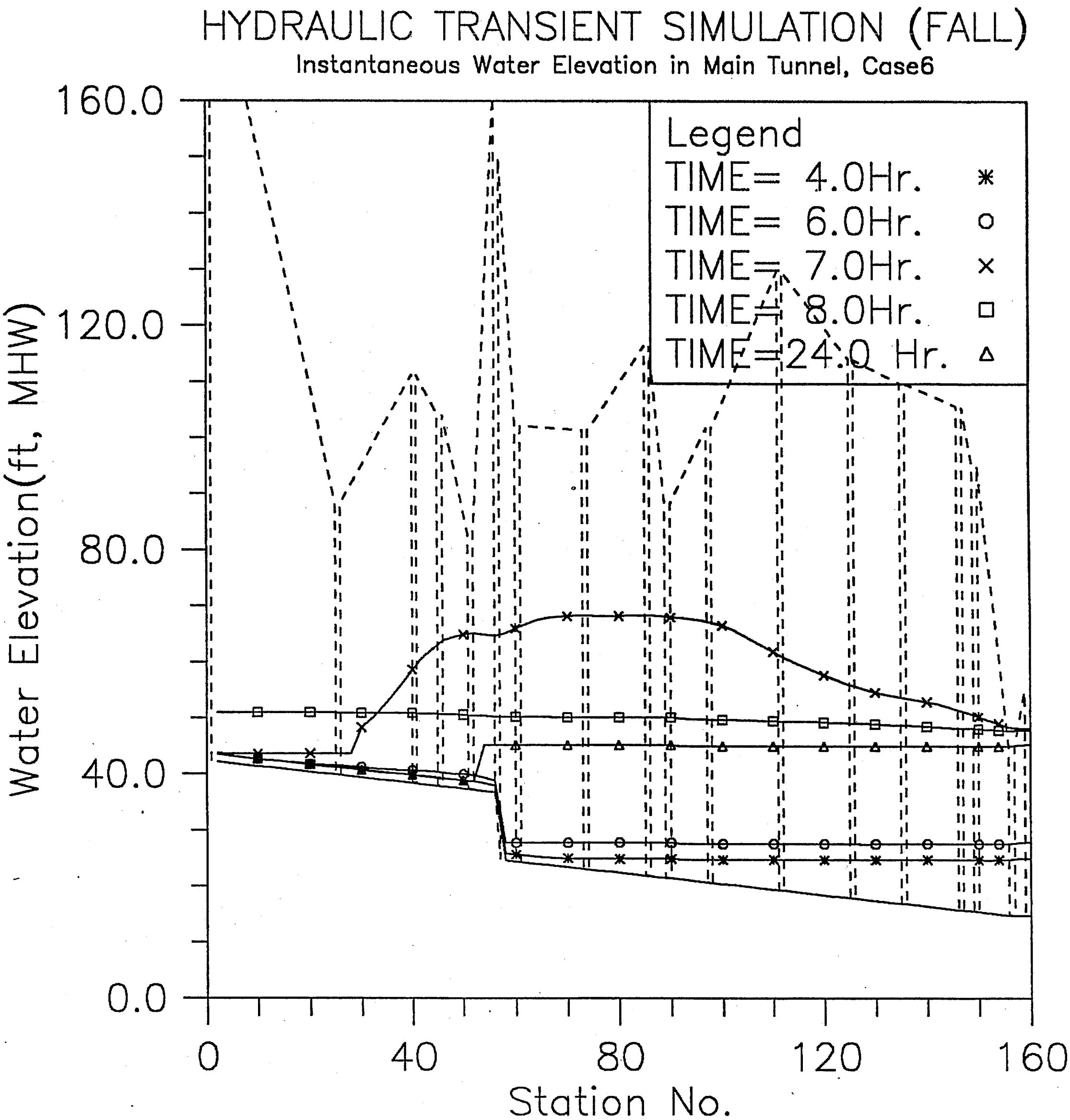

Fig. 4.1(e) Instantaneous hydraulic gradelines along the main tunnel; modeling case: design storm without flow to the WWTP, and updated design data (Case 6).

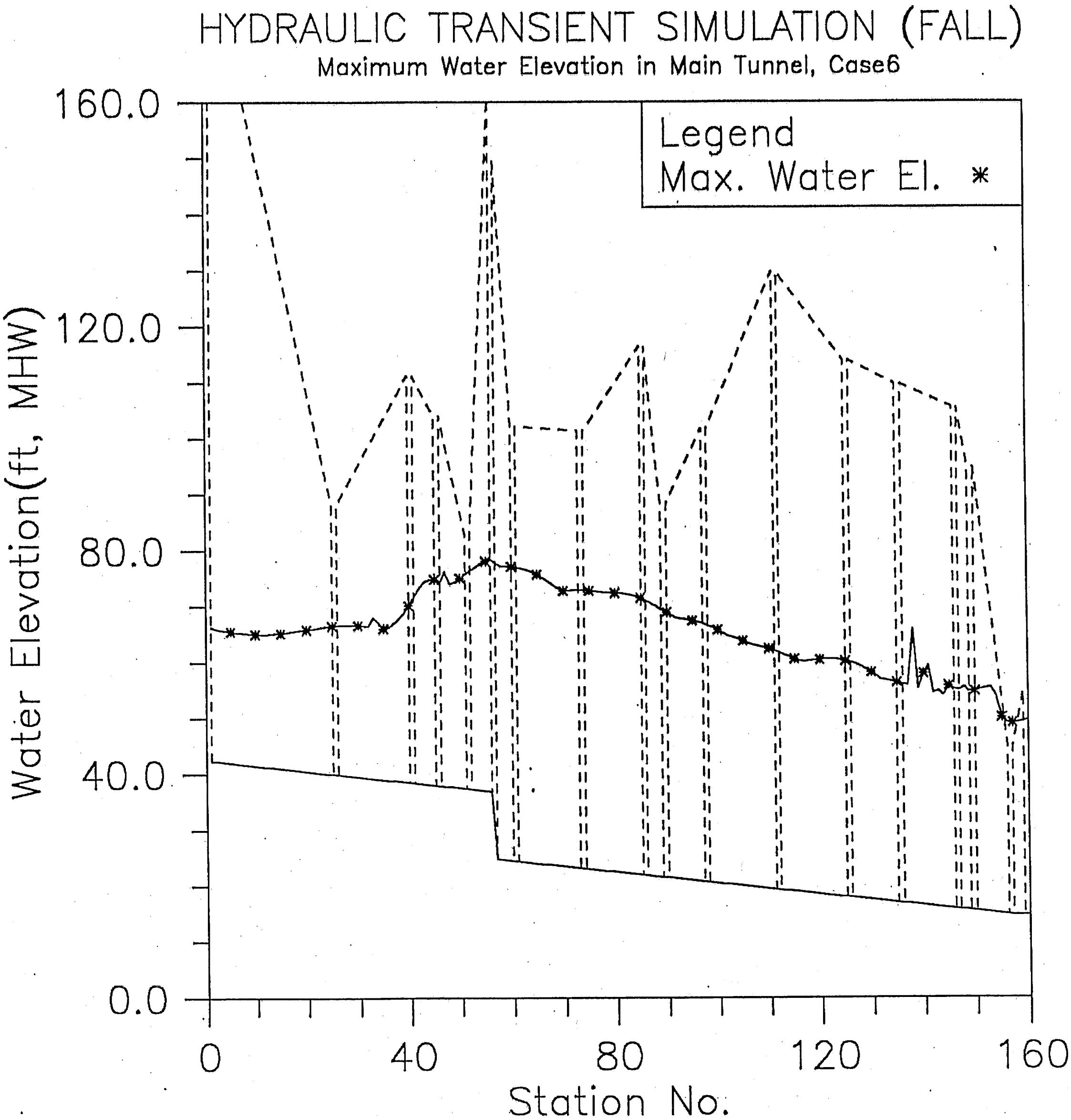

Fig. 4.1(f) The maximum water surface elevations along the main tunnel; modeling case: design storm without flow to the WWTP, and updated design data (Case 6).

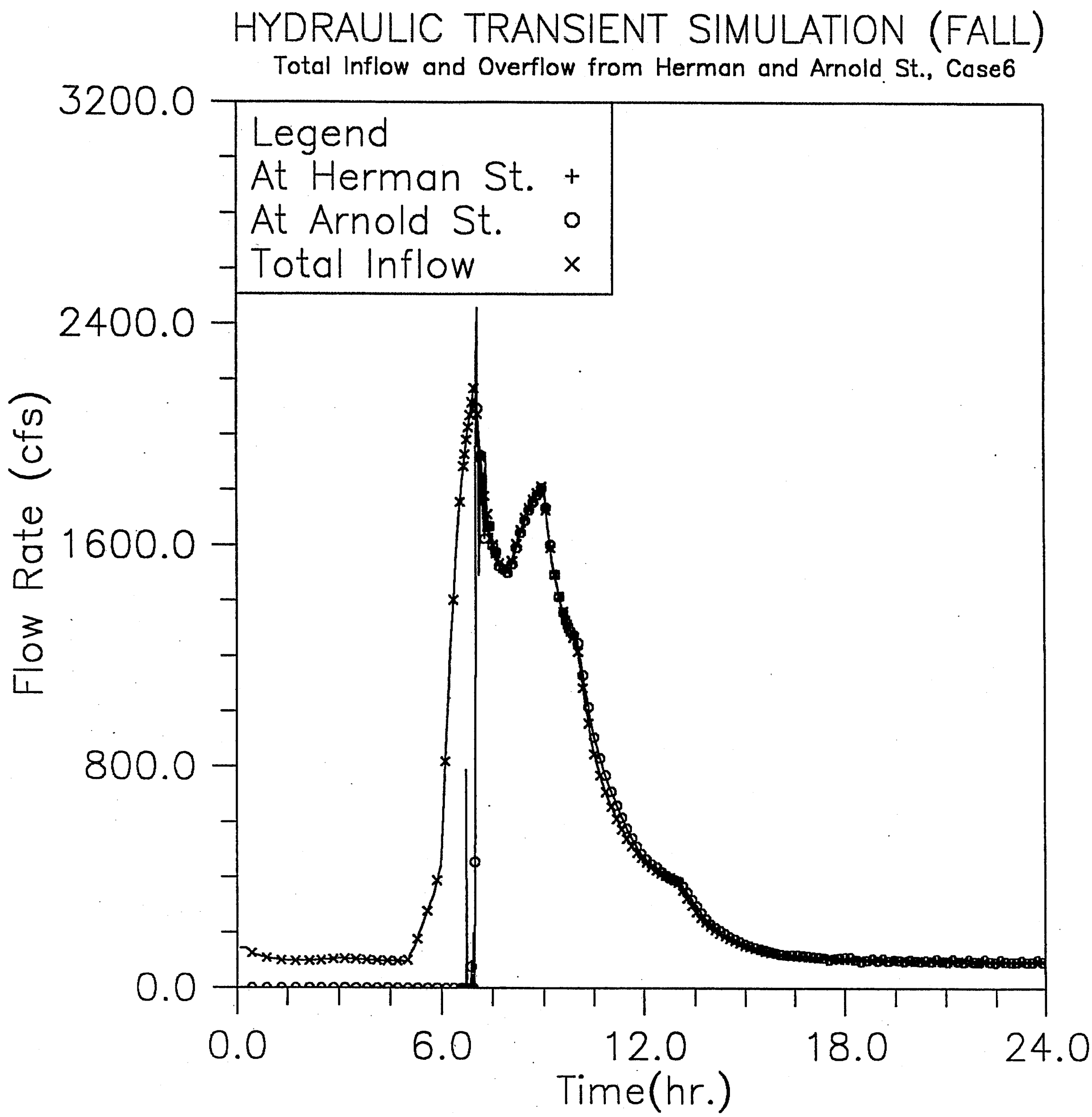

Fig. 4.1(g) Time variation of the overflow and the total inflow; modeling case: design storm without flow to the WWTP, and updated design data (Case 6).

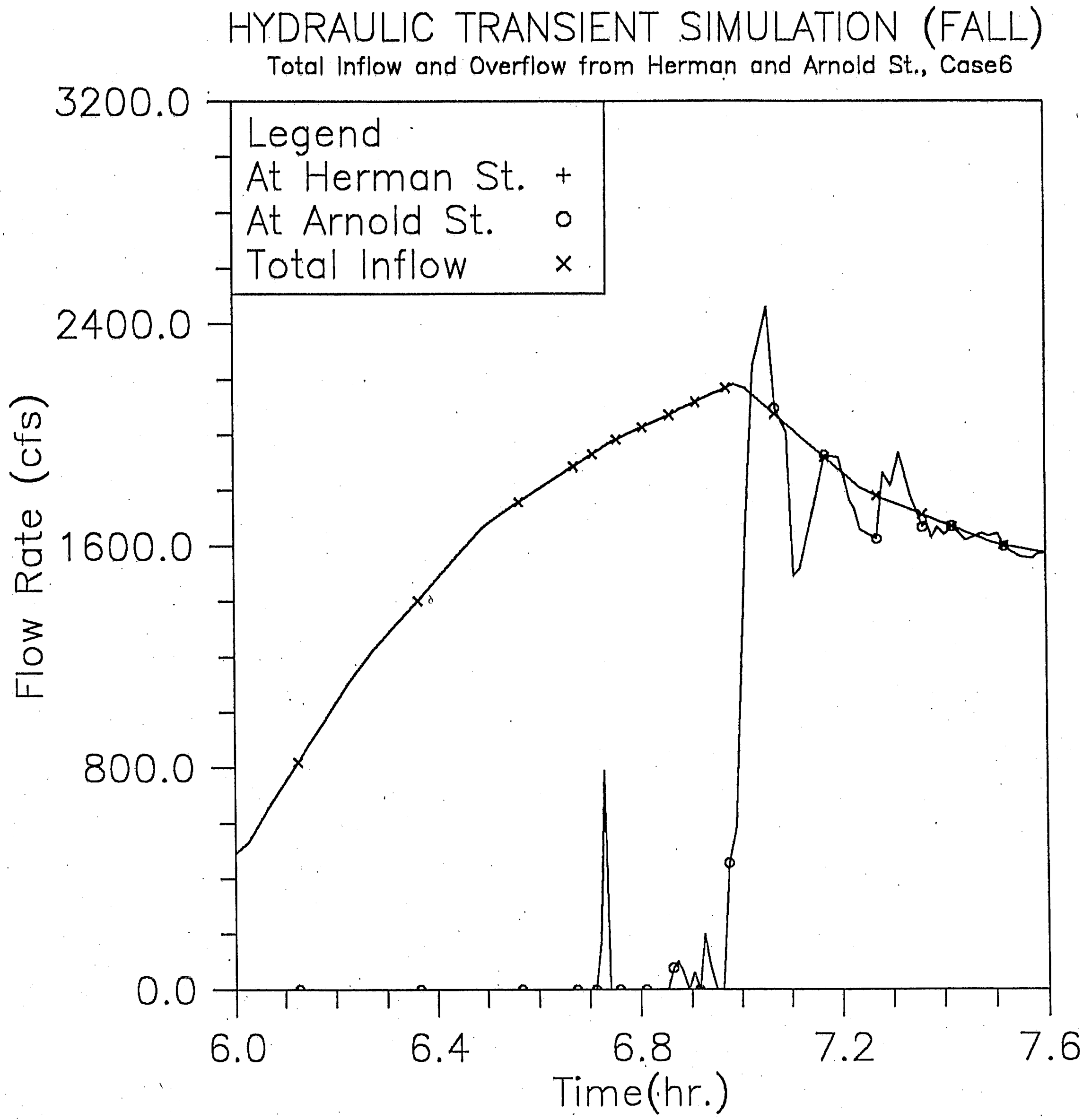

Fig. 4.1(h) Detailed time variation of the overflow and the total inflow during the initial stage of the overflow; modeling case: design storm without flow to the WWTP, and updated design data (Case 6).

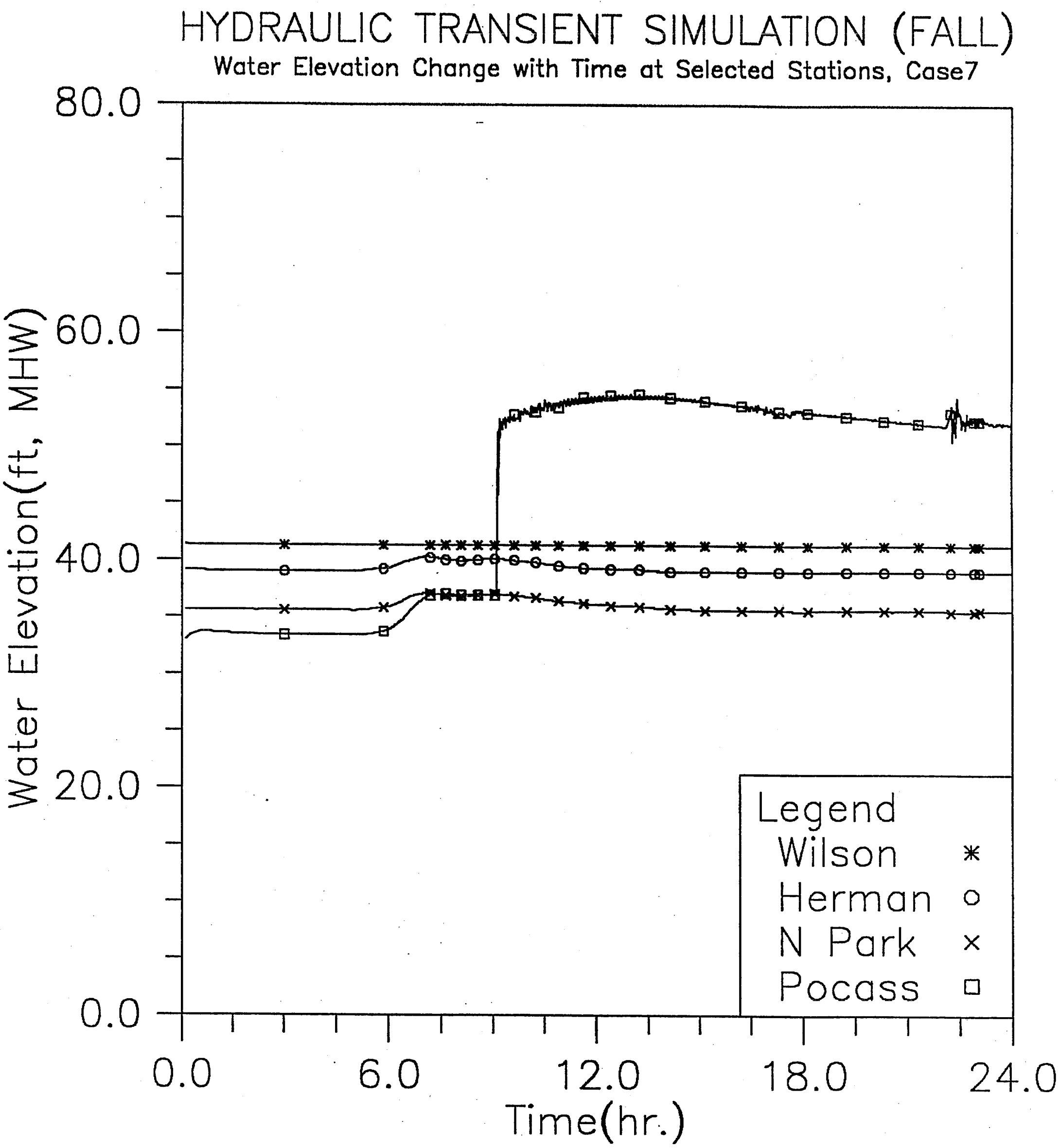

Fig. 4.2(a) Time variation of water surface elevations at four upstream dropshafts; modeling case: 3–month storm and limited outflow to the WWTP, and updated design data (Case 7).

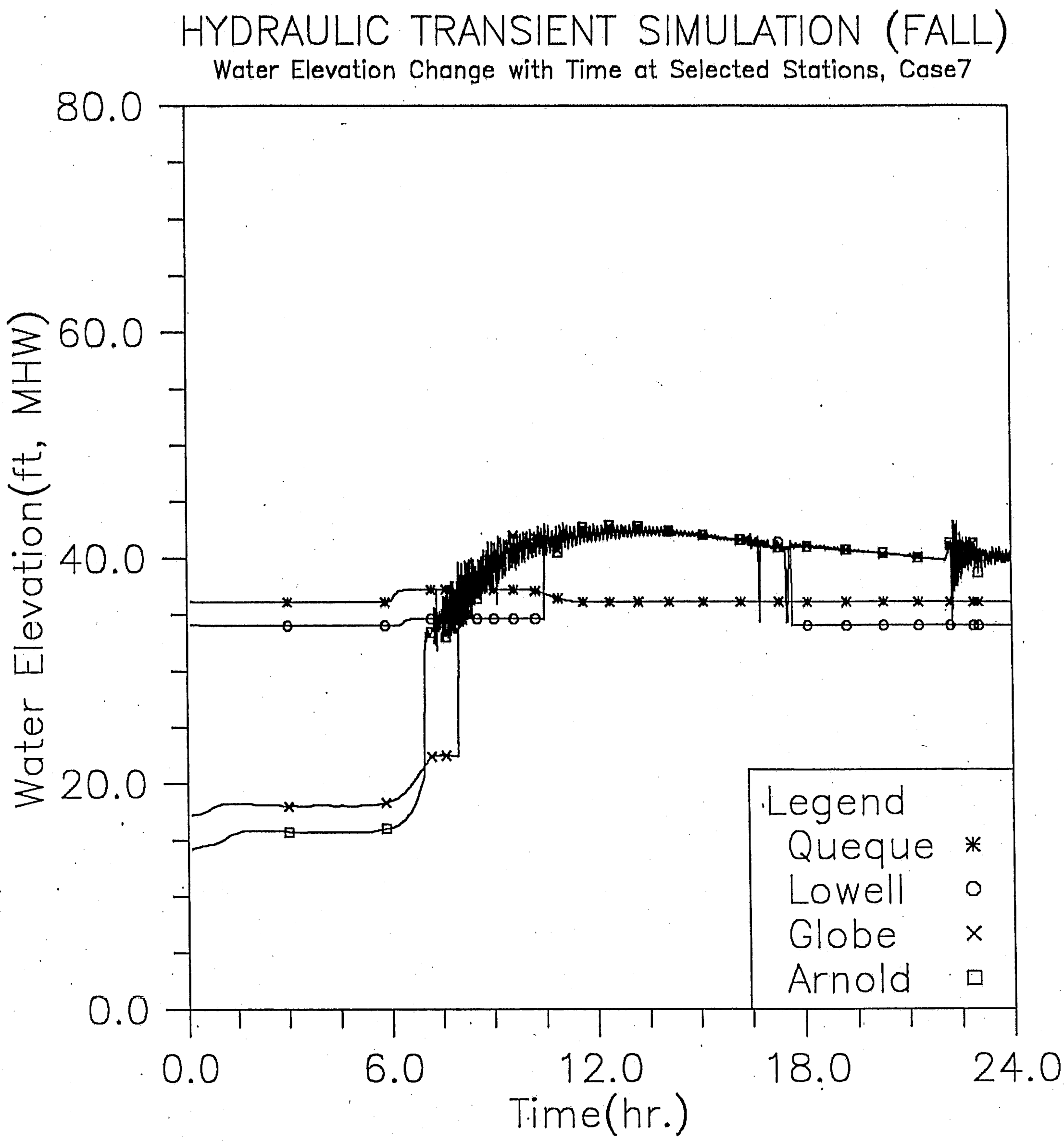

Fig. 4.2(b) Time variation of water surface elevations at Quequechan and three downstream dropshafts; modeling case: 3–month storm and limited outflow to the WWTP, and updated design data (Case 7).

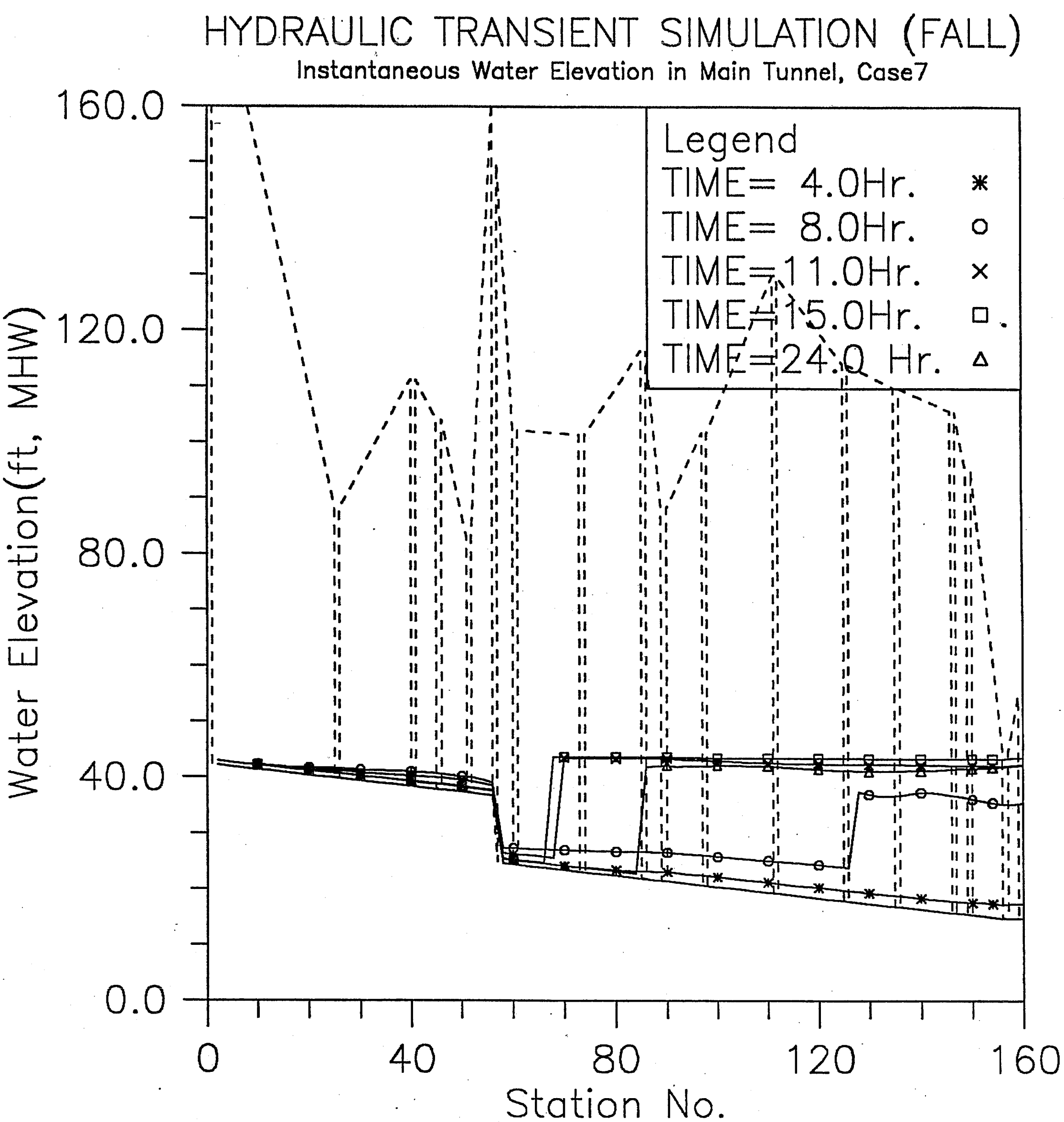

Fig. 4.2(c) Instantaneous hydraulic gradelines along the main tunnel; modeling case: 3–month storm and limited outflow to the WWTP, and updated design data (Case 7).

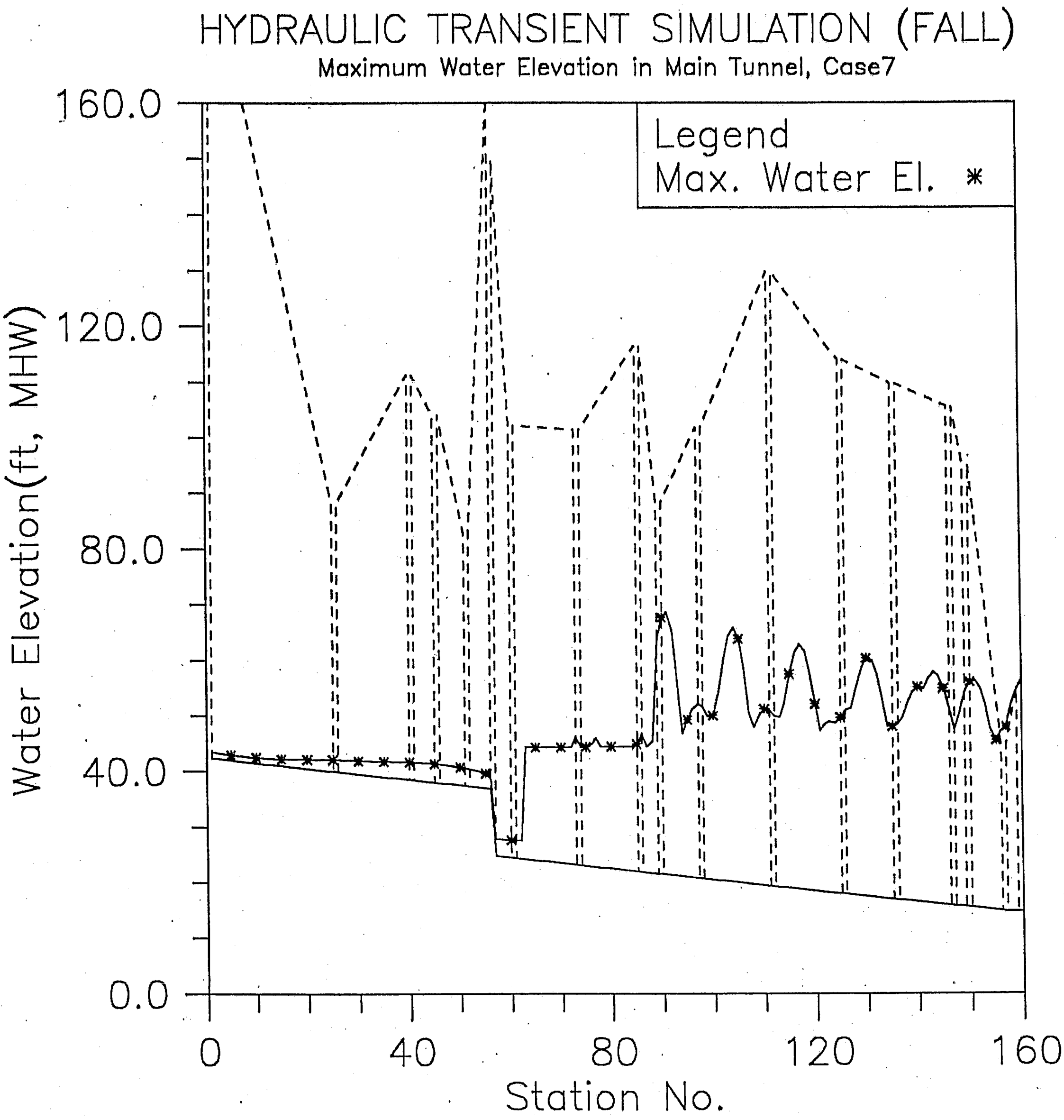

Fig. 4.2(d) The maximum water surface elevations along the main tunnel; modeling case: 3–month storm and limited outflow to the WWTP, and updated design data (Case 7).

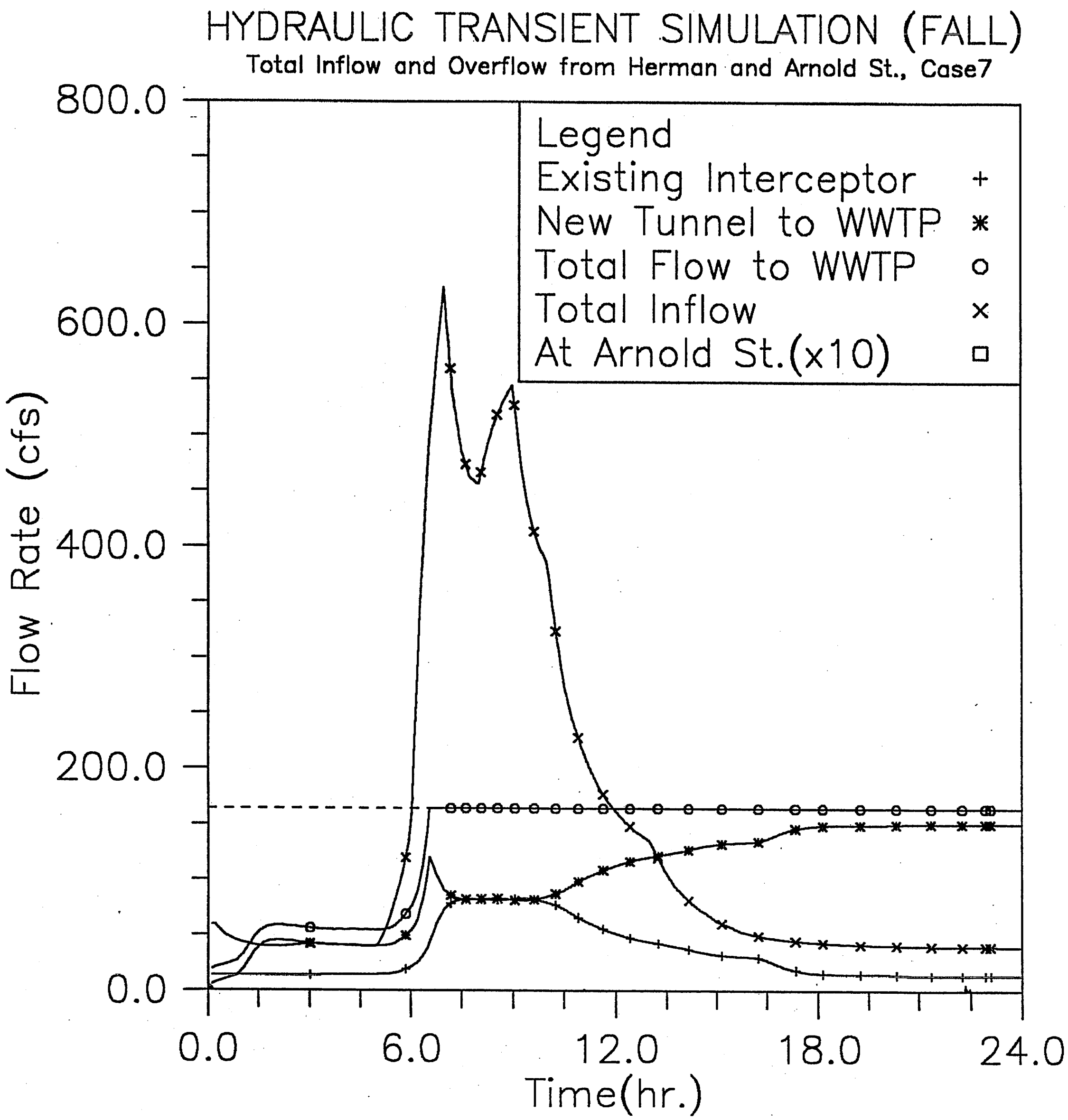

Fig. 4.2(e) Time variation of the overflow and the total inflow; modeling case: 3–month storm and limited outflow to the WWTP, and updated design data (Case 7).